Titre: Title:	Mathematical modelling and application of coupled processes in freezing soil
Auteur: Author:	Shen Mu
Date:	1991
Type:	Mémoire ou thèse / Dissertation or Thesis
Référence: Citation:	Mu, S. (1991). Mathematical modelling and application of coupled processes in freezing soil [Thèse de doctorat, Polytechnique Montréal]. PolyPublie. https://publications.polymtl.ca/57966/

UNIVERSITE DE MONTREAL

MATHEMATICAL MODELLING AND APPLICATION OF COUPLED PROCESSES IN FREEZING SOIL

par

SHEN Mu

DEPARTEMENT DE GENIE CIVIL

ECOLE POLYTECHNIQUE

THESE PRESENTEE EN VUE DE L'OBTENTION

DU GRADE DE PHILOSOPHIAE DOCTOR (Ph.D)

(GENIE CIVIL)

OCTOBRE 1991

UNIVERSITE DE MONTREAL

ECOLE POLYTECHNIQUE

Cette thèse intitulée:

MATHEMATICAL MODELLING AND APPLICATION OF COUPLED PROCESSES IN FREEZING SOIL

Présentée par: Shen Mu

en vue de l'obtention du grade de: Philosophiae Doctor (Ph.D.)

a été dûment accepté par le jury d'examen constitué de:

M. Michel Soulié	D.Sc.A., Président
M. Branko Ladanyi	D.Sc.A., directeur de recherche
M. Robert Chapuis	D.Sc.A., membre
M. Peter J. Williams	Ph.D, membre

ABSTRACT

Soil expansion during freezing is caused by soil water freezing and moisture migration from unfrozen to frozen soil. This process results in frost heaving, and it may cause damage to structures built in the permafrost or seasonally frozen ground. The understanding and simulating of soil freezing process has been a long-term goal of much research in cold regions engineering.

In this thesis, a conceptual model for calculating the amount of heaving and the resulting stresses in a freezing soil, on the basis of three coupled field: heat transfer, moisture migration and stress,is presented. This model takes into account the non-homogeneity of the frozen zone due to temperature variation, as well as the effects of frozen soil creep on stress distribution. In this model, the Clapeyron equation is used to determine the liquid water pressure and to describe the effect of stress field on the heat and moisture transfer within the freezing fringe, while the associated flow rule is used to define creep strains in frozen soil.

This model was used to simulate a test on a saturated cylindrical sample of silt under $50\,kPa$ in unidirectional open freezing system was first carried out. The predicted temperature field and the amount of heave are in a good agreement with the experimental results published by Penner (1986). However, in

addition, the simulation furnished also the complete stress field during freezing, which made it possible to take into account the effect of external loading on the amount of frost heave.

Secondly, the proposed model was used to simulate ground-pipeline interaction for a chilled pipeline experiment carried out at the pipeline test facility in Caen, France. The simulated temperature profile agrees well with the measurements, and predicted stresses acting against the pipeline seem to be of a correct order of magnitude. Because of a lack of exact information on the axial confining conditions of the pipe, it was decided to solve first two extreme pipe-confinement cases, i.e., the case of a free floating pipe and the case of a rigidly fixed pipe. It was considered that real conditions would be located between these two limiting cases. To test this assumption, and in order to take into account the possible resistance due to the longitudinal confinement of the pipe, another possible pipe confinement condition was also considered, in which the pipe resistance was represented by a virtual spring. The simulated frost heaving under this pipe confinement condition was directly controlled by the assumed spring stiffness, and was found to be always located between those of the two limiting cases.

RÉSUMÉ

L'expansion du sol pendant l'engel est causée par le gel de l'eau interstitielle et par la migration de l'humidité du sol non gelé vers le sol gelé. Ce processus produit le soulèvement du sol, qui peut endommager les structures construites dans le pergélisol ou dans le sol soumis à un gel saisonnier. Comprendre et simuler mathématiquement le processus de gel du sol a été l'objectif de nombreuses recherches en ingénierie des régions froides.

Cette thèse présente un modèle conceptuel capable de calculer le soulèvement et les contraintes dans le sol qui gèle, en se basant sur le couploge des trois champs: transfert de chaleur, migration de l'humidité et contraintes. Ce modèle tient compte de l'hétérogénéité de la zone gelée due à la variation de la température, ainsi que des effets du fluage du sol gelé sur la distribution des contraintes. On utilise l'équation de Clapeyron pour déterminer la pression dans l'eau non gelée et pour décrire l'effet du champ de contraintes sur le transfert de la chaleur et d'humidité dans la frange gelée, tandis que la loi d'écoulement associée est utilisée pour définir les déformations de fluage du sol gelé.

En utilisant ce modèle, on a d'abord simulé numériquement un essai de gel,

publié par Penner (1986). Dans cet essai, un échantillon cylindrique de silt saturé fut soumis au gel unidirectionnel sous une pression normale de $50\,kPa$. Les prédictions du champ de température et la quantité de soulèvement s'accordent bien avec les résultats expérimentaux de Penner (1986). Cependant, en plus, la simulation a fourni également le champ de contraintes complet lors du gel, ce qui permet de tenir compte de l'effet des sollicitations externes sur la quantité du soulèvement.

En second lieu, en utilisant le modèle proposé, on a également simulé l'interaction entre le sol et un gazoduc refroidi et on comparé les prédictions avec les résultats de mesures effectuées sur un gazoduc enterré, situé dans le Centre d'essais de Caen, France. Les résultats de simulation du profil de température se comparent bien avec les mesures, et les contraintes agissant sur le gazoduc ont des valeurs raisonnables. A cause de manque d'information sur les conditions de confinement du gazoduc dans le sens longitudinal, on a décidé de simuler d'abord deux cas extrêmes de confinement du tuyau, celui de flottaison libre et celui d'un encastrement rigide du tuyau. On a considéré que les conditions réelles devaient se trouver entre ces deux cas limites. Afin de vérifier cette hypothèse, et pour montrer comment on pourrait prendre en compte la résistance due au confinement longitudinal du tuyau, on a résolu également un cas intermédiaire dans lequel la résistance du tuyau fut représentée par un

ressort virtuel , fonction de la flexibilité longitudinale du tuyau. On a constaté que le soulèvement simulé dans ce dernier cas est contrôlé directement par la rigidité du ressort, en se situant entre les deux cas limites.

ACKNOWLEDGEMENT

I would like to express my great gratitude to my advisor, Prof. Branko Ladanyi of the Civil Engineering Department, for his wise guidance, encouragement and continuous support from the inception to the present form of this thesis. He has given me an invaluable help.

I would like to acknowledge Prof. P.J.Williams of Carleton University, Ottawa, for permitting me to use the results of measurements from the France-Canada joint project in Caen, France.

I would also like to acknowledge the help I received from many friends and the staff of the École Polytechnique de Montréal.

Finally, I owe a debt of gratitude to the Service des Etudes Supérieures of École Polytechnique de Montréal for the exemption of the foreign student tuition fees, and to the National Science and Engineering Research Council of Canada and Esso Resources Canada Ltd. for the financial support during my studies at École Polytechnique.

Contents

List of Figures

List of Tables

NOMENCLATURE

$[B]$	transformation matrix between strains and nodal displacements.
$[D]$	elasticity matrix
$[K]$	stiffness matrix
C	heat capacity of soil
$\overline{C}$	apparent heat capacity of soil
C^+, C^-	heat capacity of unfrozen and frozen soil
E_0	Young's modulus of soil
E_{spring}	equivalent Young's modulus of the virtual spring
F, F_0	current yield function and reference yield function
g	gravitational acceleration
g_{11}, g_{12}, g_{22}	covariant metric tensor components
G	gravitational potential
$gradT$	temperature gradient
k	hydraulic conductivity
L	latent heat of fusion
P_i, P_l	ice and liquid water pressure
$d\{P\}$	nodal loading increment vector
$P(\xi,\eta), Q(\xi,\eta)$	source terms for control of spacing and orientation of the coordinate lines

$d\{R\}$	"pseudoforce" increment vector due to the creep, the volumetric expansion and the temperature variation
r, z	coordinates in the cylindrical coordinate system
r_{rw}	minimum radius of the ice/water interface
SP	segregation potential
T	temperature
T_k, T_0	absolute temperature and the freezing point of pure water at atmospheric pressure
T_f	freezing temperature of soil
V_0	water intake flux
v_x, v_y	soil water flow velocity in the x,y direction
x, y	coordinates
x_ξ, y_ξ	first derivative of x and y with respect to ξ
x_η, y_η	first derivative of x and y with respect to η
$x_{\xi\xi}, y_{\xi\xi}$	second derivative of x and y with respect to ξ
$x_{\eta\eta}, y_{\eta\eta}$	second derivative of x and y with respect to η
Δx	spacing of gridwork in the x-direction
Δz	spacing of gridwork in the z-direction
ϵ^v	volumetric expansion strain
$\epsilon_x^v, \epsilon_y^v, \epsilon_z^v$	normal expansion strain components
$\gamma_x^v, \gamma_y^v, \gamma_z^v$	shear expansion strain components
ϵ^c	creep strain in uniaxial stress state
$\{\dot{\epsilon}^c\}$	creep strain rate

$d\{\epsilon\}$	increment vector of total strain
$d\{\epsilon^e\}, d\{\epsilon^c\}, d\{\epsilon^v\}$	increment vectors of elastic strain, creep strain and volumetric expansion strain
$d\{\delta\}$	nodal displacement vector
$\overline{\sigma}$	equivalent stress for the *von Mises* yield function
$\{\sigma\}, d\{\sigma\}$	stress vector and stress increment vector
σ_{rw}	interfacial tension of the ice/water interface
θ_i, θ_l	volumetric fraction of ice and liquid water
θ_0	initial water content
$\Delta\theta$	increment of water content by moisture migration
λ	thermal conductivity of soil
$\overline{\lambda}$	apparent thermal conductivity of soil
λ^+, λ^-	thermal conductivity of unfrozen soil and frozen soil
μ	Poisson's ratio
ξ, η	coordinates in the curvilinear system
ξ_x, η_x	first derivative of ξ and η with respect to x
ξ_y, η_y	first derivative of ξ and η with respect to y
ξ_{xx}, η_{xx}	second derivative of ξ and η with respect to x
ξ_{yy}, η_{yy}	second derivative of ξ and η with respect to y
$\Delta\xi$	spacing of gridwork in the ξ-direction
$\Delta\eta$	spacing of gridwork in the η-direction
ρ_i, ρ_l	density of ice and liquid water
Φ	soil water potential

τ	time
$\Delta\tau$	time step interval

Chapter 1

INTRODUCTION

1.1 Mechanics of Freezing in Soils

1.1.1 Freezing Process

It is well known that three conditions are necessary for frost heave and the formation of segregation ice. First, ground temperatures must be sufficiently cold and prolonged so that the soil water freezes. Second, the water table must be close to the frost front in the soil mass so that water can migrate to a growing ice lens. Third, the soil must be susceptible to the formation of segregated ice.

It is universally recognized that frost heave is caused not only by freezing of in-situ pore water, but also by water flow to the freezing front. This water flow is induced by a suction gradient that develops in the frozen soil in response to the temperature gradient in the soil mass.

As described by Konrad and Morgenstern (1980), when a soil freezes, be-

cause of the effect of particle surface forces and suction pressures acting below the ice lens, the nucleation temperature T_s required to form ice at the base of the lens is colder than the normal freezing point of water $T_f \approx 0°C$, the warmest temperature at which ice can grow. An idealization of the formation of segregated ice is shown in Figure 1.1. In this figure, the cold-side temperature is at the surface, the temperature at the frost front is equal to the normal freezing point of water T_f, and the segregation temperature T_s is located at the base of the growing ice lens. The zone between the base of the growing ice lens ($T = T_s$) and the freezing front ($T = T_f$) has been termed the frozen fringe (Miller, 1972). In the frozen fringe, liquid water exists in equilibrium with ice at a temperature below the freezing point. The amount of water that can flow to the base of the ice lens is a function of the suction gradient existing across the frozen fringe and in the unfrozen zone, and of the permeabilities of the frozen fringe and the unfrozen soil. Under steady-state conditions, water flows to the base of the growing ice lens through the frozen fringe from the underlying unfrozen soil. When the frost front advances, the temperature in the frozen fringe decreases, causing a reduction of its permeability and a decrease in the flow of water. This interrelation of heat, moisture and flow, results in the formation of finer ice lenses near the surface of a soil column where the temperature gradient is the greatest. Thicker ice lenses occur at greater depths where the temperature gradient is smaller. According to Konrad and

Morgenstern (1984), "from phenomenological point of view, the mechanics of frost heave can be regarded as a problem of impeded drainage to an ice-water interface at the segregation front".

1.1.2 Capillary Theory

In the capillary theory, the only driving force for water migration to a growing ice lens is the capillary suction which is present at a curved ice/water interface, and is given by the Kelvin equation (Williams, 1972):

$$P_i - P_l = \frac{2\sigma_{il}}{r_{il}} \tag{1.1}$$

where: P_i, P_l – ice, and liquid water pressures; σ_{il} – the interfacial tension of the ice/water interface; r_{il} – the minimum radius of the ice/water interface. According to this model, the accumulation of ice occurs only at the freezing front, and the maximum value of pressure difference $P_i - P_l$ depends only on the characteristics of soil, and not on the temperature, temperature gradient and frost penetration rate. In fact, however, it is now generally known that the moisture migration towards the growing ice lens occurs not only in the unfrozen but also in the frozen zone (Xu et al., 1985). Miller (1977) has referred to this model of ice lens growth as "primary frost heaving". Miller (1972) proposed the concept of "secondary heaving", which occurs when freezing extends below

the nominal base of the ice lens. In his model, ice in the frozen pores can move by regelation relative to the particles, and moisture can move towards the base of ice lens through a thin, partially frozen zone, which he called "frozen fringe".The phenomenon of the growing ice lens behind the freezing front was confirmed experimentally by Loch and Kay (1978), who found the thickness of frozen fringe for New Hampshire silt to be about $0.2-0.4\,cm$. This phenomenon cannot be explained on the basis of the capillary theory.

Nevertheless, as shown by Everett and Haynes (1965), Penner (1973), Sutherland and Gaskin (1973), and some others, the capillary theory can be used with some success for predicting the suction at the frost front, frost heaving rate and frost heaving pressure in essentially non-colloidal soils composed of inert particles, such as glass beads, pulverized fuel ash, and even kaolin, provided the radius r_{iw} in eq.(1.1) can be properly evaluated or indirectly measured (Williams, 1972; Sutherland and Gaskin, 1973).

1.1.3 Thermodynamic Theory

A better understanding of suction in frozen soils can be obtained by the generalized Clausius-Clapeyron equation (Kay and Perfect, 1988)

$$\frac{P_i}{\rho_i} - \frac{P_l - \pi}{\rho_l} = -L\frac{T - T_0}{T_0} \tag{1.2}$$

where:P_i, P_l – the ice pressure and hydrostatic pore water pressure, respectively; π – the osmotic pressure associated with leachable solutes; L – the latent heat of fusion, and T, T_0 – freezing temperatures ($°K$) of water in soil and in the bulk state, respectively; ρ_l, ρ_i – density of water and ice, respectively.

If appropriate values of parameters are substituted into eq.(1.2) ($\rho_l = 1000\ kg/m^3$; $\rho_i = 916.8\ kg/m^3$; $L = 3.336 \times 10^5\ J/kg$; $T_0 = 273.15°K$), and neglecting π for pure water, one gets from eq.(1.2) the rates of pressure changes with the variation of temperature (Ladanyi, 1985):

$$dP_l = 1.091 dP_i + 1.221 dT \tag{1.3}$$

with pressure in MPa and temperature in $°K$. Eq.(1.3) expresses in general the variation of suction in the pore water with the variation of the external pressure on the ice and the temperature (Konrad and Morgenstern, 1982).

If it is assumed that at the ice/water interface $dP_l = dP_i = dP$, one gets from eq.(1.3) the freezing point depression for ice

$$\frac{\partial T}{\partial P} = -0.0745 \quad °K/MPa \tag{1.4}$$

However, if only the pressure on the ice changes, with $dP_l = 0$, eq.(1.3) gives

$$\frac{\partial T}{\partial P_i} = -0.89 \quad °K/MPa \tag{1.5}$$

While in the opposite case, when $dP_i = 0$

$$\frac{\partial T}{\partial P_l} = 0.82 \quad {}^\circ K/MPa \tag{1.6}$$

Available experimental evidence (Miller et al., 1980) shows that eq.(1.5) seems to explain better than eq.(1.4) local pressure melting phenomenon in frozen soils and the freezing depression in the soil during freezing.

Finally, in an isothermal case, $dT = 0$, and eq.(1.3) yields

$$dP_l = 1.091 dP_i \tag{1.7}$$

which indicates that changes in pore water pressure will tend to follow closely those in the ice, as long as there is no substantial temperature change (Williams, 1977).

The Clapeyron equation indicates that the liquid water pressure P_l becomes negative if ice is at the atmospheric pressure ($P_i = const$) and the soil temperature decreases below the freezing point, and that there is a nearly linear relationship between the suction and the temperature when the temperature is close to $0°C$. Some experimental verification of the Clapeyron equation has been provided by Vignes and Dijkema (1974) and Biermans et al. (1978). Hoekstra (1969) and Radd and Oertle (1973) measured the pressure necessary to prevent heave as a function of temperature in a freezing soil. If one assumes

that $P_l = 0$ at the lens and that heaving pressure is equal to the ice pressure, then the measurements of heaving pressure are in a good agreement with the Clapeyron equation.

In most models of frost heaving, the ice pressure variation dP_i is assumed to be zero in order to simplify the Clapeyron equation while defining the suction. However, when the soil is constrained or under an external loading, the distribution of the stress between soil particles, ice and liquid water must be determined, as will be shown later.

1.1.4 Segregation Potential Concept

Konrad and Morgenstern (1980) have proposed a detailed model for one-dimensional frost heave. They suggested that, after an ice lens is formed, the frozen soil behind the ice lens does not participate in mass transport, but that water is transported to the ice lens from the unfrozen soil through a thin zone of partially frozen soil referred to as the frozen fringe. The driving force arrives from suction generated at the ice-fringe interface, and the fringe impedes the flow to the lens because of its low permeability. They made a simple linear analysis of the frozen fringe, by assuming that the Clausius-Clapeyron equation is valid at the base of the ice lens, that water flow is continuous across the

frozen fringe, that the fringe can be characterized by an overall permeability K_{fo}, and that the temperature in the frozen fringe varies linearly between the segregation freezing temperature T_{so}, at the lens, and the freezing temperature of bulk water T_f, at the bottom of the fringe (Figure 1.2).

According to Konrad and Morgenstern (1981), when a soil sample freezes under different cold-side step temperatures but the same warm side temperature, the water intake flux V_0 at the formation of the final ice lens is proportional to the temperature gradient in the frozen fringe (Figure 1.3):

$$V_0 = SP \cdot gradT \tag{1.8}$$

The proportionality factor SP has been termed the segregation potential. Its value, given by the slope of the straight line in Figure 1.3, was found to be a function of the total suction potential at the freezing front P_l, the suction potential at the frozen-unfrozen interface P_u, the segregation freezing temperature T_s and the overall hydraulic conductivity in the fringe K_f (Konrad, 1987).

The segregation potential, once evaluated at near steady-state conditions, and under a negligible overburden pressure, may be considered as an index property of a soil that uniquely characterizes its frost heave susceptibility. Although the value of SP is usually determined at a constant suction at the

frost front, the relationship between SP and P_u can be easily established, because the value of P_u can be determined by applying the Darcy's equation to the unfrozen zone, once the permeability (K_u) is known and the velocity of moisture migration v is measured in a freezing test (Konrad and Morgenstern, 1981; Morgenstern, 1981; Konrad, 1988)

$$P_u = \frac{v \cdot l_u}{K_u} \tag{1.9}$$

where l_u is the length of flow in the unfrozen soil. When the suction at the frost front increases, the segregation potential decreases with a concomitant decrease in the slope of the relationship V_0 versus $gradT$. In close to thermal steady-state conditions, any freezing soil at the formation of the final ice lens is possibly characterized by a set of straight lines V_0 vs $gradT$ passing through the origin (Figure 1.4). Figure 1.5 shows a correlation between SP and P_u obtained for Devon silt (Morgenstern, 1981).

It is noted that Garand and Ladanyi (1982) have used the maximum suction at the frost front (eq.(1.9)) rather than the segregation potential for comparing the frost susceptibility of a glacial till under different compaction efforts.

A detailed procedure for experimental determination of the segregation potential has been described by Konrad (1987). He recommended to use the freezing apparatus developed by Penner (1986), and to perform a freezing

test under fixed temperature boundary conditions. The value of SP is then determined at the end of transient freezing.

It is interesting to note that such a freezing test with fixed temperature boundary conditions, leads generally to a heaving behaviour which is considered to be composed of 3 phases (Konrad and Morgenstern, 1980) (Figure 1.6). In phase 1, the water intake velocity is almost constant, in phase 2 it decreases continuously with time, and finally when the frost front becomes stationary, steady state is reached and phase 3 begins. This coincides with the growth of the last ice lens, under constant boundary conditions. During that final phase, experimental data show that the rate of heave decreases monotonically with time, tending apparently to an asymptotic value (Konrad and Morgenstern, 1980; Garand and Ladanyi, 1982). One should be aware, however, that this laboratory result, which may be due to the formation of a single final ice lens across the cell, preventing nearly all further water migration into the frozen zone, is probably not applicable to the field conditions where water migration is not one-dimensional but three-dimensional, so that water can migrate around the existing ice lenses.

Konrad and Morgenstern (1984) have established that the segregation-potential of a given freezing soil decreases with increasing applied pressure,

and they expressed the influence of surcharge by the empirical power law:

$$SP = SP_0 \cdot exp(-a \cdot P_e) \tag{1.10}$$

where SP_0 is the value of SP obtained for zero applied pressure, P_e is the applied pressure (Pa) and a is a constant (Pa^{-1}). The segregation potential concept has up to now been used successfully for predicting frost heaving effect related with chilled pipelines and artificial ground freezing (Konrad and Morgenstern, 1984).

1.1.5 Problem of Stress Partition

One of the important aspects of ice segregation is the role of the overburden pressure and its effect on ice segregation. In general, the pressure in any phase will differ from the overburden pressure. When the soil is confined or an overburden imposed, the distribution of the stress between soil particles, ice and liquid water has to be determined. Following unfrozen soil mechanics principles (Bishop and Blight, 1963), Miller (1978) suggested the use of a stress partition factor to weight the relative participations of the pore pressure, based upon the Terzaghi's concept of effective stress:

$$\sigma_n = \chi \cdot P_l + (1 - \chi) P_i \tag{1.11}$$

$$P = \sigma_e + \sigma_n \tag{1.12}$$

where: σ_n, σ_e – neutral stress and effective stress; χ – stress partition function; P – overburden. Although the theoretical basis of eq.(1.11) is controversial, especially when transferred from unsaturated unfrozen soil mechanics to the mechanics of soil freezing, it has nevertheless proven to be a useful empirical formula when the value of χ was expressed on the basis of experimental results.

Hopke (1980) assumed the partition factor χ , as a first approximation, to be given by

$$\chi = \frac{\theta_i}{1 - \theta_s} \tag{1.13}$$

where θ_i and θ_s are the volume fractions of ice and soil particles, respectively. The numerical results based upon this approximation show, that the heave rate may be oscillatory, because there is a discontinuity in ice pressure at each new lens location.

On other hand, a different approach to stress partition was used by Groenevelt and Kay (1977). These authors defined the envelope pressure potentials of the liquid water and ice in a frozen soil and expressed the liquid water pressure by the equation

$$P_l = P^\star + \alpha P + \beta L \rho_i \ln \frac{T}{T_0} \tag{1.14}$$

where: $P^\star$ – reference pressure (Pa); P – external loading pressure; α, β – loading factor and frost factor, respectively. However, it is difficult to determine

the coefficients in this equation.

Some remarks on stress partition were made by Ladanyi (1985). In fact, if only mechanical effects are considered, the variation of pore matrix pressure Δu caused by an increase Δp in the overall total external pressure, can be calculated by a formula developed by Bishop (1973)

$$\frac{\Delta u}{\Delta p} = [1 + n\frac{C_m/C_s - 1}{C/C_s - 1}]^{-1} \tag{1.15}$$

where n is the soil porosity, and C_m, C_s, C are the compressibilities of the pore matrix, the soil grains and the soil skeleton. When this formula is applied to an ice-saturated sand, it is found that nearly all (99.8%) of Δp is transferred to the pore ice. However, in a 3-phase material, such as a frozen soil containing a considerable fraction of unfrozen water, the compressibility C of ice-cemented soil skeleton is greatly reduced, leading to the result that under a sudden increase of external pressure, the ice may take a much larger share of the pressure than unfrozen water.

As for the partition of stresses in a frozen soil under a deviatoric stress increment, it was found (Ladanyi, 1981) that the classical Terzaghi's law of effective stress should be extended to include the effect of shear stresses in the pore ice.

1.1.6 Frost Heaving Criteria

One important problem in which there is still some disagreement, is how to define the criterion for the start of frost heaving. Several criteria have been used up to now in published models for simulating frost heaving. Most of these criteria are simple and may be expressed by the following statement: "whenever the ice content exceeds a critical value, heaving will occur and the soil matrix will expand to make room for the excess ice". Sheppard et al. (1978) used a critical ice content equal to the porosity of the soil minus the unfrozen water. Taylor and Luthin (1978) used a critical ice content equal to 85% porosity, regardless of unfrozen water content. O'Neill and Miller (1985) used a simple criterion of neutral stress, in which heave occurs when the neutral stress exceeds the overburden pressure. However, all of these criteria for frost heaving have yet to be verified by experiments and observations. Fortunately numerically, one finds that the various criteria on the critical ice content for frost heave do not make much difference in the results of frost heave calculations.

1.1.7 External Load and Shut-off Pressure

Reductions in heaving following increases in the surcharge, have been widely reported in the literature. This phenomenon has been suggested as one of

possible ways for controlling frost action in frost susceptible soils. Some researchers (McRoberts and Nixon, 1975; Hill and Morgenstern, 1977) suggested that there is a shut-off pressure for each soil at which the effective stress at the frost front will cause no flow of water to the freezing front. When the shut-off pressure is exceeded, water is then expelled in advance of the freezing front. The shut-off pressure depends on the soil type, stress distribution and the freezing conditions.

However, Penner and Ueda (1977) expressed the opinion that no shut-off pressure should exist for soils provided that freezing is continued for a sufficiently long period. Although water may be expelled from the sample initially, the water flow must reverse from expulsion to intake, provided the experiment is not terminated too early. According to their experimental results, the cold-side temperature imposed on the sample has a significant influence on the constant heave rate observed at low pressure. At high loading, the heave rates are low and the confining pressure has an overriding influence on heave rate.

Loch and Kay (1978) reported that the expulsion of the pore water appears at an early stage in the experiment. In their experiments, the greatest expulsion occurred from the samples in which the freezing front was advancing most rapidly. This stage of expulsion which takes various lengths of time, depending on the overburden load, preceded the stage of water intake for segregation to

ice lenses. In all experiments, when the overburden pressure is increased, the heave rate is found to decrease.

Konrad and Morgenstern (1982) have attempted to estimate the true upper-bound shut-off pressure by putting $P_l = 0$ in the Clapeyron equation, which gives in the P *vs* T plot (Fig.1.7) a straight-line through the origin with the slope given by eq.(1.5), and by looking for the intersection of that line with an experimental line relating the values of the segregation temperature T_{so} with the applied pressure. As at this specific point there is zero suction at the bottom of the final ice lens, the lens will stop growing because no water flow will occur . The shut-off pressure found in this manner for Devon silt was in the range of 1.0 to $1.2 MPa$, which is still one order of magnitude lower than the ice melting pressure which for $-1°C$ would, according to eq.(1.4), be equal to about $13.5\, MPa$. In other words, one can stop heaving process by applying a pressure of about $1\, MPa$, but to reverse it mechanically, about 10 times higher pressures are necessary.

1.1.8 Effect of Freeze-Thaw Cycling

Freezing and thawing cause significant structural changes in consolidated clay slurries which cause large increases in vertical permeability. Chamberlain

and Blouin (1978) have found that when fine grained materials with high liquid limits were subjected to freeze-thaw cycling, their volume was reduced up to 20% and their vertical permeability increased up to two orders of magnitude. The increase was greatest for the soil with the largest plasticity index and, in general, the increase was smaller at highest applied stress levels. For soils where clay particles predominate, the increased permeability occurs as a result of the formation of vertical shrinkage cracks. For coarser-grained soils where more angular silts or sand particles control the compressibility, the increased permeability is probably caused by a reduction in the volume of solids in the pore spaces. This potentially beneficial effect is being explored in connection with the stabilization of uranium tailings.

1.2 Literature Review of Mathematical Models of Freezing Process in Soils

1.2.1 Models for Frost Evolution in soils

At the present time, most numerical solutions of the heat transfer problem for frozen soil are based on some form of the equations by Harlan (1973). The heat transfer equation for an isotropic soil in two dimensions is governed by

the following partial differential equation:

$$C(x,y,\tau)\frac{\partial T}{\partial \tau} + L\rho_i\frac{\partial \theta_i}{\partial \tau} = \frac{\partial}{\partial x}\{\lambda(x,y,T)\frac{\partial T}{\partial x}\} + \frac{\partial}{\partial y}\{\lambda(x,y,T)\frac{\partial T}{\partial y}\} - C_l\rho_l\frac{(\partial v_x T)}{\partial x} - C_l\rho_l\frac{(\partial v_y T)}{\partial y} \quad (1.16)$$

where: λ – thermal conductivity, $W/m^{\circ}C$; T – soil temperature, $^{\circ}C$; x, y – position coordinate, m; τ – time, s; ρ_l, ρ_i – densities of liquid water and ice,respectively, kg/m^3; C – volumetric heat capacity of the soil, $J/m^{3\circ}C$; C_l – volumetric heat capacity of water, $J/m^{3\circ}C$; v_x, v_y – fluid flow velocity in the x and y direction, respectively, m/sec; L – latent heat of water, J/kg; θ_i – volumetric ice fraction, m^3/m^3.

Works of Nixon (1975), and Taylor and Luthin (1978) have shown that the convective terms of eq.(1.16) (the third and forth terms on the right-hand side) are negligible, since most of the time the conductive term is 2 to 3 orders of magnitude greater. As a consequence, eq.(1.16) can be rewritten as

$$C\frac{\partial T}{\partial \tau} + L\rho_i\frac{\partial \theta_i}{\partial \tau} = \frac{\partial}{\partial x}(\lambda\frac{\partial T}{\partial x}) + \frac{\partial}{\partial y}(\lambda\frac{\partial T}{\partial y}) \quad (1.17)$$

Based on the different physical assumptions, different approaches have been used for treating the latent heat during phase changing. Transforming eq.(1.17), we get

$$\overline{C}\frac{\partial T}{\partial \tau} = \frac{\partial}{\partial x}(\lambda\frac{\partial T}{\partial x}) + \frac{\partial}{\partial y}(\lambda\frac{\partial T}{\partial y}) \quad (1.18)$$

with

$$\overline{C} = \begin{cases} C^+ & T > T_f \\ C^- + L\rho_i \frac{\partial \theta_i}{\partial T} & T < T_f \end{cases} \tag{1.19}$$

here $\overline{C}$ is an apparent heat capacity, which is highly variable. Bonacina et al. (1973) have suggested that the latent heat effect can be assumed to occur over a temperature range of $T_2 - T_1$ ($T_1 < T_f < T_2$), in which case the apparent heat capacity can be written as

$$\overline{C} = \begin{cases} C^+ & T > T_2 \\ \frac{C^+ + C^-}{2} + \frac{L}{T_2 - T_1} & T_1 < T < T_2 \\ C^- & T < T_1 \end{cases} \tag{1.20}$$

These relationships of apparent heat capacity have the advantage of being defined in terms of the temperature, rather than the position of the phase boundary. Thus, a problem of freezing and thawing in soils involving moving boundaries may be described by a non-linear parabolic equation.

This kind of approach, termed apparent heat capacity method and simulated to enthalpy method, often suffers from the fact that the phase change occurs over a very narrow temperature range $T_2 - T_1$, which also moves about as time proceeds. Researchers of both methods usually try to ease the steepness of the apparent heat capacity $\overline{C}$ curve by using an artificially extended temperature range for the phase change interval (Comini et al., 1974). Numerical results may be sensitive to the selection and implementation of the

$T_2 - T_1$ interval. Oscillatory problems have been reported, and remedial measures proposed (Morgan et al., 1978).

Nixon (1983) and Shen (1988) have calculated the latent heat in freezing and thawing soils by using experimental functions which relate unfrozen water content θ_i to soil temperature T, in order to match as closely as possible the characteristics of the soil. These functions result in latent heat being liberated over a range of subfreeze temperature, rather than only at the freezing point. In Nixon's method (1983), the latent heat of phase change, as prescribed by the nonlinear unfrozen water content function, was handled numerically by the Newton-Raphson iteration method, similar to that described by Ho et al. (1970). Shen (1988) has evaluated the apparent heat capacity and thermal conductivity in the finite element model without iteration from the temperature in the last time step. Obviously, some errors are introduced as compared with a solution produced by a fully iterative procedure, but these errors are of the same nature as truncation errors in any finite difference procedure and hence can be reduced to an acceptable level through the use of small time steps in the quickly varying temperature stages. The advantage of this method is that the amount of calculations in a long-term computation can be reduced to a level reasonable for personal computer processing. Shen (1988) and Shen and Ladanyi (1989) simulated successfully the thawing highway embankment

in permafrost, located in Qinghai-Xizang (Tibet) Plateau, China, using the finite difference method and curvilinear coordinate system which is generated numerically by the coupled Poisson's equations.

For a pure substance such as water and for coarse grained, water saturated soil media, phase change occurs almost as a step at the freezing temperature T_f. Thus, artificial extension of the phase change interval may introduce physically realistic depiction of behavior of the medium. Numerous approaches have been developed using a step change characterization of freeze/thaw by treating this as a moving boundary problem. Therefore, another form of eq.(1.18) (constant C) is solved over each phase zone, featuring continuous coefficients and temperature, with appropriate jump conditions attached to a moving boundary

$$\begin{aligned} C^+\frac{\partial T}{\partial \tau} &= \frac{\partial}{\partial x}(\lambda^+\frac{\partial T}{\partial x}) + \frac{\partial}{\partial y}(\lambda^+\frac{\partial T}{\partial y}) \qquad T > T_f \\ C^-\frac{\partial T}{\partial \tau} &= \frac{\partial}{\partial x}(\lambda^-\frac{\partial T}{\partial x}) + \frac{\partial}{\partial y}(\lambda^-\frac{\partial T}{\partial y}) \qquad T < T_f \\ C^+\frac{\partial T}{\partial n} - C^-\frac{\partial T}{\partial n} &= L \cdot v_s \qquad \textit{on moving boundary} \end{aligned} \tag{1.21}$$

here v_s is the velocity of the interface in normal direction. When one does this on a fixed numerical mesh, the phase boundary moves across it, requiring some kind of special treatment in its vicinity (Goodrich, 1978). Unfortunately, this kind of method is difficult to use in multi-dimensional problems. Lynch and

O'Neill (1981) have developed a finite element method using a moving finite element mesh, in which the mesh motion effect appears as a velocity term in the governing equation. This technique has proved to be highly accurate, but rather complicated. O'Neill (1983) has developed an algorithm for two-dimensional freezing and thawing problem using a fixed mesh finite element scheme. This method is considered to be capable of solving phase change in a substance with discrete phase change temperatures, such as pure water or coarse grained water saturated media.

1.2.2 Models for Frost Heaving in Soils

Soil expansion during freezing is caused by soil water freezing and moisture migration from unfrozen to frozen soil. This process results in frost heaving, and it may cause damage to structures built in the permafrost or seasonally frozen ground. The understanding and simulating of soil freezing process has been a long-term goal of much research in cold regions engineering.

Since the 1970's, several theories based on different points of view have been proposed for describing the mechanism of frost heave and ice segregation in freezing soils. Many mathematical models have been set up on the basis of various theories and assumptions for the mechanism of soil freezing and

thawing processes. With the advent and widespread use of computers, the mathematical models have become quite complicated in some respects, and have required a very considerable amount of calculation. However, because of lack of a common understanding of the basic physical phenomena, the process of ice segregation in these models or theories was not always clear. On the whole, any further development of mathematical models had to be based on an increasing understanding of the physics of observed phenomena and their possible quantification.

Mathematical modelling of frost heaving in freezing soil has been the subject of many studies since the 1970's. The first efforts at modelling coupled heat and moisture transport in freezing soil were by Harlan (1973) and Guymon and Luthin (1974). Most of the mathematical models have included simultaneous heat and moisture transfer in a one-dimensional column.

Harlan (1973) and Guymon and Luthin (1974) have developed models of one-dimensional heat and moisture transfer in a partially frozen soil. Harlan calculated the liquid water pressure from the equation based on the Gibbs free energy. Sheppard et al. (1978) used the Clapeyron equation to determine the water pressure, with the assumption that the soil is under zero loading and ice

at atmospheric pressure:

$$P_l = L\rho_l \ln \frac{T_k}{T_0} \tag{1.22}$$

where:P_l – liquid water pressure (Pa); ρ_l – density of liquid water (kg/m^3); L – latent heat of fusion (J/kg); T_k – the absolute temperature of soil ($°K$); T_0 – freezing point of pure water at atmospheric pressure ($°K$).

Taylor and Luthin (1978), and Jame and Norum (1980) solved the coupled heat and moisture equations and avoided calculating the liquid water pressure by using experimental unfrozen water content data. In their models, the moisture transfer is driven by a gradient in frozen water content under unsaturated conditions. This is expressed in the same way in both frozen and unfrozen soils. Ice pressure and Clapeyron equation were not used in their model. Because of a lack of knowledge of the relationship between soil water diffusivity in frozen and unfrozen soil, respectively, an impedance factor, assumed to be a function of total water content, was introduced to reduce the diffusivity value for the soil in the frozen state.

Guymon et al. (1980) proposed a one-dimensional frost heave model for unidirectional freezing in a moist silt with water table. They assumed that a portion of water in freezing soil would not freeze, and all water in addition to this amount that freezes in excess of the soil porosity would result in heaving.

In 1984, they developed a two-dimensional model of coupled heat and moisture flow in frost susceptible soil based on published equations of simultaneous heat and moisture transfer. Several numerical examples such as highway embankment freezing and frost heaving have been carried out by the Galerkin finite element methods. Up to now, most of the available mathematical models are valid only for one-dimensional problems.

Guymon et al. (1981) pointed out that there is considerable measurement error in many of the physical parameters that are incorporated in mathematical models of frost heaving and concluded that it would probably never be possible to calculate precisely the amount of frost heaving from a predictive point of view. They suggested that probabilistic concepts should be coupled with deterministic approaches. Chamberlain (1980) studied in the field the frost heaving for a small section of a roadway in Hanover, NH, with sandy silts as the base material. The measured variations of frost heaving at 455 discrete points were fitted to a β-probability distribution, suggesting that frost heave can be evaluated as a probabilistic process.

Hopke (1980) developed a model of frost heaving that included applied load, based on the Clapeyron equation and capillary concepts. In his model, the ice pressure is assumed to be zero at freezing front, and to be equal to the local mean pressure at the coldest side of the freezing fringe. The simulated

results using estimated soil parameters were compared with experimental data published by Penner and Ueda (1977), but the model predicted too much heave at low overburden pressure and high temperature gradients. The simulated heaving rate is oscillatory, because there is a discontinuity in ice pressure at each new lens location. Hopke speculated that other mechanisms not included in the model have to limit frost heave under these circumstances.

Gilpin (1980) and O'Neill and Miller (1985) proposed respectively two models of frost heaving being able to predict ice lensing. The pressure relationships used in the Gilpin's model are equivalent to a special case of the Clapeyron equation. Assumed are also quasi-steady temperature profiles and constant thermal properties for each zone. Gilpin provided an expression for "separation pressure" by virtue of which the soil particles are forced apart when heave occurs. This model predicts ice lensing and heaving rates as a function of soil properties (e.g. thermal conductivities and particle size) and externally applied boundary conditions (temperature boundary conditions and applied loading). The simulated results are qualitatively in agreement with experimentally observed phenomenon, e.g. initiation of lenses and overburden effect, as well as with early time water expulsion and its reversal. O'Neill and Miller (1985) proposed a numerical model for simulating frost heave in saturated, granular, solute-free soil. The Clapeyron and capillary equations were used to relate

temperature, pressures and phase composition. In this model, a stress partition factor was used to apportion participation of pore pressure. Whenever the neutral stress builds up to overcome the overburden, a new lens is initiated. This model predicts the rhythmic formation of lenses in a recognized pattern which are more closely spaced during later slower freezing.

The models proposed by Gilpin (1980) and O'Neill and Miller (1985) are difficult to apply to multidimensional problems. Up to now, the majority of models of frost heaving do not consider the discrete ice lensing, because of a lack of understanding of the mechanism of ice lens initiation. Booth (1981) demonstrated experimentally that the occurrence of visible ice lenses in a frozen soil represents a change only in the scale of segregation, and as such does not affect the rates of heaving or water intake of soil as it freezes. Therefore, in applications of mathematical models of frost heaving to practical problems an exact prediction of ice lensing is in fact not required.

1.3 Scope and Organization of This Thesis

Up to now, most of the investigations on modelling and numerical simulation of frost heaving in soil have been only based on the coupled heat and moisture transport in freezing soils. However, these models do not consider

the effects of external loading. Although many mathematical models of frost heaving have included the effect of external loading, the external loading is only considered as a factor influencing frost heaving. However, these models are difficult to be extended to 2-D cases. To our knowledge, Blanchard and Frémond (1985) were the first ones to propose a model for coupled heat, moisture and stress fields. Their model considers the existence of liquid water in the frozen zone and the deformability of the soil which is assumed to be elastic for unfrozen soil and Norton-Hoff viscoplastic for frozen soil. They have simulated the frost heaving and thaw settlement around a chilled and heated pipeline, using this model. Unfortunately up to now, only the isotherms, heaving and hydraulic head after 48 hours have been published, without any information on the associated stress field.

The objective of this thesis is to propose a model for coupled heat, moisture and stress field in freezing soil. The goal of this research was to develop a model which can predict the stresses and deformations due to the heat and moisture transfer in a freezing soil, applicable to engineering design, and to keep calculation costs at a minimum. The model has a wide field of potential applications to all problems involving frost heaving and frost pressures against structures. However, at present, the main interest in such models is in the area of natural gas transport through partially chilled pipelines traversing discontinuous

permafrost regions. For this reason, the validity of the proposed model was tested against the measurements made on a large scale buried chilled pipeline test that have been going on since 1982 in Caen, France.

The thesis is organized as follows:

- Chapter 2 describes the basic assumptions and equations of the proposed model used for coupling heat, moisture and stress fields.
- Chapter 3 presents a numerical simulation by the proposed model of a uni-directional freezing test published by Penner (1986). The results of the simulation for temperature and heave are shown to agree well with the experimental measurements, giving an experimental validation of the proposed model.
- In Chapter 4, the first freezing cycle of the Canada-France Chilled Pipeline Ground Freezing Test is simulated by using this model. Because of the lack of exact information on the confining conditions of the pipe in the longitudinal sense, three possible pipe confinement conditions are considered in this simulation. In addition, the sensitivity of prediction results has been tested by varying the soil hydraulic conductivity and the temperature boundary conditions.
- In the final Chapter 5, conclusions are summarized and implications, as

well as recommendations for further research are discussed.

1.4 Summary

The propose of this chapter was to provide a brief review of the most important developments that occurred during the last two decades in research on the mechanics and modelling of frost heaving in soils. Up to now, most models of frost heaving have been based on the coupled heat and moisture transport in freezing soils. Only a few models considered external loading as a factor influencing frost heave, while the stress field in the soil due to loading, volumetric expansion and creep was neither considered nor calculated in these models.

Chapter 2

PROPOSED MATHEMATICAL MODEL

From the practical viewpoint, the prediction of stress and deformation fields during frost heaving is considered to be of a great importance for the prediction of stability of structures in cold regions. A complete analysis of this problem must be able to deal with the coupling of heat, moisture and stress fields. Although many mathematical models of frost heaving have included the effect of external loading, the applied load was considered only as a factor influencing the frost heave, while the stress field in the soil due to loading, volumetric expansion and creep was not taken into account and calculated in these models. Blanchard and Frémond (1985) were the first ones to propose a model for coupling the heat, moisture and stress fields on the basis of the principle of conservation of energy, mass and momentum. They have up to now applied this model for simulating heat and moisture transfer around a chilled pipeline, but no information on the stress field has yet been published. This thesis presents another different model for coupling together the heat, moisture and stress effects. The main difference between the two models is that in the thesis:

(1) the Clapeyron equation is used to determine the liquid water pressure and to describe the effect of stress field on the heat and moisture transfer; (2) creep strains in the frozen portion are considered and the associated flow rule is used to determine them; (3) the incremental initial strains approach is used to define the stress distribution produced by the volumetric strains of freezing soil caused by the phase change of water and moisture transfer. The results of simulation of both temperature field and amount of heave, published by Shen and Ladanyi (1987, 1988), were found to be in a good agreement with experimental results published by Penner (1986). In addition, the simulation furnished also the complete stress field during freezing, and made it possible to take into account the effect of external loading. This study was the first one able to simulate the stress variation in a freezing soil. On the other hand, experimental information on this stress variation is lacking. This is due to the fact that, because of a lack of appropriate instruments and methods, it has been found difficult up to now to accurately measure stress field in frozen soil. To our knowledge, Williams and Wood (1984, 1985) were the first ones to measure the internal pressure variation in a freezing soil, using small pressure transducers. The transducers press against small copper tubes which extend 1.1 cm into the soil over which small oblong rubber membranes are fitted. The membranes are filled with silicon oil the freezing temperature of which is $-50°C$. Smith and Onysko (1990) used a similar method to observe the internal pressure around a chilled

pipeline in the Caen experiment. In that case, pressure transducers of the same design were installed in a vertical profile beneath the pipe, at 80, 100, 120 and 140 cm depth below the surface. Their measurements are interesting and are interpreted in a thermodynamic-rheological context. However, these measured pressures are average pressures in the soil, or rather, average pressures acting on small deformable tubes buried in the freezing soil. In particular, when the elastic modulus of the sensor is different from that of enclosing medium, the sensor will change the local stress field. Thus, the measurements cannot be directly compared with our simulated stress variation in the freezing soil. Therefore, the ability to calculate stress and deformation fields in freezing soil on the basis of the temperature, moisture and external loading appears to be an important step towards a more accurate prediction of the stability of structures in frozen soils.

This thesis presents an extended version of this model and its application to the solution of some practical problems of ground-structure interaction.

2.1 Basic Assumptions

During freezing, the transfer of heat, moisture and the variation of stresses in the soil are all interrelated, so the analysis must deal with the coupling of all

these effects. The mathematical model requires three systems of equations for expressing the interrelationship among the laws of heat and moisture transfer and a varying stress field.

The basic assumptions made in the model are as follows:

- Moisture transport in frozen and unfrozen zones occurs only by the liquid water form. The air phase and vapor transfer have negligible effects in net water transfer.
- Effect of salt exclusion is negligible.
- The soil is consolidated under external pressure before freezing, and the effect of consolidation in the unfrozen zone is negligible during the freezing process.
- The volume of soil particles remains constant in the freezing process.
- Both unfrozen and frozen soil are isotropic bodies.
- The freezing point depression of water in the soil under loading is negligible.
- The sign rule in this thesis is that all tensile stresses and strains are positive.

2.2 Basic Equations for Heat and Moisture Transfer

On the basis of the above assumptions, the generalized moisture transport equation for steady or unsteady flow in a saturated or partially saturated soil during freezing can be written as (Sheppard et al., 1978)

$$\frac{\partial \theta_l}{\partial \tau} + \frac{\rho_i}{\rho_l}\frac{\partial \theta_i}{\partial \tau} = \frac{1}{\rho_l g}[\frac{\partial}{\partial x}(k\frac{\partial \Phi}{\partial x}) + \frac{\partial}{\partial y}(k\frac{\partial \Phi}{\partial y})] \tag{2.1}$$

and

$$\Phi = P_l + G \tag{2.2}$$

where: ρ_l, ρ_i – density of liquid water and ice (kg/m^3), respectively; θ_l, θ_i – volumetric fraction of liquid water and ice (m^3/m^3), respectively; k – hydraulic conductivity (m/s); x, y – coordinates (m); τ – time (sec); Φ – soil water potential (Pa); P_l – pressure of liquid water (Pa); g – gravitational acceleration (m/sec^2); G – gravitational potential (Pa). The volumetric fraction of ice or liquid water is related to the gravimetric ice or liquid water content by

$$\theta = \frac{\rho_d}{\rho_l} w \tag{2.3}$$

where w is ice or liquid water content by mass (kg/kg).

In most cases, the effect of the gravitational component on water flow in

the frozen zone is negligible, so that eq.(2.1) can be rewritten as

$$\frac{\partial \theta_l}{\partial \tau} + \frac{\rho_i}{\rho_l}\frac{\partial \theta_i}{\partial \tau} = \frac{1}{\rho_l g}\{\frac{\partial}{\partial x}(k\frac{\partial P_l}{\partial x}) + \frac{\partial}{\partial y}(k\frac{\partial P_l}{\partial y})\} \tag{2.4}$$

The heat transport equation may be written as

$$C\frac{\partial T}{\partial \tau} = \frac{\partial}{\partial x}(\lambda\frac{\partial T}{\partial x}) + \frac{\partial}{\partial y}(\lambda\frac{\partial T}{\partial y}) + L\rho_i\frac{\partial \theta_i}{\partial \tau} \tag{2.5}$$

where: C – volumetric heat capacity of soil ($Jm^{-3}{}^{\circ}C^{-1}$); λ – thermal conductivity of soil ($Wm^{-1}{}^{\circ}C^{-1}$); T – temperature ($^{\circ}C$); L – latent heat of fusion ($3.336 \times 10^5\ J/kg$).

In eq.(2.5), the component for thermal vapor transport is neglected, because the heat flow from this source is much smaller than that from thermal conduction (Nixon, 1975; Taylor and Luthin, 1978).

In order to be able to predict the effect of the stress in soil on the ice pressure, the Clapeyron equation including the ice pressure term (Kay and Groenevelt, 1974) is adopted

$$\frac{P_l}{\rho_l} - \frac{P_i}{\rho_i} = L \cdot \ln\frac{T_k}{T_0} \tag{2.6}$$

here: T_k – the absolute temperature ($^{\circ}K$); T_0 – the freezing point of pure water at atmospheric pressure ($273.15^{\circ}K$); P_i – the pressure of ice (Pa). Because the role of ice pressure is poorly understood, it is difficult to use directly the

Clapeyron equation for predicting liquid water pressure. To be able to use the Clapeyron equation, some simplified assumptions about ice pressure are proposed (shown in Fig. 2.1). We assumed that the ice pressure P_i at the freezing front is zero, and that at the coldest end of the freezing fringe it is equal to the local mean pressure. This assumption is the same as in the Hopke's model (1980), and it is close to the profiles of liquid water and ice pressure in saturated soil suggested by Miller (1972). The frost heaving is assumed to start when the ice content exceeds its critical value equal to 85% of soil porosity, regardless of the unfrozen water content (Taylor and Luthin, 1978).

Once the ice pressure is defined according to the above assumption, the liquid water pressure P_l can be determined from the Clapeyron equation (2.6)

$$P_l = \frac{\rho_l}{\rho_i} P_i + L\rho_l \ln \frac{T_k}{T_0} \tag{2.7}$$

Substituting eq.(2.7) and eq.(2.4) into eq.(2.5), and rearranging gives:

$$\overline{C}\frac{\partial T}{\partial \tau} = \frac{\partial}{\partial x}(\overline{\lambda}\frac{\partial T}{\partial x}) + \frac{\partial}{\partial y}(\overline{\lambda}\frac{\partial T}{\partial y}) + \frac{\rho_l L}{\rho_i g}[\frac{\partial}{\partial x}(k\frac{\partial P_i}{\partial x}) + \frac{\partial}{\partial y}(k\frac{\partial P_i}{\partial y})] \tag{2.8}$$

with

$$\overline{C} = C + \rho_l L \frac{\partial \theta_l}{\partial T} \tag{2.9}$$

$$\overline{\lambda} = \lambda + \frac{k\rho_l L^2}{T_k g} \tag{2.10}$$

In fact, the effect of stress in soils on the heat transfer is very small and may be neglected. The third term on the right side of eq.(2.8) is neglected in this analysis, and it can be rewritten as

$$\overline{C}\frac{\partial T}{\partial \tau} = \frac{\partial}{\partial x}(\overline{\lambda}\frac{\partial T}{\partial x}) + \frac{\partial}{\partial y}(\overline{\lambda}\frac{\partial T}{\partial y}) \tag{2.11}$$

The basic equations about heat and moisture transfer in the proposed model are eq.(2.11), eq.(2.4) and eq.(2.7). In these equations, the relationship between the liquid water content in freezing soil and the temperature, $\theta_l = f(T)$, must be determined experimentally.

2.3 Basic Equations for Calculating Stresses and Deformations

In a freezing process, the volume change of freezing soil is caused by the fact that water in soil is partly changed into ice and the moisture content varies by moisture transport. If the volume of soil particles is assumed to remain constant in the freezing and thawing process, the volumetric expansion strain ϵ^v can be given as

$$\begin{aligned} \epsilon^v &= 0.09 \cdot \theta_i + \Delta\theta \\ &= (\frac{\rho_w}{\rho_i} - 1)(\theta_0 + \Delta\theta - \theta_l) + \Delta\theta \end{aligned} \tag{2.12}$$

where: θ_0 – initial water content (m^3/m^3); $\Delta\theta$ – increment of water content by moisture migration (m^3/m^3).

Because both frozen and unfrozen soil are assumed to be isotropic, the normal expansion strains are equal in each direction, while the shear strains due to the expansion are zero. They are given by

$$\epsilon_x^v = \epsilon_y^v = \epsilon_z^v = \frac{1}{3}\epsilon^v \tag{2.13}$$

$$\gamma_{xy}^v = \gamma_{yz}^v = \gamma_{zx}^v = 0 \tag{2.14}$$

where: ϵ_x^v, ϵ_y^v, ϵ_z^v – normal strain components due to soil expansion; γ_{xy}^v, γ_{yz}^v, γ_{zx}^v – shear strain components due to soil expansion.

In numerical analysis, the creep deformations are usually determined by a step-by-step procedure in the time domain. The creep strain increment $d\{\epsilon^c\}$ in each time step is computed as

$$d\{\epsilon^c\} = \{\dot{\epsilon}^c\} \cdot \Delta\tau \tag{2.15}$$

in which $\Delta\tau$ is the size of the time step and $\{\dot{\epsilon}^c\}$ is the creep strain rate vector in the time step.

In the uniaxial stress state, the creep strain in frozen soil can be described by a power form equation as (Ladanyi, 1975)

$$\epsilon^c = [\frac{\sigma}{\sigma_{ct}}]^n [\frac{\dot{\epsilon}_c \tau}{b}]^b \tag{2.16}$$

and the reference stress σ_{ct} is given by

$$\sigma_{ct} = \sigma_{c0}[1 + \frac{T}{T_c}]^{\omega} \tag{2.17}$$

where: σ, ϵ^c – stress and creep strain in uniaxial stress state; σ_{c0}, n, b, ω – experimental coefficients; $\dot{\epsilon}_c$, T_c – reference values of strain rate and temperature.

For a homogeneous isotropic viscoplastic material, the relationship between creep strain rates and stresses can be expressed by the associated flow rule (Zienkiewicz and Cormeau, 1974; Soo et al., 1985)

$$\{\dot{\epsilon}^c\} = \gamma \cdot [\frac{F}{F_0}]^m \cdot \frac{\partial F}{\partial \{\sigma\}} \tag{2.18}$$

where: F, F_0 – current yield function and reference yield function; γ – fluidity coefficient depending on material properties and time.

If the ***von Mises*** yield function is used, because this yield function can be expressed by the equivalent stress, the eq.(2.18) can be written as

$$\{\dot{\epsilon}^c\} = \gamma \cdot [\frac{\overline{\sigma}}{\overline{\sigma}_0}]^m \cdot \frac{\partial \overline{\sigma}}{\partial \{\sigma\}} \tag{2.19}$$

where $\overline{\sigma}$ is the equivalent stress and $\overline{\sigma}_0$ is the equivalent stress for the reference yield function.

In the stress state, $\overline{\sigma}$ reduces to σ as in eq.(2.16), and the last term at the right hand side of eq.(2.19) reduces to 1. Taking the time derivative of equation (2.16), gives

$$\dot{\epsilon}^c = b \cdot [\frac{\sigma}{\sigma_{ct}}]^n \cdot [\frac{\dot{\epsilon}_c}{b}]^b \cdot \tau^{b-1} \tag{2.20}$$

which compared with eq.(2.19) gives

$$\gamma = [\frac{\dot{\epsilon}_c}{b}]^b \cdot b \cdot \tau^{b-1} \tag{2.21}$$

$$\overline{\sigma}_0 = \sigma_{ct} \tag{2.22}$$

$$m = n \tag{2.23}$$

In eq.(2.20), the creep parameters in the uniaxial stress state may be generalized for corresponding parameters in multiaxial states. Using eq.(2.15), eq.(2.16) and eqs.(2.22) to (2.23), the vector of creep strain increment in each time step can be written as

$$d\{\epsilon^c\} = b \cdot [\frac{\overline{\sigma}}{\overline{\sigma}_0}]^n \cdot [\frac{\dot{\epsilon}_c}{b}]^b \cdot \tau^{b-1} \cdot \frac{\partial \overline{\sigma}}{\partial \{\sigma\}} \cdot \Delta\tau \tag{2.24}$$

The total strain increment $d\{\epsilon\}$ in frozen soil consists of the increments of elastic strain $d\{\epsilon^e\}$, creep strain $d\{\epsilon^c\}$ and volumetric expansion strain $d\{\epsilon^v\}$

$$d\{\epsilon\} = d\{\epsilon^e\} + d\{\epsilon^c\} + d\{\epsilon^v\} \tag{2.25}$$

The stress-strain relationship for frozen soil in multiaxial stress state can be expressed by

$$\{\epsilon^e\} = [D]^{-1} \cdot \{\sigma\} \tag{2.26}$$

where $\{\epsilon^e\}$ is the elastic strain vector, and $[D]$ is the elasticity matrix. Because the Young's modulus and Poisson's ratio of frozen soil are related to the temperature of the soil, taking the differential of eq.(2.26) gives

$$d\{\epsilon^e\} = \frac{d[D]^{-1}}{dT} \cdot \{\sigma\} \cdot dT + [D]^{-1} \cdot d\{\sigma\} \tag{2.27}$$

Substituting eq.(2.27) into eq.(2.25), and rearranging gives

$$d\{\sigma\} = [D](d\{\epsilon\} - d\{\epsilon^c\} - d\{\epsilon^v\} - \frac{d[D]^{-1}}{dT} \cdot \{\sigma\} \cdot \Delta T) \tag{2.28}$$

From the finite element method, the strain increment vector $d\{\epsilon\}$ can be related to the nodal displacement vector $d\{\delta\}$ as

$$d\{\epsilon\} = [B] \cdot d\{\delta\} \tag{2.29}$$

where $[B]$ is the transformation matrix between strains and nodal displacements. Applying the theorem of minimum potential energy, a system of equations for the elements can be formed as

$$[K] \cdot d\{\delta\} = d\{P\} + d\{R\} \tag{2.30}$$

with

$$[K] = \int_v [B]^{-1} \cdot [D] \cdot [B] \cdot dv \tag{2.31}$$

$$d\{R\} = \int_v [B]^{-1} \cdot [D] \cdot (d\{\epsilon^v\} + d\{\epsilon^c\} + \frac{d[D]^{-1}}{dT} \cdot \{\sigma\} \cdot \Delta T) \cdot dv \tag{2.32}$$

where: $[K]$ – the stiffness matrix; $d\{P\}$ – nodal loading increment vector; $d\{R\}$ – "pseudoforce" increment vector due to the creep, the volumetric expansion and the temperature variation.

On the basis of the above system of equations, the stress and deformation increments at each time step can be calculated by the finite element method.

2.4 Summary

In this chapter, a conceptual model for calculating heaving and stresses in a freezing soil, on the basis of coupled heat, moisture and stress field, is presented. This model takes into account the non-homogeneity of the frozen zone due to temperature variation, as well as the effects of frozen soil creep on stress distribution. In this model, the Clapeyron equation is used to determine the liquid water pressure and to describe the effect of stress field on the heat and moisture transfer within the freezing fringe, while the associated flow rule is used to define creep strains in frozen soil.

Chapter 3

SIMULATION OF A UNIDIRECTIONAL SOIL FREEZING TEST

3.1 Description of Test

Using the proposed model, a numerical simulation for the frost heaving experiment published by Penner (1986) was carried out. Penner measured the frost heaving, ice lens growth and frost penetration during open system freezing of a saturated soil under 50 kPa overburden pressure. His experimental data provide a good opportunity for checking the validity of the proposed model.

In Penner's test, the test samples were cylinders 10 cm long and 10 cm in diameter. The frost cell is shown in Fig.3.1. Soil samples for the frost cell were prepared from sieved, air-dry soils by adding sufficient water to bring the moisture content to just above the predetermined liquid limit. The wet soil was then stored in a container for several days to equilibrate. It was placed in layers in the cell and consolidated in steps, to a final pressure of $500kPa$. The pressure was then reduced to $50kPa$ and the sample was allowed to expand

to its equilibrium volume before the freezing run was initiated. The moisture content of samples after consolidation was about 20% by weight.

Experiments with the frost cell were carried out inside a constant temperature chamber which was held close to the mean temperature of the samples. Freezing of the sample was from the bottom upwards, and resistance to movement of the unfrozen portion was reduce by the use of a lubricated teflon film inside the cell. The external water supply was held level with the porous plate at the top of the cell. The temperature baths that supply liquid coolant to heat exchangers at the ends of the sample were located outside the constant-temperature chamber. A dedicated multi-tasking HP minicomputer was used to control the temperature of the liquid coolant, and to measure sample temperatures, water intake and heave. The used method of control was capable of maintaining the sample end temperatures to within $\pm 0.004°C$, and also changing the end temperature of sample according to a pre-selected rate in the ramped temperature mode. The temperature boundary conditions are shown in Fig.3.2.

Because the freezing and the external water supply were both unidirectional, and the test samples were cylinders, the heat and moisture transfer

eq.(2.11) and eq.(2.4) may be simplified as follows:

$$\overline{C}\frac{\partial T}{\partial \tau} = \frac{\partial}{\partial z}(\overline{\lambda}\frac{\partial T}{\partial z}) \tag{3.1}$$

$$\frac{\partial \theta_l}{\partial \tau} + \frac{\rho_i}{\rho_l}\frac{\partial \theta_i}{\partial \tau} = \frac{1}{\rho_l g}[\frac{\partial}{\partial z}(k\frac{\partial P_l}{\partial z})] \tag{3.2}$$

and

$$\frac{\partial T}{\partial r} = \frac{\partial \theta_l}{\partial r} = \frac{\partial \theta_i}{\partial r} = 0 \tag{3.3}$$

where r and z are the coordinates in the cylindrical coordinate system. Therefore, the heat and moisture transfer are one-dimensional problems, but the mechanical equations are axially symmetrical.

3.2 Soil Properties

The soil heat capacity and thermal conductivity are calculated according to the following relationships (Kay et al., 1977)

$$C = C_s\theta_s + C_l\theta_l + C_i\theta_i + C_a\theta_a \tag{3.4}$$

$$\lambda = \lambda_s^{\theta_s} \cdot \lambda_l^{\theta_l} \cdot \lambda_i^{\theta_i} \cdot \lambda_a^{\theta_a} \tag{3.5}$$

where C_s, C_l, C_i, C_a are heat capacities of soil grains, water, ice and air, respectively; while λ_s, λ_l, λ_i and λ_a are their conductivities. θ_s, θ_l, θ_i and θ_a are volumetric fractions of each phase in the soil, respectively.

Table 3.1: Thermal constants used in calculation

	soil grains	water	ice
C $(MJ/m^3{}^\circ C)$	2.2	4.18	1.93
λ $(W/m^3{}^\circ C)$	1.95	0.602	2.22

As the soil is saturated, the volumetric air fraction in the soil is zero. The constants used in this simulation and given in Table 3.1, have been selected according to Harlan and Nixon (1978).

The unfrozen water content is calculated from the temperature in the frozen soil by the one-point method (Xu Xiaozu et al., 1985):

$$\theta_u = \theta_0 |T|^n \tag{3.6}$$

with

$$n = \frac{\ln \frac{\theta_u|_{T=-1^\circ C}}{\theta_0}}{\ln \frac{T_f}{T_r}} \tag{3.7}$$

where: θ_u – the unfrozen water content; θ_0 – the initial water content; $\theta_u|_{T=-1^\circ C}$ – the unfrozen water content at $-1^\circ C$; T_f – the freezing temperature of soil (°); T_r – the reference temperature $(-1^\circ C)$. The error of predicting the unfrozen water content by this method is *1-3%* on average.

Because no information about the effect of stress on the hydraulic conductivity is presently available, the hydraulic conductivity of frozen soil in this simulation is considered to be only a function of temperature. The relationship

Table 3.2: Coefficients in creep equation

state	b	n	ω	$\sigma_{ct}(MPa)$	T_r	$\dot{\epsilon}_c$
Compression	0.45	2.50	0.97	0.18	-1.0	10^{-5}
tension	0.44	2.33	1.0	1.83	-1.0	10^{-5}

between the hydraulic conductivity and temperature was deduced from the experimental data published by Horiguchi and Miller (1983), using a regression analysis:

$$k = \begin{cases} 3.072 \times 10^{-11} e^{13.438T} & -0.3°C < T < T_f \\ \\ 5.453 \times 10^{-13} & T < -0.3°C \end{cases} \quad (m/s) \tag{3.8}$$

The creep equation of frozen soil is defined from compression and tension tests under uniaxial state of stress. The corresponding experimental parameters in the creep eq.(2.16) and eq.(2.17) shown in Table 3.2 originate from Vyalov (1962) and Eckardt (1982).

The Young's modulus of unfrozen soil is considered to be constant and equal to $11.2MPa$ (Lambe and Whitman, 1969). The stress-strain curve and the relationship between the initial tangent modulus of frozen soil E_0 and the temperature is defined by using the results published by Zhu Yuanlin and Carbee (1984), and the E_0 is represented as follows

$$E_0 = 4 \times 10^2 (\frac{T}{T_r})^{0.636} \quad (MPa) \tag{3.9}$$

where T_r – the reference temperature ($-1°C$). The Poisson's ratio of both unfrozen and frozen soils used in the calculation is assumed to be 0.3.

3.3 Numerical Analysis Scheme

For reducing the amount of calculation, the heat and moisture transport eq.(3.2) and eq.(3.2) were solved by the finite difference method, but the mechanical equations were still calculated by the finite element method. Because of a difference in dimensions of both systems of equations, the grid systems for calculating heat, moisture transfer and stress field are different. The two grid system with the vertical coordinate of each grid point made to coincide (shown in Fig.3.3), were set up for calculating by both the finite difference method and the finite element method. The three nodes linear elements were used in the calculation of stress and deformation by the finite element method.

For an interior difference node (j,n), where j is the spatial node (vertical) and n is the time increment, the heat transfer equation (3.2) can be approximated by the predictor-corrector implicit scheme:

Predictor:

$$-a\cdot\ \overline{\lambda}_n^{j-\frac{1}{2}}\cdot T_{n+\frac{1}{2}}^{j-1}+[\overline{C}_n^j+a\cdot\overline{\lambda}_n^{j-\frac{1}{2}}+b\cdot\overline{\lambda}_n^{j+\frac{1}{2}}]\cdot T_{n+\frac{1}{2}}^{j}-b\cdot\overline{\lambda}_n^{j+\frac{1}{2}}\cdot T_{n+\frac{1}{2}}^{j+1}$$
$$=\overline{C}_n^j\cdot T_n^j \qquad (3.10)$$

Corrector:

$$\begin{aligned} -a\cdot\overline{\lambda}^{j-\frac{1}{2}}_{n+\frac{1}{2}}\cdot T^{j-1}_{n+1}+[\overline{C}^{j}_{n+\frac{1}{2}}+a\cdot\overline{\lambda}^{j-\frac{1}{2}}_{n+\frac{1}{2}}+b\cdot\overline{\lambda}^{j+\frac{1}{2}}_{n+\frac{1}{2}}]\cdot T^{j}_{n+1} \\ -b\cdot\overline{\lambda}^{j+\frac{1}{2}}_{n+\frac{1}{2}}\cdot T^{j+1}_{n+1}=\overline{C}^{j}_{n+\frac{1}{2}}\cdot T^{j}_{n}+a\cdot\overline{\lambda}^{j-\frac{1}{2}}_{n+\frac{1}{2}}\cdot T^{j-1}_{n} \\ -[a\cdot\overline{\lambda}^{j-\frac{1}{2}}_{n+\frac{1}{2}}+b\cdot\overline{\lambda}^{j+\frac{1}{2}}_{n+\frac{1}{2}}]\cdot T^{j}_{n}+b\cdot\overline{\lambda}^{j+\frac{1}{2}}_{n+\frac{1}{2}}\cdot T^{j+1}_{n} \end{aligned} \tag{3.11}$$

with

$$a = \frac{\Delta\tau}{\Delta z_j(\Delta z_j+\Delta z_{j+1})} \tag{3.12}$$

$$b = \frac{\Delta\tau}{\Delta z_{j+1}(\Delta z_j+\Delta z_{j+1})} \tag{3.13}$$

where Δz – the positional node spacing; $\Delta\tau$ – the time step interval.

As for the moisture transfer equation (3.2), it may be expressed in an explicit difference scheme:

$$\begin{aligned} (\theta_i)^{j}_{n+1} = (\theta_i)^{j}_{n}+\frac{\rho_l}{\rho_i}[a\cdot k^{j-\frac{1}{2}}_{n+1}\cdot(P_l)^{j-1}_{n+1}-(a\cdot k^{j-\frac{1}{2}}_{n+1}+b\cdot k^{j+\frac{1}{2}}_{n+1})\cdot(P_l)^{j}_{n+1} \\ +b\cdot k^{j+\frac{1}{2}}_{n+1}\cdot(P_l)^{j+1}_{n+1}]-\frac{\rho_l}{\rho_i}[(\theta_l)^{j}_{n+1}-(\theta_l)^{j}_{n}] \end{aligned} \tag{3.14}$$

here a and b are also defined by eqs.(3.13) and (3.13) , respectively.

In each time step, first the temperature in each node is calculated, then the moisture content is defined according to the temperature and ice pressure at each node. Once the heat and moisture field are determined, the volumetric strain can de calculated from the variation of moisture field within the time step, using eq.(2.12), and the creep strain increment is determined on the

basis of stress level and soil temperature in the time step by eq.(2.24). The displacement increment field in the time step can be calculated according to the incremental initial strain method in FEM analysis:

$$[K]\Delta\{\delta^n\} = \Delta\{R^n\} \tag{3.15}$$

where $[K]$ is the global stiffness matrix, related to the soil temperature in the time step; $\Delta\{\delta^n\}$ is the nodal displacement increment vector in the time step n; $\Delta\{R^n\}$ is the equivalent nodal force increment vector.

Once a nodal displacement increment is defined, the nodal stresses can be calculated by the constitutive law. Then the nodal average stress can be determined for calculating heat and moisture transport in the next time step.

3.4 Results and Discussion

In this chapter, the simulation of Penner's experiments of frost heaving (Penner, 1986, Soil 1, Run 1) was carried out. In addition, the prediction of frost heaving and stress fields for another loading was also undertaken.

Figure (3.4) compares the simulated frost penetration under $50kPa$ applied loading, with the experimental curve published Penner (1986). In the

early stage of test, the calculated penetration is seen to be slightly smaller than experimental data, but after 2000 min, the calculated results are in good agreement with the measurements.

The comparison between experimental and simulated total frost heaving under $50kPa$ is shown in Fig.3.5 . The model predicts a smaller heave in the initial stage. The precision of simulation becomes better after early stage of test.

The calculated moisture distribution in the sample under the $50kPa$ and $300kPa$ applied loading are shown in Figs.3.6 and 3.7. Because the dry density of tested soils was not given in the Penner's paper (1986), the dry density was assumed to be 1750 kg/m^3 according to other experiments under similar conditions published by Penner and Ueda (1977). According to our simulation, the moisture increase near the cold side is not very large, because the frost penetration progresses very quickly in the initial freezing stage. Later, the total moisture content smoothly increases to a maximum value behind the advancing front, when the applied loading is small. For the case of applied large loading, the total moisture content slightly decreases behind the advancing front, and the total migrated moisture content is much smaller than under the small applied loading. This simulated results are in agreement with those obtained

experimentally or observed in the field. Discrete ice lenses cannot be predicted by the proposed model.

The stress fields in the soil under the $50kPa$ and $300kPa$ loading during freezing are shown in figures (3.8), (3.9) and (3.10). Before the soil is frozen, the initial stress field defined by the finite element method according to the elastic theory, is found to be uniform. When soil is partially frozen, the soil water changes into ice and the moisture migrates. This causes a volumetric variation in frozen soil, and results in a change in stresses. This phenomenon is very similar to thermal stresses in structures. In the frozen portion, the vertical stress σ_z remains uniform. However, the radial stress σ_r and the tangential stress σ_θ vary with the amount of expansion, because of lateral confinement of the frost chamber. A comparison of the stress field and moisture fields, shows that maximum values of σ_r and the tangential stress σ_θ appear at the same level as the maximum moisture contents. The effect of the stress field on the distribution of ice and the liquid water pressure can be determined by the Clapeyron equation with simplified assumptions, as shown in figure (2.1). In two previous papers (Shen and Ladanyi, 1987, 1988), the calculated stress field was too high, because the expansion strains have not been subtracted from the total strain in calculating the elastic strains. These results have been corrected in this thesis.

Figures (3.11) and (3.12) show the calculated relationships between the frost heaving, the frost heaving rate and the external loading. The predicted results are seen to simulate very well the often observed effect of applied loading on frost heaving, shown that, when the applied loading increases, the frost heaving and heaving rate decrease rapidly.

3.5 Summary

In this chapter, a model that makes it possible to calculate the deformation and stress fields in the soil during freezing under an applied loading is proposed. This model, based on coupling of heat moisture and stress fields is then used for simulating the results of a unidirectional freezing test in a saturated soil under a overburden of $50kPa$, published by Penner (1986). The simulated temperature field and frost heaving are found to be in a good agreement with the experimental results. The variation of stress fields during freezing is also predicted by this model.

Chapter 4

SIMULATION OF A CHILLED PIPELINE GROUND FREEZING TEST

4.1 Description of Test

4.1.1 Background

The freezing of soil around a buried chilled pipeline leads to heaving of soil. The amount of frost heaving depends on the type of soil and the ground water conditions. When a chilled pipeline crosses a transition zone between two initially unfrozen soils with different frost heaving susceptibilities, differential heaving in the soils occurs. This leads to deformation of the buried pipeline and to associated stresses in the pipeline, which may lead to pipe failure. Williams (1986a) has discussed the history and the state-of-the-art of constructing oil and gas pipelines in cold regions. In practice, determination of the complex interaction between the frost heaving soils and pipeline has presented some design difficulties. It is important not only to understand the heaving characteristics of the soil but also the reaction of the annulus of frozen

soil around the pipe, deformation of the pipeline and the state of stress in the pipe. An understanding of heaving characteristics is required to predict the behaviour of freezing soils beneath the chilled pipeline. A knowledge of the pipeline displacements and related strains in the pipe can be used to determine the state of stress in the pipeline.

The Canada-France co-operative experiment of chilled pipeline ground freezing which started in 1982, is located at the "Station de Gel" at the Centre de Géomorphologie du Centre National de la Recherche Scientifique, Caen, Normandy, France. The purpose of this project is to study the behaviour of buried pipelines under freezing and thawing conditions. The investigation of heaving and stresses developed in the pipeline, as well as the complex physical interaction that occurs when a chilled pipeline traverses two soils with different frost susceptibilities, represents an integral part of this test. Various instruments monitor the soil and pipeline at the test facility and provide the data for a comprehensive analysis.

This project is a response to the need for fundamental knowledge of freeze-thaw phenomena related to chilled gas pipelines in arctic and subarctic environments. The main feature of this full scale experiment is the precise control of the physical, thermal and hydrologic variables. Such control is not possible in field experiments where the changeable nature of soil, ground water and

weather conditions prevent the study of relevant variables independently. This project does not attempt to model any particular field situation. It attempts only to produce the type of conditions necessary for a study of relations of frost heaving of chilled pipelines to various factors, including the relation of pipe reaction to the frost heaving phenomena. This experiment gives an opportunity for validating the proposed mathematical model of frost heaving in soils.

4.1.2 Test Facility

The controlled environment test facility of the CNRS in Caen was built in the 1960's to investigate the effects of freezing on highway test sections. For the pipeline experiment, the refrigeration system was improved and several other modifications were made to the test hall. The facility in Caen provides a temperature-controlled hall $18m$ long by $8m$ wide with adjacent rooms to accommodate instrumentation and mechanical equipments, which can be filled with soil to a depth of $2m$. The base of the room has been specially prepared in order to isolate the thermal and hydraulic regime of the soils and ensure careful control of the experimental conditions. A $18m$ long, $273mm$ diameter steel pipeline with an independent refrigeration system was buried in the soils at an invert elevation of $30cm$ below the surface. The pipe ends are free, to simulate

infinite length conditions. Figures (4.1) and (4.2) show the longitudinal and transversal section of the facility, respectively. As shown in these figures, two different soil types, a slightly frost susceptible sand and a highly frost susceptible silt have been filled on each half of the trough.

4.1.3 Operation Conditions

The experimental conditions were selected to simulate the autumn start-up of a chilled gas pipeline in a discontinuous permafrost or seasonally frozen ground. The first period began on September 21, 1982. In order to minimize the temperature gradients and heat fluxes once freezing starts, the initial conditions for the experiment called for soil temperature approaching $0°C$ at the surface. Freezing from the surface was initiated on September 21, 1982. The air temperature in the room was lowered to $-5°C$ for 6 hours, then raised to $-0.75°C$. Freezing around the pipe was initiated on September 23, 1982 by lowering air temperature in the pipe to $-5°C$, after which the temperature was raised to $-2°C$. These temperatures of $-0.75°C$ *(room air)* and $-2°C$ *(pipe air)* were maintained for the duration of the freezing cycle, except for several very short interruptions. The water table was regulated at an approximate depth of $90cm$ below the original ground surface (initially the table had been maintained at $60cm$ depth but due to excessive heave of the pipe and only

limited frost penetration, after 3 months it was lowered to 90cm depth). On the lateral sides, the heat flux and water flux were isolated.

4.1.4 Instrumentation

In the first freezing cycle, the temperature profiles beneath the centreline of the pipe were measured automatically by thermocouples with a data acquisition unit. Also, regular measurements were taken, manually: of temperature using thermistors; of stand pipe water levels; of frost depth tubes;of moisture potentials using tensiometers; of pressure cell; and of pipe deflections and pipe curvature using strain gauges and devices. Volumetric unfrozen water content profiles beneath the centreline of the pipe have been determined from the Time Domain Reflectometry (T.D.R.) probes, installed in the two soils. The deformation of the pipe and elevation of the soil surface were periodically measured by the rods fixed to the pipe and placed on the soil surface. The water table level was monitored by 12 piezometers and 6 observation wells. The soil heave was observed on two sets of telescoping aluminium heave tubes, placed on the pipe axis in each soil. Each set consisted of 10 tubes, spaced every 10 cm below the pipe, to measure differential heave. Heave on the soil surface was measured by levelling a grid of surveying nails.

Table 4.1: Physical properties of Caen silt

Granulometry	30.4% sand; 56.5% silt; 13.1% clay
Density of particles	2665 ± 7 $(\mp 0.3\%)$ kg/m^3
Mineralogy (X-ray)	quartz with a small amount of chlorite and calcite
Salt content	specimen No.1: equivalent to 0.73-0.95 g NaCl/L saturated specimen No.2: equivalent to 0.37-0.50 g NaCl/L saturated

4.1.5 Properties of Caen Silt

The samples of Caen silt were sent to Carleton University for laboratory analysis. The test results are shown in Table (4.1).

The unfrozen water content was measured by the TDR method on specimens of dry density between 1.504 and 1.514 g/cm^3 and a saturation percentage between 82 and 94. (For this density the volumetric water content for the saturated soil is from 37.8% to 40.3%). The measured unfrozen water at $-1°C$ is about 18% by volume.

The thermal properties were measured by utilizing a special heated needle technique which was developed by the Geotechnical Science Laboratories of Carleton University. The measured thermal conductivity and heat capacity of Caen silt at $5°C$ are 1.97 $W/m°C$ and 2.72 $MJ/m^3°C$ on average, respectively.

Experiments for determining the hydraulic conductivity of the Caen silt were also carried out at Carleton University. The soil specimens were prepared as a normally consolidated, saturated sediment. The experimental results are shown in figure (4.3). The relationship between hydraulic conductivity and soil temperature was obtained from the experimental data using a regression analysis:

$$k = \begin{cases} 1.075 \times 10^{-9} e^{13.438T} & -0.3°C < T < T_f \\ 8.0499 \times 10^{-13} & T < -0.3°C \end{cases} \quad (m/s) \qquad (4.1)$$

The strain-rate-controlled uniaxial compression tests with the Caen silt were carried out in the Laboratories of the Northern Engineering Centre of École Polytechnique de Montréal *(CINEP)*. All these tests were made at three different temperatures: $-1°C$, $-2°C$ and $-5°C$, respectively. The samples were about $37.5\,mm$ in diameter, and $77.5\,mm$ in length. The average degree of saturation was 91%. The relationship between the Young's modulus and temperature may be defined from these experimental data by using a regression analysis:

$$E = 13.75(\frac{T}{T_r})^{1.18} \qquad MPa \qquad (4.2)$$

where T_r - the reference temperature $(-1°C)$. The Young's modulus of unfrozen soil is considered to be constant and equal to $11.2\,MPa$ (Lambe and

Whitman, 1966). When the Young's modulus E of frozen soil predicted by the eq.(4.2) is smaller than $11.2\,MPa$, the value of E is assumed to be equal to $11.2\,MPa$. The Poisson's ratio of both unfrozen and frozen soil is assumed to be 0.3.

4.2 Numerical Analysis Scheme

Although the proposed model is capable of solving a three-dimensional problem, this project is simulated as a two-dimensional case for minimizing costs. The heat and moisture transport equation were solved by the finite difference method using a boundary-conforming curvilinear coordinate system, because the finite difference method requires normally much smaller memory and amount of calculation than the finite element method. In practical computations, a high numerical efficiency is very important when using a personal computer or a small computer system to simulate such problem. The mechanical equations will still be calculated by the finite element method. The two numerical methods use two grid meshes with same grid points for the convenience of interchanging the data.

4.2.1 Mesh Generation

In the past decade, the numerical generation of curvilinear coordinate systems has provided the powerful tool for the development of finite difference solutions of partial differential equations in regions with arbitrarily shaped boundaries. Although this method has been developed from computational fluid dynamics and aerodynamics, the techniques are equally applicable to heat and mass transfer problems in cold regions, and to other areas.

Normally, the procedures for generation of curvilinear coordinate systems may be separated into two types: (1) numerical solution of partial differential equations, e.g. elliptic or hyperbolic generation systems; (2) construction by algebraic interpolation. In this simulation, the mesh system was generated by the coupled Poisson's equations (Thompson et al., 1985)

$$\xi_{xx} + \xi_{yy} = P(\xi, \eta) \tag{4.3}$$

$$\eta_{xx} + \eta_{yy} = Q(\xi, \eta) \tag{4.4}$$

The source terms P and Q can control the spacing and orientation of the coordinate lines. However, the forms of the source terms require artful selection and depend on the problem. Thomas and Middlecoff (1980) suggested for the source terms to have the forms:

$$P(\xi, \eta) = \phi(\xi, \eta) \cdot (\xi_x^2 + \xi_y^2) \tag{4.5}$$

$$Q(\xi,\eta) = \psi(\xi,\eta) \cdot (\eta_x^2 + \eta_y^2) \tag{4.6}$$

in which the functions ϕ, ψ on the boundaries are defined as

$$\phi = -\frac{x_\xi x_{\xi\xi} + y_\xi y_{\xi\xi}}{x_\xi^2 + y_\xi^2} \qquad on\ \ boundaries\ \ \eta = const \tag{4.7}$$

$$\psi = -\frac{x_\eta x_{\eta\eta} + y_\eta y_{\eta\eta}}{x_\eta^2 + y_\eta^2} \qquad on\ \ boundaries\ \ \xi = const \tag{4.8}$$

The values of these functions on the boundaries can be computed by using central-difference operators replacing differential operators:

$$\begin{aligned}
(x_\xi)_{i,j} &\sim \frac{1}{2 \cdot \Delta\xi}(x_{i+1,j} - x_{i-1,j}) \\
(x_\eta)_{i,j} &\sim \frac{1}{2 \cdot \Delta\eta}(x_{i,j+1} - x_{i,j-1}) \\
(x_{\xi\xi})_{i,j} &\sim \frac{1}{\Delta\xi^2}(x_{i+1,j} - 2x_{i,j} + x_{i-1,j}) \\
(x_{\eta\eta})_{i,j} &\sim \frac{1}{\Delta\eta^2}(x_{i,j+1} - 2x_{i,j} + x_{i,j-1})
\end{aligned} \tag{4.9}$$

Once the function ϕ is defined at each point of the horizontal boundaries $\eta = const$ in the considered domain, its value at interior mesh points can be calculated by linear interpolation along vertical mesh lines $\xi = const$. Similarly, η is computed by interpolation along the horizontal mesh lines $\eta = const$ between the boundaries.

Substituting equations (4.5), (4.6) into equations (4.3) and (4.4), and transforming it to ξ, η coordinates by interchanging the roles of dependent and independent variables, yields a quasilinear elliptic systems of equations:

$$g_{22}(x_{\xi\xi} + \phi x_\xi) - 2g_{12}x_{\xi\eta} + g_{11}(x_{\eta\eta} + \psi x_\eta) = 0 \tag{4.10}$$

$$g_{22}(y_{\xi\xi} + \phi y_{\xi}) - 2g_{12}y_{\xi\eta} + g_{11}(y_{\eta\eta} + \psi y_{\eta}) = 0 \qquad (4.11)$$

with

$$\begin{aligned} g_{11} &= x_{\xi}^2 + y_{\xi}^2 \\ g_{12} &= x_{\xi}x_{\eta} + y_{\xi}y_{\eta} \\ g_{22} &= x_{\eta}^2 + y_{\eta}^2 \end{aligned} \qquad (4.12)$$

The equations (4.10) and (4.11) are solved by SOR *(successive over-relaxation)* iteration in the rectangular computational domain to generate the grid in the physical domain. This method of evaluating the parameters ϕ and ψ insures that the grid distribution throughout the interior of the domain will be governed by grid point distribution assigned on the boundaries, and that the grid lines will be locally orthogonal to the boundaries. Therefore, the distribution of grid points generated by this method is easily controlled, and has very good character.

Figure (4.4) shows the stretching 34×37 mesh used for solving heat and moisture transport equations by the finite difference method, which is generated by the above generation system. This grid mesh has smooth and regular character, and guarantees the preservation throughout the domain of the grid point distribution specified on the boundaries. The grid mesh was generated using a PC-286 personal computer with a mathematical co-processor, which

consumed less than 2 minutes.

Figure (4.5) shows the triangular finite element mesh which is used for calculating mechanical equations. The three nodes constant strain elements were used in the simulation. This triangular mesh was generated by simply cutting quadrilaterals from the finite difference mesh, shown in figure (4.4). This mesh has 2376 triangular elements totalling 1258 nodes. These two mesh systems have exactly the same number and coordinates as the grid nodes.

4.2.2 Transformed Heat and Moisture Equations

When a general boundary-conforming curvilinear coordinate system is used in the solution of partial difference equations, the equations must first be transformed to the curvilinear coordinate system. The transformed equations are of the same type as the original ones, but are more complicated in that they contain more terms and variable coefficients. On the other hand, the domain is greatly simplified since it is transformed to a fixed rectangular region regardless of its shape in physical space.

The heat transfer equation (2.11) transformed to the curvilinear coordinate system (ξ, η), can be written as:

$$g \cdot \overline{C} \cdot \frac{\partial T}{\partial \tau} = g_{22} \cdot \frac{\partial}{\partial \xi}(\overline{\lambda} \cdot \frac{\partial T}{\partial \xi}) - 2g_{12} \cdot \frac{\partial}{\partial \xi}(\overline{\lambda} \cdot \frac{\partial T}{\partial \eta}) +$$

$$g_{11} \cdot \frac{\partial}{\partial \eta}(\overline{\lambda} \cdot \frac{\partial T}{\partial \eta}) + A_1 \cdot \overline{\lambda} \cdot \frac{\partial T}{\partial \xi} + A_2 \cdot \overline{\lambda} \cdot \frac{\partial T}{\partial \eta} \qquad (4.13)$$

with

$$\begin{aligned} A_1 &= (y_\xi \cdot Dx - x_\xi \cdot Dy)/\sqrt{g} \\ A_2 &= (x_\eta \cdot Dy - y_\eta \cdot Dx)/\sqrt{g} \\ Dx &= g_{22} \cdot x_{\xi\xi} - 2g_{12} \cdot x_{\xi\eta} + g_{11} \cdot x_{\eta\eta} \\ Dy &= g_{22} \cdot y_{\xi\xi} - 2g_{12} \cdot y_{\xi\eta} + g_{11} \cdot y_{\eta\eta} \\ \sqrt{g} &= x_\xi \cdot y_\eta - x_\eta \cdot y_\xi \end{aligned} \qquad (4.14)$$

where: $\sqrt{g}$ is the Jacobian; and g_{11}, g_{12}, g_{22} are covariant metric components, defined by the equation (4.12).

In the transformed $\xi - \eta$ plane, the outward normal derivative of an arbitrary function T at the boundary of the region has the following forms:

$$\frac{\partial T}{\partial n} = \frac{1}{\sqrt{g}}(\sqrt{g_{22}} \cdot \frac{\partial T}{\partial \xi} - \frac{g_{12}}{\sqrt{g_{22}}} \cdot \frac{\partial T}{\partial \eta}) \qquad for\ constant\ \xi \qquad (4.15)$$

or

$$\frac{\partial T}{\partial n} = \frac{1}{\sqrt{g}}(\sqrt{g_{11}} \cdot \frac{\partial T}{\partial \eta} - \frac{g_{12}}{\sqrt{g_{11}}} \cdot \frac{\partial T}{\partial \xi}) \qquad for\ constant\ \eta \qquad (4.16)$$

If the $\xi - \eta$ coordinate lines are locally orthogonal around the boundaries of interest, equations (4.15) and (4.16) reduce simply to

$$\frac{\partial T}{\partial n} = \frac{\sqrt{g_{22}}}{\sqrt{g}} \cdot \frac{\partial T}{\partial \xi} \qquad for\ constant\ \xi \qquad (4.17)$$

or

$$\frac{\partial T}{\partial n} = \frac{\sqrt{g_{11}}}{\sqrt{g}} \cdot \frac{\partial T}{\partial \eta} \qquad for\ \ constant\ \ \eta \tag{4.18}$$

The moisture transfer equation (2.4) transformed to the curvilinear system (ξ, η), may be written as:

$$\begin{aligned} g \cdot \frac{\rho_i}{\rho_l} \frac{\partial \theta_i}{\partial \tau} \;=\; & g_{22} \cdot \frac{\partial}{\partial \xi}(k \cdot \frac{\partial P_l}{\partial \xi}) - 2g_{12} \cdot \frac{\partial}{\partial \xi}(k \cdot \frac{\partial P_l}{\partial \eta}) + g_{11} \cdot \frac{\partial}{\partial \eta}(k \cdot \frac{\partial P_l}{\partial \eta}) + \\ & A_1 \cdot k \cdot \frac{\partial P_l}{\partial \xi} + A_2 \cdot k \cdot \frac{\partial P_l}{\partial \eta} - g \cdot \frac{\partial \theta_l}{\partial \tau} \end{aligned} \tag{4.19}$$

where the definitions of coefficients A_1, A_2 and covariant metric components g_{11}, g_{12}, g_{22} are the same as above.

4.2.3 Finite Difference Scheme

A numerical solution of the transformed problem can be obtained using standard technique once the problem is discretized. Since the transformed domain is stationary and rectangular, the computation can always be done on a fixed uniform square grid.

In the calculation, the non-homogeneous distributed grid mesh (shown in Fig.4.4) was used. As for the heat transfer equation (4.13), it can be approximated by the alternating direction implicit *(ADI)* method (Warming and Beam, 1979):

$$(1 - \frac{\Delta\tau}{2} \cdot L_\xi) \cdot \Lambda T^\star \;=\; \Delta\tau \cdot (L_\xi + L_\eta - \frac{2g_{12}}{g\bar{c}} \cdot \frac{\partial}{\partial \xi} \cdot \bar{\lambda} \cdot \frac{\partial}{\partial \eta}) \cdot T^n$$

$$(1 - \frac{\Delta\tau}{2} \cdot L_\eta) \cdot \Lambda T^n = \Lambda T^\star \tag{4.20}$$

$$T^{n+1} = \Lambda T^n + T^n$$

with

$$L_\xi = (A_1 \cdot \overline{\lambda} \cdot \frac{\partial}{\partial \xi} + g_{22} \cdot \frac{\partial}{\partial \xi} \cdot \overline{\lambda} \cdot \frac{\partial}{\partial \xi}) / (g \cdot \overline{C}) \tag{4.21}$$

$$L_\eta = (A_2 \cdot \overline{\lambda} \cdot \frac{\partial}{\partial \eta} + g_{11} \cdot \frac{\partial}{\partial \eta} \cdot \overline{\lambda} \cdot \frac{\partial}{\partial \eta}) / (g \cdot \overline{C}) \tag{4.22}$$

Replacing differential operators by central-difference operators, the ADI scheme may be obtained from equation (4.21). This ADI scheme is unconditionally stable. When the $\xi - \eta$ coordinate lines are orthogonal, the mixed derivative term of equation (4.19) is zero, and the ADI scheme has a second order accuracy in time. If the mixed derivative is included, the scheme is first order accurate.

As for the moisture transfer equation (4.19), it may be approximated by an explicit difference scheme:

$$\begin{aligned}(\theta_i)_{i,j}^{n+1} = {} & (\theta_i)_{i,j}^n - \frac{\rho_l}{\rho_i}[(\theta_l)_{i,j}^{n+1} - (\theta_l)_{i,j}^n] + \frac{\rho_l \cdot \Delta\tau}{\rho_i \cdot g}\{g_{22}[k_{i+\frac{1}{2},j}^{n+1} \cdot (P_l)_{i+1,j}^{n+1} \\ & -(k_{i+\frac{1}{2},j}^{n+1} + k_{i-\frac{1}{2},j}^{n+1}) \cdot (P_l)_{i,j}^{n+1} + k_{i-\frac{1}{2},j}^{n+1} \cdot (P_l)_{i-1,j}^{n+1}] - \\ & \frac{g_{12} \cdot k_{i,j}^{n+1}}{2}[(P_l)_{i+1,j+1}^{n+1} - (P_l)_{i-1,j+1}^{n+1} - (P_l)_{i+1,j-1}^{n+1} + \\ & (P_l)_{i-1,j-1}^{n+1}] + g_{11}[k_{i,j+\frac{1}{2}}^{n+1} \cdot (P_l)_{i,j+1}^{n+1} - (k_{i,j+\frac{1}{2}}^{n+1} + k_{i,j-\frac{1}{2}}^{n+1}) \cdot (P_l)_{i,j}^{n+1} \\ & +k_{i,j-\frac{1}{2}}^{n+1} \cdot (P_l)_{i,j-1}^{n+1}] + \frac{A_1 \cdot k_{i,j}^{n+1}}{2}[(P_l)_{i+1,j}^{n+1} - (P_l)_{i-1,j}^{n+1}]\end{aligned}$$

$$+\frac{A_2 \cdot k_{i,j}^{n+1}}{2}[(P_l)_{i,j+1}^{n+1} - (P_l)_{i,j-1}^{n+1}]\} \tag{4.23}$$

where $\Delta\tau$ is the interval of time step.

4.3 Numerical Simulation

4.3.1 Initial Condition and Boundary Conditions

Because of symmetry, only half of the structure was considered. The meshes used in this simulation are shown in figures (4.4) and (4.5). In the freezing period, the temperature of the pipe was held constant at $-2°C$, and the temperature of ground surface was at $-0.75°C$. The external loading was zero on the ground surface. On the lower boundary and on the sides, zero heat flux conditions (Neumann conditions) were used, because of insulations and symmetry. The initial temperature of ground was considered to be uniform at $4°C$. The initial moisture content was 40% and the initial dry density was $1510\,kg/m^3$. The soil was considered to be saturated. No external loading acted on the ground surface, and the gravity was neglected. On the bottom and on the sides, the simply-supported conditions were used, because the friction between the soil and the wall was neglected.

When a chilled pipeline crosses initially unfrozen nonhomegeneous soils, differential heaving of soils occurs. Therefore, the confining condition of the

pipe in the longitudinal direction is quite a complex three-dimensional problem. Because of a lack of exact information on the confining conditions of the pipe, two extreme pipe-confinement cases were initially considered, i.e., in which the pipe is either rigidly fixed or is free floating, as shown in figure (4.6). It was thought that the true pipe-confinement condition determined by its longitudinal rigidity and fixity will be located between these two limiting cases. Obviously, the free floating pipe-confinement conditions result in larger frost heaving but smaller stresses acting in the pipe, while the fixed condition gives less frost heaving but larger stress. In order to take into account the possible pipe resistance due to its longitudinal confinement, a third possible confinement condition was considered, shown in figure (4.7), in which the resistance of pipe was represented by a independent linear spring. The Young's modulus of the virtual spring was determined by the fixed beam formula (Ladanyi and Lemaire, 1984). If an external loading P acts on the centre point of the pipeline with the length L, which is considered as a fixed beam, the maximum deflection of pipeline Δ_{max} is governed by the following formula:

$$\Delta_{max} = \frac{L^3}{192EI} P \tag{4.24}$$

Therefore, the equivalent Young's modulus of the virtual spring will be determined approximately by

$$E_{spring} = \frac{P}{\Delta_{max}} = \frac{192EI}{L^3} = 2.085 \quad MPa \tag{4.25}$$

where: E – Young's modulus of the pipeline steel ($E = 210\ GPa$); I – moment of inertia of the pipeline section ($I = 3.688 \times 10^{-5}$); L – length of the fixed pipeline ($L = 9\ m$).

For the fixed pipe confinement condition, all nodes on the pipe boundary were fixed in calculating the stress and displacement fields by the finite element method, and no element was inside the pipe. For other two pipe confinement conditions, the pipe was considered to be an undeformable body with a very high Young's modulus. The pipe was divided into nine triangular elements in these two cases.

Then, the simulation of this complex three-dimensional problem may be simplified by simulating these three two-dimensional cases, which minimizes computing costs and difficulties.

4.3.2 Results and Discussion

Using the proposed model, a numerical simulation for the first period of Canada-France pipeline ground freezing experiment has been carried out. The heat and moisture transport equations were solved by the finite difference method and the curvilinear coordinate system, which are described above. The mechanical equations were solved by the finite element method. The used

finite element mesh was composed by the three nodes triangular elements, shown in figure (4.5).

Figures (4.8) and (4.9) show the simulated isothermal and moisture isolines after 400 hours. From figure (4.9), it was found that most of moisture accumulation appears below the pipeline. This phenomenon leads to serious heaving under the chilled pipeline which is buried in frost heaving susceptible soil. Figure (4.10) compares the simulated frost penetration under the centreline of pipeline with the measurements. The calculated values are seen to be larger than experimental data made in the first year of the test. Although there were some differences in initial and boundary conditions, the main discrepancy is found to be due to some measuring errors which occurred in the first year of the experiment, giving an abnormal frost penetration curve.

The calculated temperature and moisture profiles under the pipeline and far from the pipeline ($3.5\,m$ from the centreline of the pipeline) are shown in figure (4.11). According to our simulation, the moisture accumulation near the ground surface and the pipeline is not very large, because the frost penetration progresses very quickly in the initial freezing stage. Most of moisture in the soil was frozen in-situ in this stage. Later, as the rate of the frost penetration in soil slows down, a lot of moisture migrates from unfrozen soil to frozen soil. Therefore, the total moisture content smoothly increases to a maximum value

behind the advancing freezing front. Discrete ice lenses cannot be predicted by this model.

Figure (4.12) shows the calculated frost heaving of the surface above the pipe for different pipe confinement conditions. In this figure, the curves 1 and 4 indicate the surface frost heaving for the two limiting cases. The true frost heaving should be located between these two curves. The curve 3 shows the frost heaving of the ground surface at points far from the pipeline. Far from the pipe, the freezing is unidirectional from top to bottom. Therefore, in the initial freezing stage, the frost heaving is very small, even smaller than that above the fixed pipe. The curve 2 shows the frost heaving above the pipe with a virtual spring confinement. Because the resistance from the spring increases in direct proportion to the heaving of the pipe, the difference of heaving between this case and the free floating pipe case increases with the total frost heaving. This difference clearly varies with the stiffness of the virtual spring.

Figure (4.13) shows the measured elevation of soil surface on January 5, 1983, after about 2700 hours. Comparison of this measured contour and the simulated heaving of the soil surface shown in figure (4.12), shows that the calculated surface heavings far from the pipe (curve 3 in figure (4.12)) and above the pipe are in good agreement with the experimental measurements.

Because the ends of the pipe were free in this experiment, the true pipe confinement condition in longitudinal direction was close to an extreme condition in which the pipe is free floating. Therefore, the simulated frost heaving under this pipe confinement condition (curve 1 in figure (4.12)) is quite close to the measured one. However, calculated surface heaving under other two pipe confinement conditions is too small, because the assumed resistance is too strong for simulating these experimental conditions.

Figures (4.14) and (4.15) show deformed meshes after 400 and 1600 hours, in the rigidly fixed pipe confinement case. Figures (4.16) and (4.17) show the same kind of meshes in the free floating pipe case. The deformed meshes under the virtual spring pipe confinement condition after 400 and 1600 hours were shown in figures (4.18) and (4.19). In order to clearly present the distribution of heaving in the soil, the displacements at each grid point were amplified in the figures (4.14) to (4.19). The amplification factor was 10 for nodal displacement. These figures show clearly the effect of the pipe confinement condition and the distribution of frost heaving. From a comparison of heaving distributions with moisture distributions, it was found that serious heaving occurs below the pipe and behind the advancing freezing front, where the moisture was accumulated. This simulated distribution of frost heaving agree well with the measured results published by Smith and Williams (1990), shown in figure

(4.20). When the pipe was rigidly fixed, the heaving in the soil under the pipe was confined by the pipe. It caused the heaving soil to expand downward and compress the unfrozen soil below.

Before being frozen, the soil is free of stress because there is no external loading, because the gravity stress is neglected. The principal stress field after 400 hours of freezing is shown in figure (4.21). According to this figure, the maximum expansion stresses appear under the pipeline. Figure (4.22) shows the simulated stress profiles under the centreline of the pipeline and far from the pipeline (3.5 m from the centreline). From comparison of profiles of stress (Fig.4.8) and moisture (Fig.4.11), it is clearly seen that the maximum expansion stresses appear at the same depth as the maximum moisture accumulations. Figure (4.23) shows the stresses acting on the pipeline for the rigidly fixed case. The stress concentration under the pipeline is caused by the longitudinal confinement of the pipeline. In the section far from the pipeline, the vertical stress and the shear stress remain zero, and the lateral stress varies with the amount of moisture accumulation, because of lateral confinement of the test room. Figure (4.24) shows the normal and shear stresses acting on the free floating pipe. Obviously, the free floating pipe confinement condition results in smaller stresses acting on the pipe. In fact, the resistance of frozen soil above the pipe is acting against pipe uplift. The resistance depends on the

type and temperature of the frozen soil and on the depth of the buried pipe. It is well known that the diagram of soil reactions can be obtained by differentiating twice the moment diagram, or rather the second differential of the deflection line. Figure (4.25) shows the result of such a calculation, published by Ladanyi and Lemaire (1984), made on the basis of the results of observations of pipeline deflections by deformation gauges during the first year of the Caen experiment. By integrating the simulated normal stresses acting on the pipe (shown in figures 4.23 and 4.24), the average uplift pressure acting on the pipe from the soil beneath the pipe were found to be 138 kPa in the fixed pipe case, and 81 kPa in the free floating case. The total uplift force is equal to multiply average uplift pressure by the diameter of the pipe. The maximum uplift pressure acting on the pipe, published by Ladanyi and Lemaire (1984), was 73 kPa. Their results were obtained by differentiating twice the moment diagram, on the basis of the results of observations of pipeline deflections by deformation gauges, as shown in figure (4.25). Because only a two-dimensional section was considered in our simulation, there are some differences between the simulated uplift pressure and the maximum uplift pressure published by Ladanyi and Lemaire (1984). On the other hand, the precision of calculated stresses in the soil, especially that of stresses on boundaries, was lower, when the three nodes constant strain elements were used in calculating stress and displacement fields. Unfortunately, no appropriate method existed at that time

for accurately measuring the stress field in frozen soil, so that the calculated stress field could not have been compared with the measurements. In order to study the ultimate resistance of frozen soil against the pipe uplift, a test is being planned to be carried out in the Caen pipe test facility.

In order to predict the sensitivity of the results to the pipe temperature, a numerical simulation for the pipe temperature at $-5°C$ was also carried out, with all other initial and boundary conditions unchanged. These conditions correspond to the second and the third freezing cycle. Figures (4.26) and (4.27) show the predicted isotherms in the silt section after different times. Comparison of the predicted isotherms (Fig.4.27) with the measured ones (Fig.4.28), shows that the predicted ones agree well with the measurements. Figure (4.29) shows the predicted frost heaving of the surface. In the figure, curves 1, 2 and 4 indicate the frost heaving of the surface above the pipe for different pipe confinement conditions, and curve 3 shows the frost heaving of the ground surface far from the pipeline. Figure (4.30) shows the measured surface contour in the silt section after different times. The predicted surface heaves above the pipe for the free floating case is seen to be in very good agreement with the measurements. Far from the pipe, the predicted heave is slightly larger than the measured one. This comparison of the simulated frost heave for the two different pipe temperatures shows that the variation of the pipe temperature

strongly affects the initial progress of frost penetration and frost heaving, but, the effects decrease with time.

For checking the sensitivity of results to the assumed hydraulic conductivity of freezing soil, another relationship between hydraulic conductivity and temperature, suggested by Dr. J.F.Nixon (private communication, 1991), was used for comparison

$$k = 5.1 \times 10^{-13}(\frac{T_r}{T})^{1.14} \tag{4.26}$$

Where T_r - the reference temperature ($-1°C$). As this relationship gives lower hydraulic conductivities than equation (4.1), the resulting frost heaving is also smaller. Using this function, the simulated frost heaves of surface for the pipe temperatures of $-2°C$ and $-5°C$, are shown in figures (4.31) and (4.32). The simulated frost heaving was much smaller than those found for the previously relationship (eq.4.1) between the hydraulic conductivity and temperature. The simulated results indicate that, frost heaving of the pipeline is very sensitive to the hydraulic conductivity of the freezing soil.

4.4 Summary

The freezing of soil water around a buried chilled pipeline leads to soil heaving, which is affected by the presence of the pipe. This process may

eventually cause pipeline failure. Using the proposed model for coupled heat, moisture and stress fields, a numerical simulation of ground-pipeline interaction for a chilled pipeline was carried out and compared with measurements. The predictions of the temperature profile agree well with the measurements, and stresses acting against the pipeline are seen to be of a correct order of magnitude. Because of a lack of exact information on the confining conditions of the pipe in the longitudinal sense, it was decided to solve first two extreme pipe-confinement cases, i.e., the case of a free floating pipe and the case of a rigidly fixed pipe. It was considered that the true conditions would be located between these two limiting cases. To test this assumption, and in order to take into account the possible resistance from the longitudinal confinement of the pipe, another possible pipe confinement condition was also considered, in which the resistance of pipe was represented by a virtual spring. The simulated frost heaving under this pipe confinement condition was directly controlled by the assumed spring stiffness, and was found to be always located between those of the two limiting cases. In addition, the sensitivity of prediction results has been tested by varying the soil hydraulic conductivity and the temperature boundary conditions. The simulated results indicate that, the frost heaving of the pipeline is highly sensitive to the assumed hydraulic conductivity of the freezing soil.

Chapter 5

CONCLUSION

During the past two decades, many mathematical models for simulating the heat and moisture transport during frost heaving process have been developed. However, all of these models were based only on the coupling of heat and moisture transfer, and did not consider the effect of the external loading and the generation of internal stresses. Since 1980's, some mathematical models of frost heaving which included applied loading have, in fact, also been proposed (Hopke, 1980; Gilpin, 1980; O'Neill and Miller, 1985), but in all of them the applied external loading was only considered as a factor affecting frost heaving, while the resulting deformation and stress fields were not considered. However, for the prediction of stability of structures in cold regions, the prediction of stress and deformation fields during frost heaving is considered to be of a great importance. In fact, the stress and deformation fields in soil during freezing depend not only on the heat and moisture transfer conditions, but also strongly on the deformation boundary conditions and the external loading. This analysis of these simultaneous effects requires the coupling of

heat, moisture and stress fields. In this thesis, a conceptual model for calculating stresses and strains associated with soil freezing, on the basis of coupled heat, moisture and stress fields, is proposed. This model takes into account the non-homogeneity of the frozen zone due to the temperature distribution, as well as the effects of frozen soil creep on stress distribution. In this model, the Clapeyron equation is used to determine the liquid water pressure and to describe the effect of stress field on the heat and moisture transfer within the freezing fringe, while the associated flow rule is used to define creep strains in frozen soil. The contribution of this proposed model is that it gives a practical approach for calculating the interaction between the stresses, deformations as well as the heat and moisture transfer during soil freezing.

Using this model, a numerical simulation of a test on a saturated cylindrical sample under $50\,kPa$ in unidirectional freezing was first carried out. The experimental data for that test published by Penner (1986) provided a good opportunity for checking the feasibility of the proposed model. The simulated results of both frost penetration and amount of heave were found to be in a good agreement with the experimental ones. In addition, the frost heaving and stress field in the sample under several different loadings were also simulated. The simulated relationships between the frost heaving, the heaving rate and the applied loading, show that, when the applied loading increases, the frost

heaving and heaving rate decrease rapidly. The predicted results are seen to simulate very well the often observed effect of applied loading on frost heaving. This simulation model is able to predict the amount of water (ice) accumulation behind the advancing freezing front, but not the position of discrete ice lenses. The variation of stress field during freezing is also predicted by this model. The simulated stress field shows that, the maximum value of lateral stress appears at the same place as the maximum moisture contents. This phenomenon is very similar to the thermal expansion stresses in structures. Because no appropriate method existed at that time for accurately measuring stress field in frozen soil, the simulated stress field could not have been compared with measurements.

Since 1970's, construction of several gas pipelines have been considered in the North for natural gas from the Arctic to the southern consumers. For security reasons, and for protecting the northern environment, these pipelines were usually buried. One of the suggested methods consists in transporting the gas at below freezing temperature. This would avoid the thawing od ice-rich soils and their loss of stability. But, on the other hand, it would result in a freezing of unfrozen soils in the discontinuous permafrost area. The freezing of soil water around a buried chilled pipeline leads to heaving of soil, which is affected by the presence of the pipe. This leads to deformation of the pipeline and may result in its failure. In this thesis, a numerical simulation

of the initial phases of the co-operative Canada-France chilled pipeline ground freezing experiment, was carried out by using the proposed model.

Because of a lack of exact information on the confining conditions of the pipe in the longitudinal sense, it was decided to solve first two extreme pipe-confinement cases, i.e., the case of a free floating pipe and the case of a rigidly fixed pipe. It was considered that the true conditions would be located between these two limiting cases. In order to check the assumption and to take into account the possible resistance from the longitudinal confinement of the pipe, another possible pipe confinement condition was also considered, in which the resistance of pipe was represented by a virtual spring. The simulated frost heaving under this pipe confinement condition was directly controlled by the assumed spring stiffness, and was found to be always located between those for the two limiting cases. Because the ends of the pipeline were free in the experiment, the comparison of the simulated surface heaving and the measured one shows that the true pipe confinement condition is close to the free floating pipe conditions and the simulated one agrees quite well with the measurements. The calculated progress of frost penetration is also in good agreement with the measurements, and the stresses acting against the pipeline are seen to be of a correct order magnitude. Up to now, it was not possible to compare with measurements, because of a lack of appropriate instruments and methods.

In addition, the sensitivity of prediction results was tested by varying the soil hydraulic conductivity and the temperature boundary conditions. The simulated results indicate that, the frost heaving of the pipeline is highly sensitive to the hydraulic conductivity of the freezing soil. The variation of temperature of the pipe strongly affects the progress of frost penetration and heaving in the initial freezing stage. Afterwards, the effects of the pipe temperature are much smaller than those of the hydraulic conductivity of the soil.

The proposed model in this thesis has contributed to solving the problem of coupling the heat, moisture transfer and stress field. Up to now, it has been found difficult to accurately measure stresses in frozen soil. Therefore, the ability to calculate stress and deformation fields during soil freezing appears to be an important step towards a more accurate prediction of stability of structures in frozen soils. On the other hand, as usual, the development of theories is much faster than experimentation, so that some real weakness still exist in the area of proper knowledge of some basic material parameters and in a correct selection of assumptions included in the simulation model. A tentative list of such problems that still require further investigation is given in the following:

- More accurate measurement of the hydraulic conductivity of freezing soil, as a function, not only of temperature, but also of solutes, internal

stresses and ice lensing. In fact, the hydraulic conductivity of soil is the most important parameter affecting the frost heaving in soil.

- Better knowledge on stress sharing between ice and water in the soil pores during soil freezing.

- A proper selection of the criterion for the start of frost heaving, in terms of soil porosity, unfrozen water content, degree of saturation, and internal stress.

- Measurement of internal stresses during freezing in both frozen and adjacent unfrozen soil.

- Extension of the existing one-dimensional frost heaving models to the three-dimensional case, which are able to simulate ice lensing in the frozen zone.

- Inclusion of frozen soil strength and creep properties into frost heaving models.

- Taking into account the effect of freeze thaw cycling on both freezing and thawing response of soils.

Although some assumptions and answers to above questions have already been given, some controversy and deficiencies still exists in many points, so

that more study will be needed before solutions to freezing problems could be approached with confidence.

References

[1] **Biermans, M. & Dijkema, K. & DeVries, D.A., 1978**, Water Movement in Porous Media Towards an Ice Front., J. of Hydro., 37, pp.137-148.

[2] **Bishop, A.W. & Blight, G.E., 1963**, Some Aspects of Effective Stress in Saturated and Partly Saturated Soils, Geotechnique, 13, pp.177-197.

[3] **Blanchard, D. & Fremond, M., 1985**, Soils Frost Heaving and Thaw Settlement, Proc. 4th International Symposium on Ground Freezing, pp.209-216.

[4] **Bonacina, C. & Comini,G. & Fasano, A. & Primicerio, M., 1973**, Numerical Solution of Phase-Change Problems, Int. J. Heat Mass Transfer, Vol.16,pp.1825-1832.

[5] **Booth, D.B., 1981**, Macroscopic Behavior of Freezing Saturated Silty Soil, Cold Regions Science and Technology, 4, pp.163-174.

[6] **Chamberlain, E.J., 1980**, Determining Differential Frost Heave by the Probabilistic Method, CRREL in house-laboratory independent Research Progress Report 43.

[7] **Chamberlain, E.J. & Blouin, S.E., 1978**, Densification by Freezing and Thawing of Line Material Dredged from Waterways, Proc. 3rd Int. Conf. on Permafrost, pp.622-628.

[8] **Comini, G. & Guidice, S.D. & Lewis, R.W. & Zienkiewicz, O.C., 1974**, Finite Element Solution of Non-Linear Heat Conduction Problems with Special Reference to Phase Change, Int. J. for Numerical Methods in Engineering, 8, pp.613-624.

[9] **Eckardt, H., 1982**, Creep Tests with Frozen Soil under Uniaxial Tension and Uniaxial Compression, Proc. 4th Canadian Permafrost Conference, pp.394-405.

[10] **Everett, D.H. & Haynes, J.M., 1965**, Capillary Properties of Some Model Pore Systems with Special Reference to Frost Damage, RILEM Bull., New Ser. 27, pp.31-38.

[11] **Garand, P. & Ladanyi, B., 1982**, Frost Susceptibility Testing of Compacted Glacial Till, Proc. the 3rd Int. Symp. on Ground Freezing, pp.277-284.

[12] **Gilpin, R.R., 1980**, A Model for the Prediction of Ice Lensing and Frost Heave in soils, Water Resources Res., 16(5), pp.918-930.

[13] **Goodrich, L., 1978**, Efficient Numerical Technique for One-Dimensional Thermal Problems with Phase Change, Int. J. of Heat and Mass Transfer, Vol.21, pp.615-621.

[14] **Groenevelt, P.H. & Kay, B.D., 1977**, Water and Ice Potentials in Frozen Soils, Water Resources Research, 13(2), pp.445-449.

[15] **Guymon, G.L. & Harr, M.E. & Berg, R.L. & Hromadka, T.V., 1981**, A Probabilistic-Deterministic Analysis of One-Dimensional Ice Segregation in a Freezing Soil Column, Cold Regions Science and Technology, 5, pp.127-149.

[16] **Guymon, G.L. & Hromadka, T.V. & Berg, R.L., 1984**, A One Dimensional Frost Heave Model Based upon Simulation of Simultaneous Heat and Water Flux, Cold Regions Science and Technology, 3, pp.253-262.

[17] **Guymon, G.L. & Hromadka, T.V. & Berg, R.L., 1984**, Two-Dimensional Model of Coupled Heat and Moisture Transport in Frost-Heaving Soils, J. of Energy Resources Technology, ASME, 106, pp.336-342.

[18] **Guymon, G.L. & Luthin, J.N., 1974**, A Coupled Heat and Moisture Transport Model for Arctic Soil, Water Resources Research, 9(5), pp.1314-

1323.

[19] **Harlan, R.L., 1973**, Analysis of Coupled Heat-Fluid Transport in Partially Frozen Soil, Water Resources Res., 9(5), pp.1314-1323.

[20] **Harlan, R.L. & Nixon, J.F., 1973**, Ground Thermal Regime. In: Geotechnical Engineering for Cold Regions. O.B.Andersland and D.M.Anderson (Eds.), McGraw-Hill, pp.103-150.

[21] **Hill, D.W. & Morgenstern, N.R., 1977**, Influence of Load and Heat Extraction on Moisture Transfer in Soils, Proc. Int. Symp. on Frost Action in Soil, Lulea, Vol.1, pp.76-91.

[22] **Ho, D.M. & Harr, M.E. & Leonards, G.A., 1970**, Transient Temperature Distribution in Insulated Pavements – Predictions vs. Observations, Can. Geotech. J., 7, pp.275-284.

[23] **Hoekstra, P., 1969**, Water Movement and Freezing Pressures, Proc. Soil Sci. Soc. of Amer., 33, pp.512-518.

[24] **Hopke, S.W., 1980**, A Model for Frost Heave Including Overburden, Cold Regions Sci. Tech.,3, pp.111-127.

[25] **Horiguchi, K. & Miller, R., 1983**, Hydraulic Conductivity Functions of Frozen Materials, Proc. 4th International Conference on Permafrost, pp.504-508.

[26] **Jame, Y.W. & Norum, D.I., 1980**, Heat and Mass Transfer in a Freezing Unsaturated Porous Medium, Water Resources Res., 16(4), pp.811-819.

[27] **Kay, B.D. & Groenevelt, P.H., 1974**, On the Interaction of Water and Heat Transport in Frozen and Unfrozen Soils: I. Basic Theory; The Vapor Phase. Soil Sci. Soc. Amer. Proc., Vol.38, pp.395-400.

[28] **Kay, B.D. & Perfect, E., 1988**, State of the Art: Heat and Mass Transfer in Freezing Soils, Proc. 5th Int. Symp. on Ground Freezing, pp.3-21.

[29] **Kay, B.D. & Sheppard, M.I. & Loch, J.P.G., 1977**, A Preliminary Comparison of Simulated and Observed Water Redistribution in Soils Freezing under Laboratory and Field Conditions, Proc. Int. Symp. on Frost Action in Soils, Lulea, Sweden, pp.29-40.

[30] **Konrad, J.M., 1987**, Procedure for Determining the Segregation Potential of Freezing Soils, Geotech. Testing J., ASTM, 10(2), pp.51-58.

[31] **Konrad, J.M., 1988**, Influence of Freezing Mode on Frost Heave Characteristics, Cold Regions Science and Technology, 15, pp.161-175.

[32] **Konrad, J.M. & Morgenstern, N.R., 1980**, A Mechanistic Theory of Ice Formation in Fine-Grained Soils, Canadian Geotech. J., 17, pp.473-486.

[33] **Konrad, J.M. & Morgenstern, N.R., 1981**, The Segregation Potential of a Freezing Soil, Canadian Geotech. J., 18, pp.482-491.

[34] **Konrad, J.M. & Morgenstern, N.R., 1982**, Effects of Applied Pressure on Freezing Soils, Can. Geotech. J., 19, 494-505.

[35] **Konrad, J.M. & Morgenstern, N.R., 1983**, Frost Susceptibility of Soils in Terms of Their Segregation Potential, Proc. of the 4th Int. Conf. on Permafrost, Fairbanks, pp.660-665.

[36] **Konrad, J.M. & Morgenstern, N.R., 1984**, Frost Heave Prediction of Chilled Pipelines Buried in Unfrozen Soils, Canadian Geotech. J., 21, pp.100-115.

[37] **Ladanyi, B., 1972**, An Engineering Theory of Creep of Frozen Soils. Canadian Geotech. J., 9, pp.63-79.

[38] **Ladanyi, B., 1975**, Bearing Capacity of Strip Footings in Frozen Soils, Canadian Geotech. J., 12, pp.253-262.

[39] **Ladanyi, B., 1981**, Mechanical Behaviour of Frozen Soils, Proc. Int. Symp. on Structured Media, Ottawa, pp.205-245.

[40] **Ladanyi, B., 1985**, Stress Transfer Mechanism in Frozen Soils, Proc. of the 10th CANCAM, London, Ontario, pp.11-23.

[41] **Ladanyi, B. & Lemaire, C., 1984**, Behavior of a Buried Pipeline under Differential Frost Heave Conditions, Proc. of Cold Regions Engineering Special Conf., Montral, pp.161-176.

[42] **Ladanyi, B. & Shen Mu, 1989**, Mechanics of Freezing and Thawing in Soils. Special Lecture, Proc. of Int. Symp. on Frost in Geotechnical Engineering, Saariselka, Finland, pp.73-103.

[43] **Lambe, T.W. & Whitman, R.V., 1969**, Soil Mechanics, John Wiley & Sons Inc., New York.

[44] **Loch, J.P.G. & Afifi, S.S., 1973**, Thaw Consolidation of Alaskan Silts and Granular Soils, Proc. the 2nd Int. Conf. on Permafrost, pp.325-334.

[45] **Loch, J.P.G. & Kay, B.D., 1978**, Water Redistribution in Partially Frozen, Saturated Silt under Several Temperature Gradients and Overburden Loads, J. Soil Sci. Soc. of Amer, 43, 3, pp.400-406.

[46] **Lynch, D. & O'Neill, K., 1981**, Continuously Deforming Finite Elements for the Solution of Parabolic Problems, with and without Phase Change, Int. J. for Num. Methods in Engrg., Vol.17, pp.81-96.

[47] **McRoberts, E.C. & Nixon, J.F., 1975**, Some Geotechnical Observations on the Role of Surcharge in Soil Freezing, Proc. of Conf. on Soil Water Problems in Cold Regions, pp.42-57.

[48] **Miller, R.D., 1972**, Freezing and Heaving of Saturated and Unsaturated Soils, Highway Res. Rec., No.393, pp.1-11.

[49] **Miller, R.D., 1977**, Lens Initiation in Secondary Heaving, Proc. Int. Symp. on Frost Action in Soils, Lulea, 2, pp.68-74.

[50] **Miller, R.D., 1978**, Frost Heaving in Non-Colloidal Soils, Proc. 3rd Int. Conf. on Permafrost, pp.707-713.

[51] **Morgan, K. & Lewis, R.W. & Zienkiewicz, O.C., 1978**, An Improved Algorithm for Heat Conduction Problems with Phase Change, Int. J. for Num. Methods in Engrg., Vol.12, pp.1191-1195.

[52] **Morgenstern, N.R., 1981**, Geotechnical Engineering and Frontier Resource Development, Geotechnique, 31, 3, pp.305-365.

[53] **Nixon, J.F., 1975**, The Role of Convective Heat Transport in the Thawing Soils, Can. Geotech. J., 12, pp.425-429.

[54] **Nixon, J.F., 1983**, Practical Applications of Versatile Geothermal Simulator, ASME winter annual meeting, Paper 82-WA/HT-14.

[55] **Nixon, J.F., 1986**, Pipeline Frost Heave Predictions Using a 2-D Thermal Model, ASCE, Research on Transportation Facilities in Cold Regions, pp.67-86.

[56] **Nixon, J.F. & Morgenstern, N.R. & Reesor, S.N., 1983**, Frost Heave - Pipeline Interaction using Continuum Mechanics, Canadian Geotech. J., 20, pp.251-261.

[57] **O'Neill, K., 1983**, The Physics of Mathematical Frost Heave Models: A Review. Cold Regions Science and Technology, 6, pp.275-291.

[58] **O'Neill, K., 1983**, Fixed Mesh Finite Element Solution for Cartesian Two-Dimensional Phase Change, J of Energy Resources Techno., ASME, Vol.105, pp.436-441.

[59] **O'Neill, K. & Miller, R.D., 1985**, Exploration of a Rigid Ice Model of Frost Heave, Water Resources Res., 21(3), pp.281-296.

[60] **Penner, E., 1973**, Frost Heaving Pressures in Particulate Materials, Proc. OECD Symp. on Frost Action in Roads, Paris, 1, pp.379-385.

[61] **Penner, E., 1986**, Aspects of Ice Lens Growth in Soils. Cold Regions Sci. Tech., 13, pp.91-100.

[62] **Penner, E. & Ueda, T., 1977**, The Dependence of Frost Heaving on Load Application – Preliminary Results. Proc. Int. Symp. Frost Action in Soils, Lulea, Vol.1, pp.92-101.

[63] **Radd, F.J. & Oertle, D.H., 1973**, Experimental Pressure Studies of Frost Heave Mechanisms and the Grouth-Fusion Behaviour of Ice, Proc. 2nd Int. Conf. on Permafrost, North Amer. Contribution, pp.377-384.

[64] **Shen Mu, 1987**, Numerical Analysis of Creep Deformation and Stress of the Artificial Freezing Shaft Wall. Journal of Glaciology and Geocryology, 9(2), Lanzhou, pp.139-148.

[65] **Shen Mu, 1988**, Numerical Analysis of Temperature Field in a Thawing Embankment in Permafrost. Canadian Geotechnical Journal, 25, pp.163-166.

[66] **Shen Mu, 1990**, Problem of the Coupled Heat, Moisture and Stress in Freezing Soil. In: Interaction among Temperature, Moisture and Stress Fields in Frozen Soil. An Weidong(Ed.), Lanzhou University Press, pp.211-225.

[67] **Shen Mu & Ladanyi, B., 1987**, Modelling of Coupled Heat, Moisture and Stress Field in Freezing Soil. Cold Regions Science and Technology, 14, pp.237-246.

[68] **Shen Mu & Ladanyi, B., 1988**, Calculation of the Stress Field in Soils during Freezing. Proc. of 5th International Symp. on Ground freezing, Nottingham, England, pp.121-126.

[69] **Shen Mu & Ladanyi, B., 1989**, Numerical Solutions for Freezing and Thawing of Soils Using Boundary-Fitted Curvilinear Coordinate Systems. Proc. of Int. Symp. on Frost in Geotechnical Engineering, Saariselka, Finland, pp.391-400.

[70] **Shen Mu & Ladanyi, B., 1990**, Modelling of Freezing Process in Soil. Presented at the Int. Colloquium on Free Boundary Problems, Montreal.

[71] **Shen Mu & Ladanyi, B., 1991**, Soil-Pipe Interaction during Frost Heaving around a Buried Chilled Pipeline. Proc. of 6th Int. Cold Regions Engineering Conference, West Lebanon, NH , pp.11-21.

[72] **Sheppard, M.I. & Kay, B.D. & Loch, J.P.G., 1978**, Development and Testing of a Computer Model for Heat and Mass Flow in Freezing Soils. Proc. of the 3rd Int. Conf. on Permafrost, pp.76-81.

[73] **Smith, M.W. & Onysko, D., 1990**, Observations and Significance of Internal Pressure in Freezing Soil. Proceedings of the 5th Canadian Permafrost Conference, Québec, pp.75-81.

[74] **Smith, S.L. & Williams, P.J., 1990**, Ice Lens Orientation around a Chilled Buried Pipe. Proceedings of the 5th Canadian Permafrost Conference, Québec, pp.83-87.

[75] **Soo, S. & Wen, R.K. & Andersland, O.B., 1985**, Finite Element Models for Structure Creep Problems in Frozen Ground, Proc. of the 4th Int. Symp. on Ground Freezing, Vol.2, pp.23-28.

[76] **Sutherland, H.B. & Gaskin,P.N., 1973**, Pore Water and Heaving Pressures Developed in Partially Frozen Soils, Proc. 2nd Int. Conf. on Permafrost, North Amer. Contribution, pp.409-418.

[77] **Taylor, G.S. & Luthin, J.N., 1978**, A Model for Coupled Heat and Moisture Transfer during Soil Freezing, Canadian Geotech. J., Vol.15, pp.548-555.

[78] **Thomas, P.D. & Middlecoff, J.F., 1980** Direct Control of the Grid Point Distribution in Meshes Generated by Elliptic Equations, AIAA Journal, Vol.18, No.6, pp.652-656.

[79] **Thompson, J.F. & Wassi, Z.U.A. & Masstin, C.W., 1985**, Numerical Grid Generation – Foundations and Applications, North-Holland, New York.

[80] **Vialov, S.S., 1965**, The Strength and Creep of Frozen Soils and Calculations for Ice-Soil Retaining Structures, CRREL Transl. 76.

[81] **Vignes, M. & Dijkema, K.M., 1974**, A Model for the Freezing of Water in a Dispersed Medium, J. of Colloid and Interface Sci., 49, 2, pp.165-172.

[82] **Warming, R.F. & Beam, R.M., 1979**, An Extension of A-Stability Alternating Direction Implicit Method, BIT, 19, pp.395-417.

[83] **Williams, P.J., 1972**, Use of the Ice-Water Surface Tension Concept in Engineering Practice, Highway Research Record, 393, pp.19-29.

[84] **Williams, P.J., 1977**, Thermodynamic Conditions for Ice Accumulation in Freezing Soils, Proc. Int. Symp. on Frost Action in Soils, 1, pp.42-53.

[85] **Williams, P.J., 1983**, Investigation of Soil Freezing in Association with a Buried Chilled Pipeline in a Large-Scale Test Facility - Phase 2 (Final Report). for Earth Physics Branch, EMRC.

[86] **Williams, P.J., 1986**, Pipelines and Permafrost – Science in Cold Climate. The Carleton University Press.

[87] **Williams, P.J., 1986**, The Third Cycle of the Canada-France Ground Freezing Experiment (Final Report). for Geological Survey of Canada.

[88] **Williams, P.J., 1986**, Investigations of Frost Heave as a Cause of Pipeline Deformation. for Earth Physics Branch, EMRC.

[89] **Williams, P.J. & Wood, J.A., 1984**, Internal Stresses in Soils during Frost Heaving. for Earth Physics Branch, EMRC.

[90] **William, P.J. & Wood, J.A., 1985**, Internal Stresses in Frozen Ground. Canadian Geotech. J., 22, pp.413-416.

[91] **Xu Xiaozu & Oliphant, J.L. & Tice, A.R., 1985**, Prediction of Unfrozen Water Contents in Frozen Soils by a Two-Points or One-Point Method, Proc. 4th Int. Symp. on Ground Freezing, 2, pp.83-87.

[92] **Zhu Yuanlin & Carbee, D.L., 1984**, Uniaxial Compressive Strength of Frozen Silt at Constant Deformation Rates, Cold Regions Sci. Technol., 9(1), pp.3-15.

[93] **Zhu Yuanlin & Carbee, D.L., 1987**, Creep and Strength Behavior of Frozen Silt in Uniaxial Compression, CREEL Report 87-10.

[94] **Zhu Yuanlin & Carbee, D.L., 1987**, Tensile Strength of Frozen Silt, CRREL Report 87-15.

[95] **Zienkiewica, O.C. & Cormean, I.C., 1974**, Viscoplasticity-Plasticity and Creep in Elastic Solids – a Unified Numerical Solution Approach, Int. J. Numerical Methods. in Engineering, 8, pp.821-845.

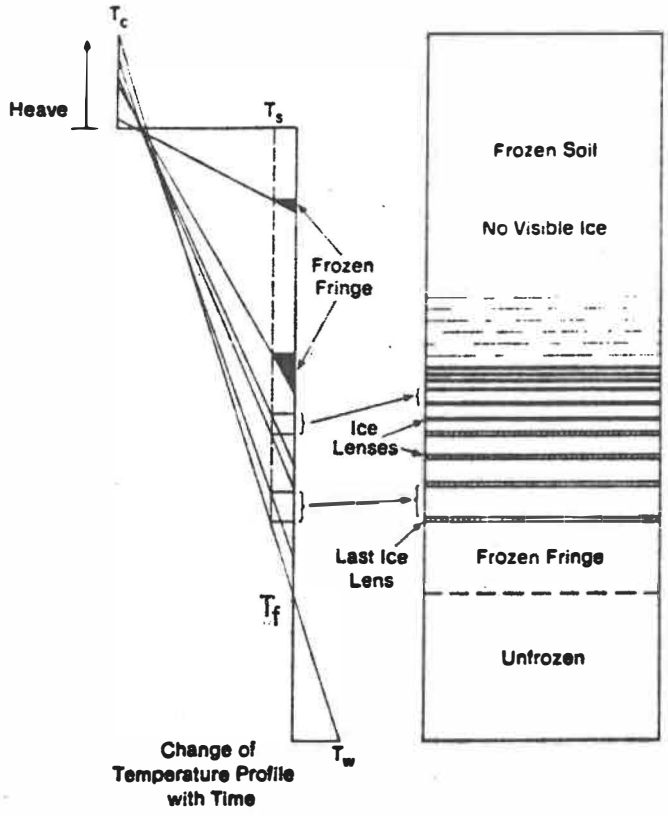

Figure 1.1: Schematic rhytmic ice lens formation (after Konrad and Morgenstern, 1980)

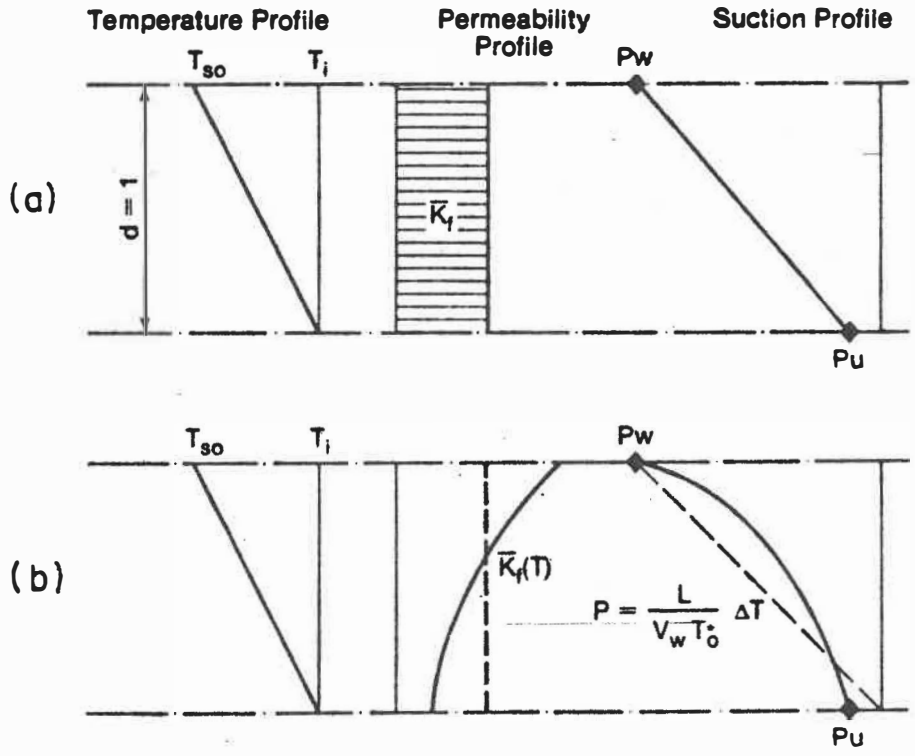

Figure 1.2: Characteristics of the frozen fringe: (a) simplified, (b) actual shape (after Konrad and Morgenstern, 1981)

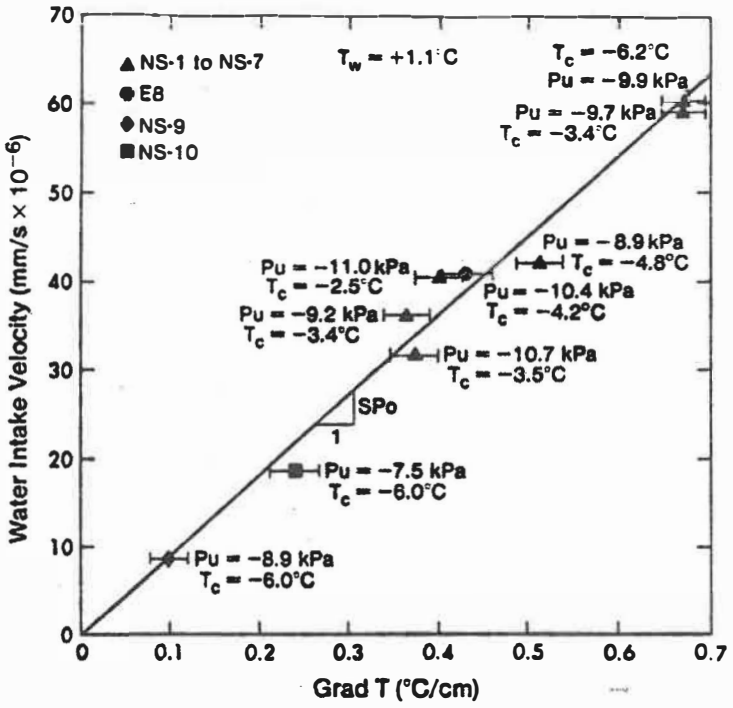

Figure 1.3: Relation between water intake velocity and temperature gradient across the active system, at the formation of the final ice lens (after Konrad and Morgenstern, 1981)

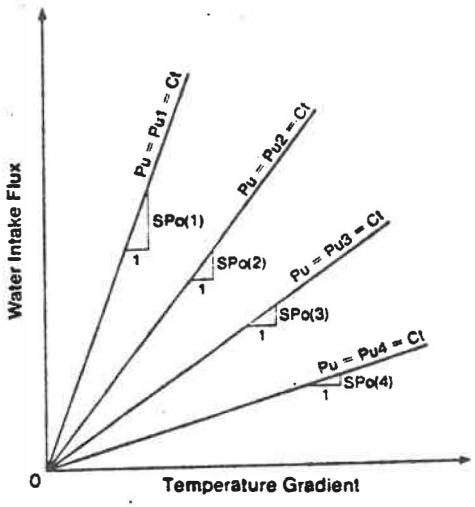

Figure 1.4: Conceptual relationship between the water intake flux and temperature gradient at different suctions at the frost front (after Konrad and Morgenstern, 1981)

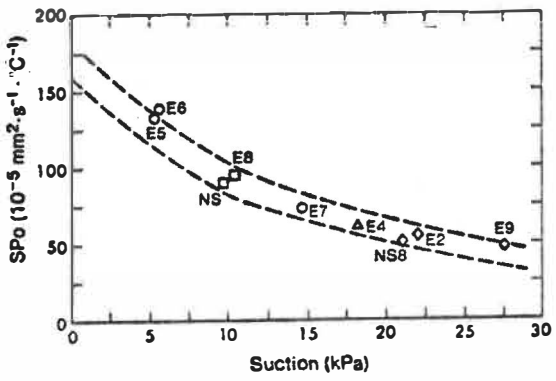

Figure 1.5: Segregation potential vs. suction at the frost front for Devon silt (after Konrad and Morgenstern, 1981)

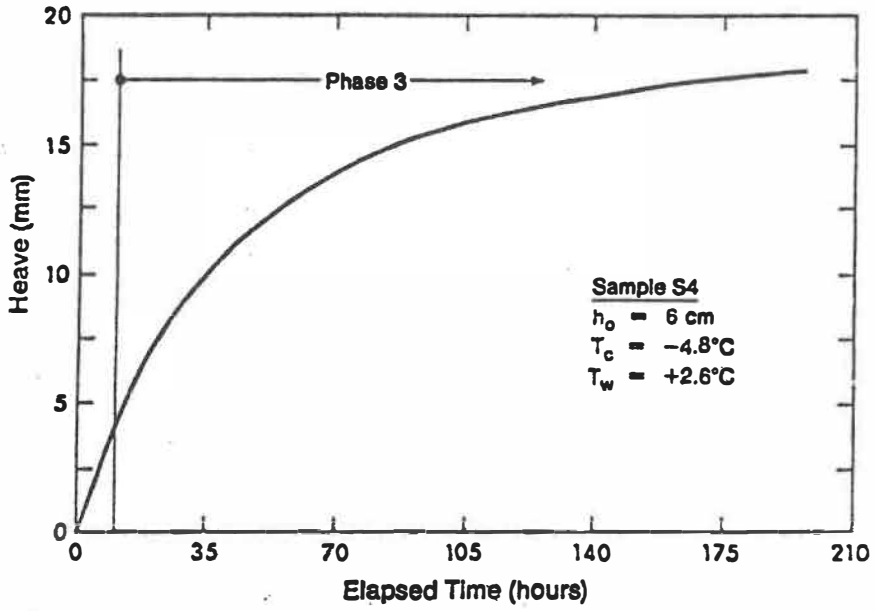

Figure 1.6: Result of a typical laboratory frost heave test with fixed thermal boundary conditions (after Konrad and Morgenstern, 1981)

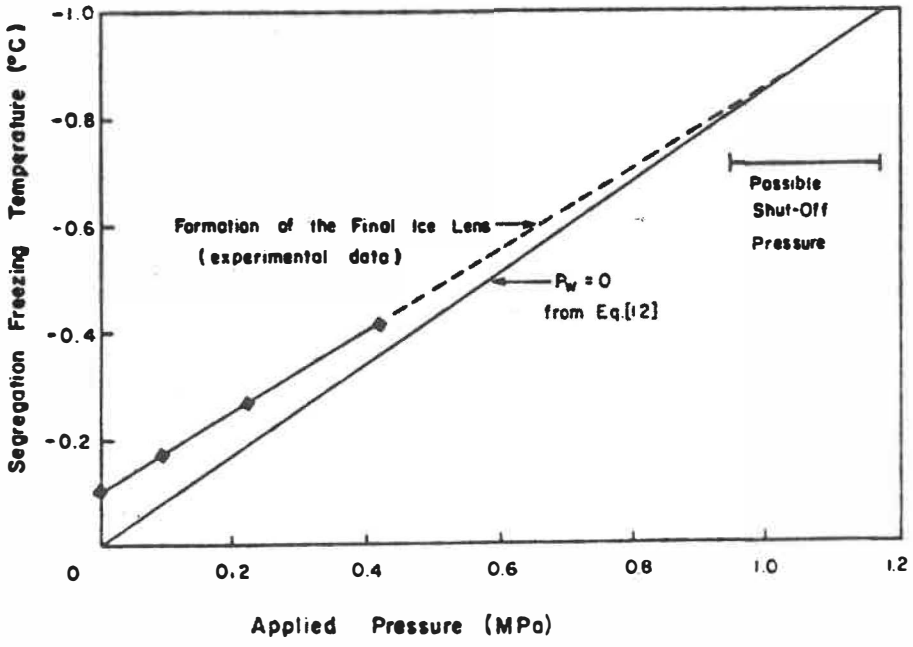

Figure 1.7: Determination of the shut-off pressure for Devon silt (after Konrad and Morgenstern, 1982)

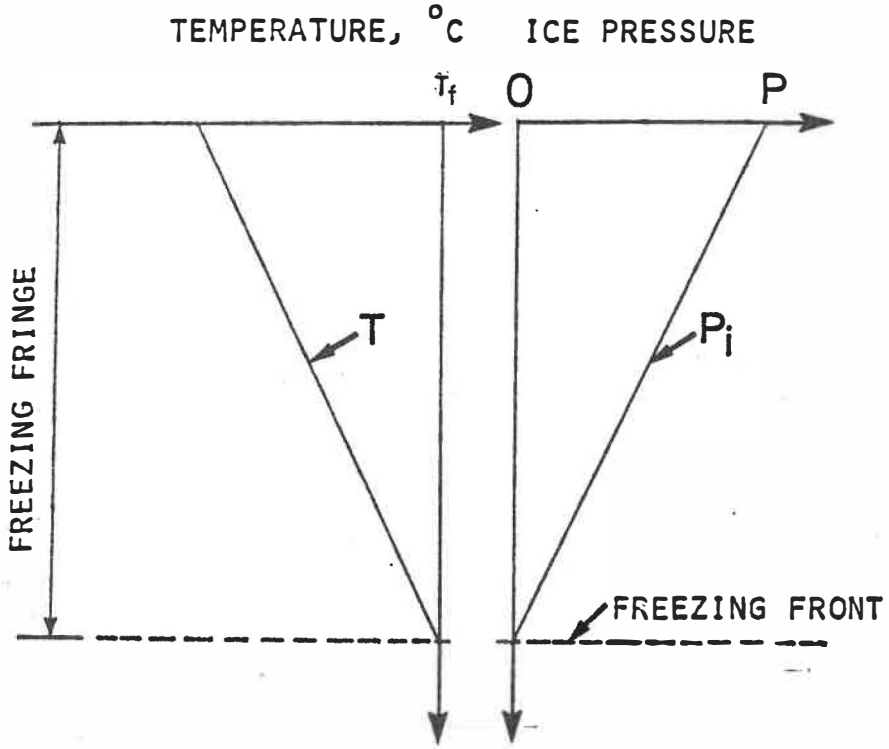

Figure 2.1: Idealized distribution of temperature and ice pressure within the freezing fringe, adopted in the model

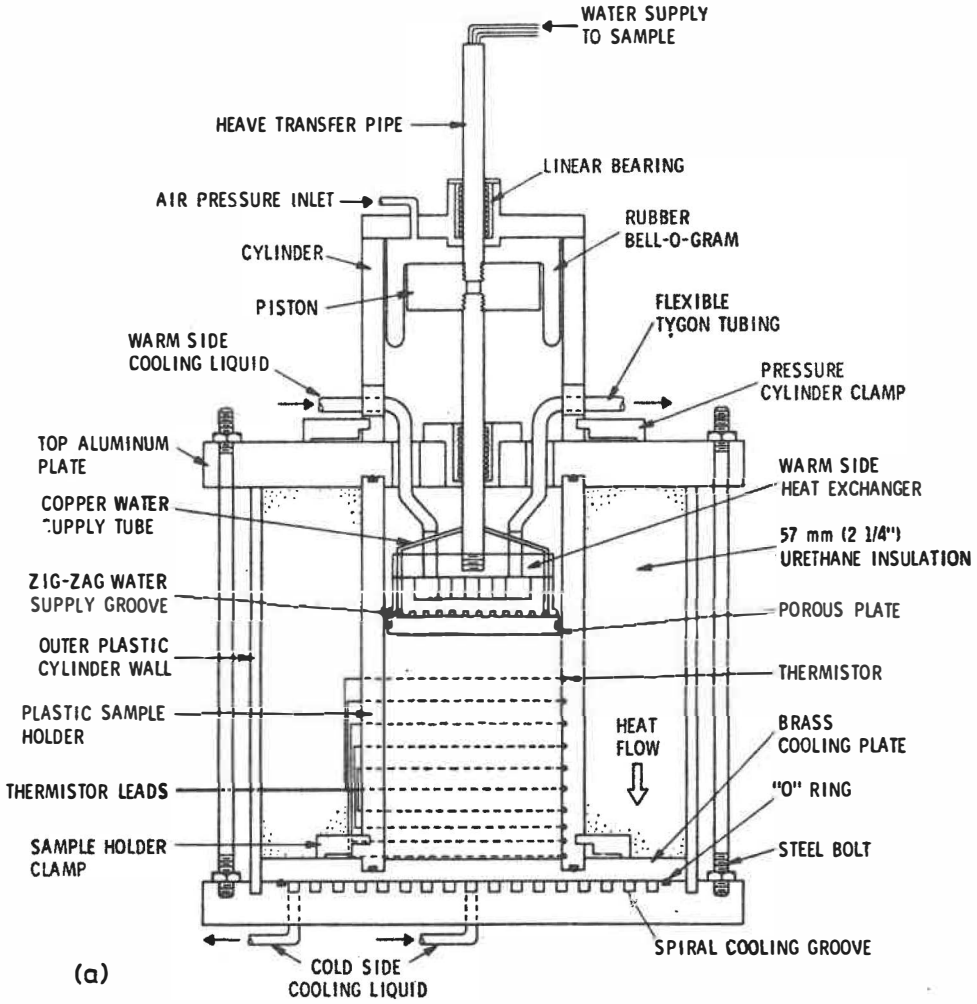

Figure 3.1: Frost cell used in the test (after Penner, 1986)

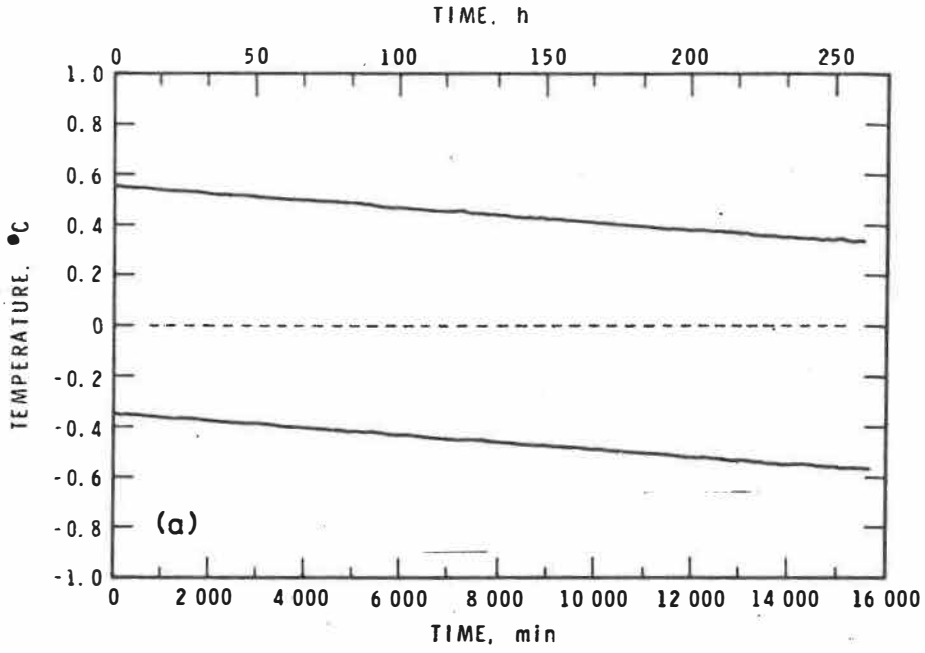

Figure 3.2: Temperature boundary conditions (after Penner, 1986)

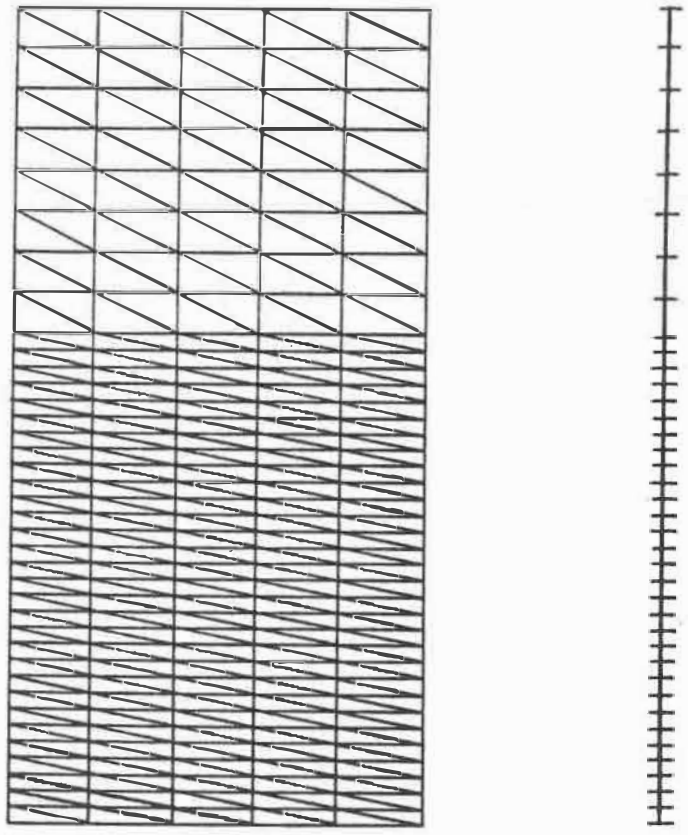

Figure 3.3: The grid system used in the simulation: (a) mesh for finite element method; (b) grid for finite difference method

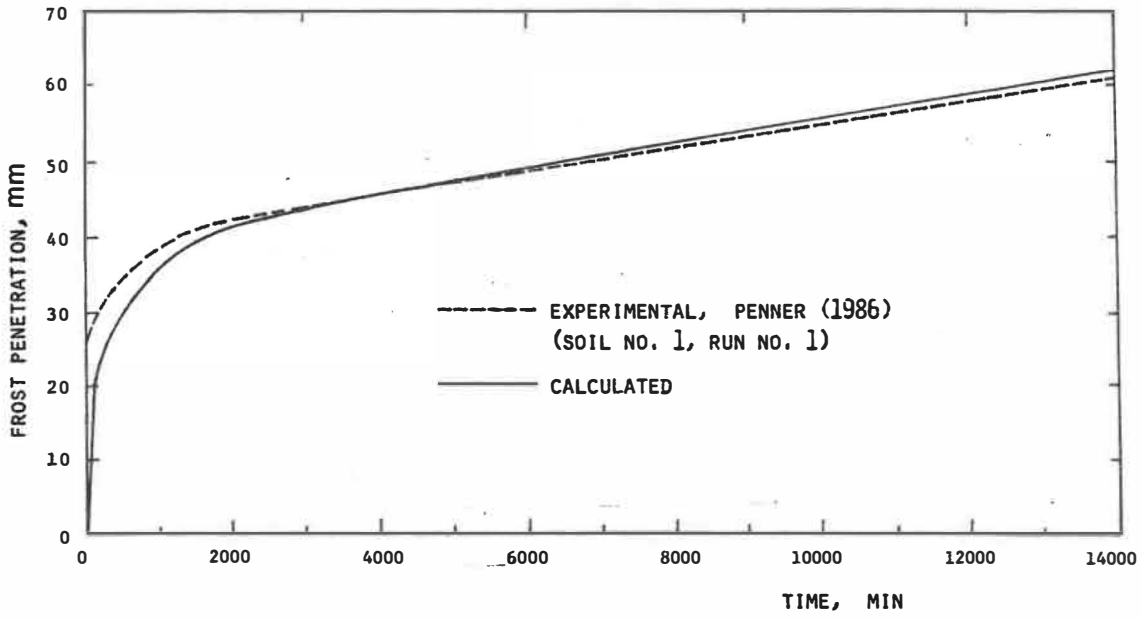

Figure 3.4: Comparison of calculated frost penetration with that measured by Penner (1986)

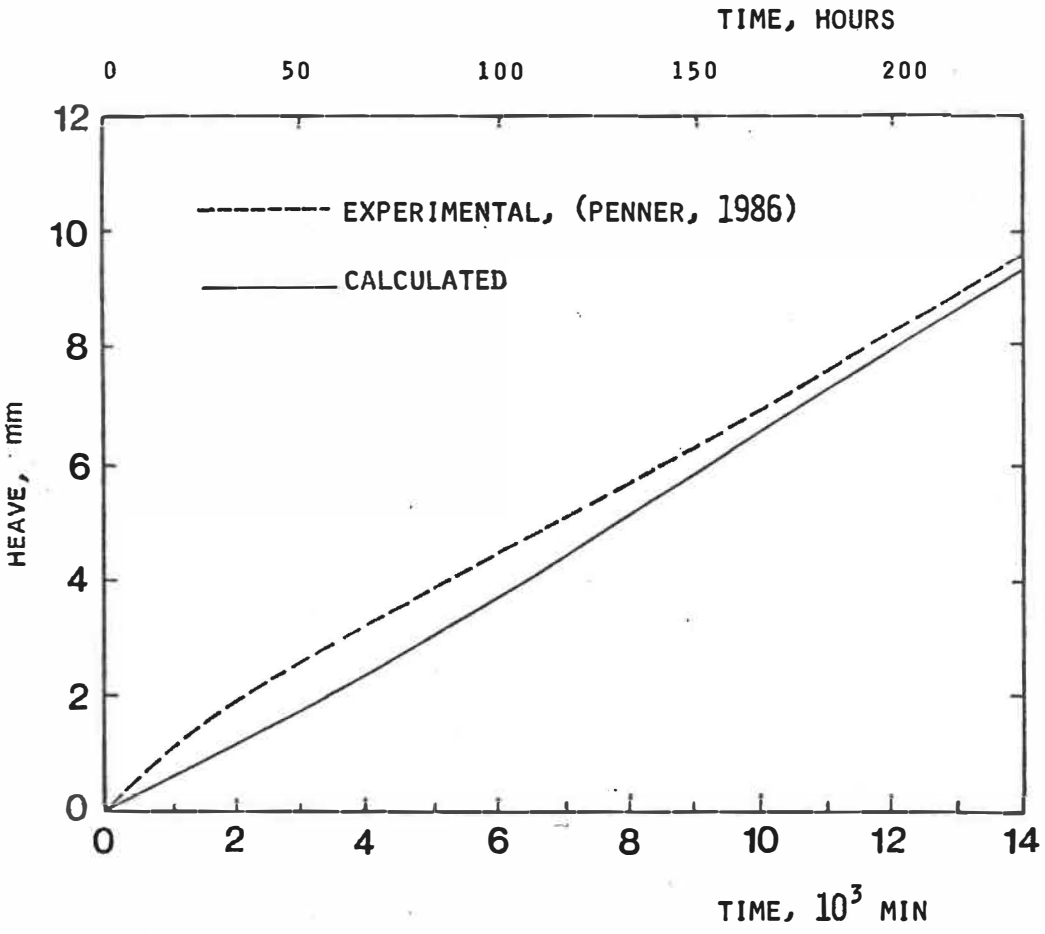

Figure 3.5: Comparison of calculated frost heave with experimental data by Penner (1986)

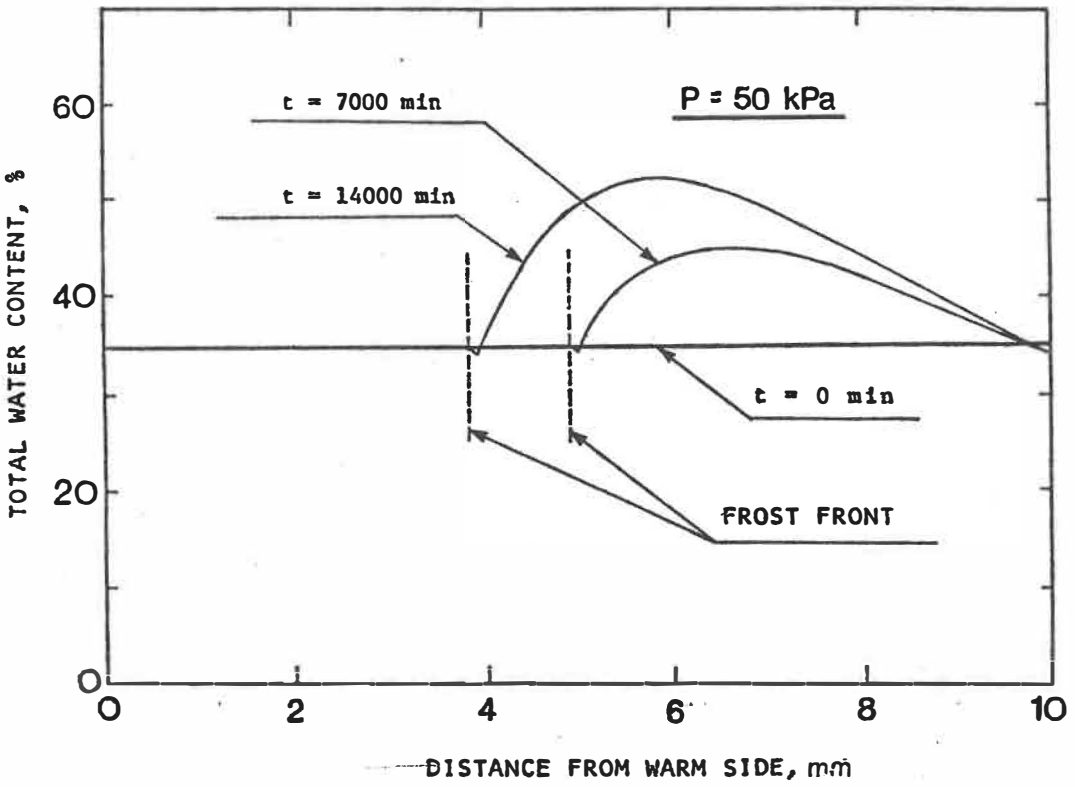

Figure 3.6: Calculated moisture distribution in the sample after 7000 and 14000 min, under 50 kPa

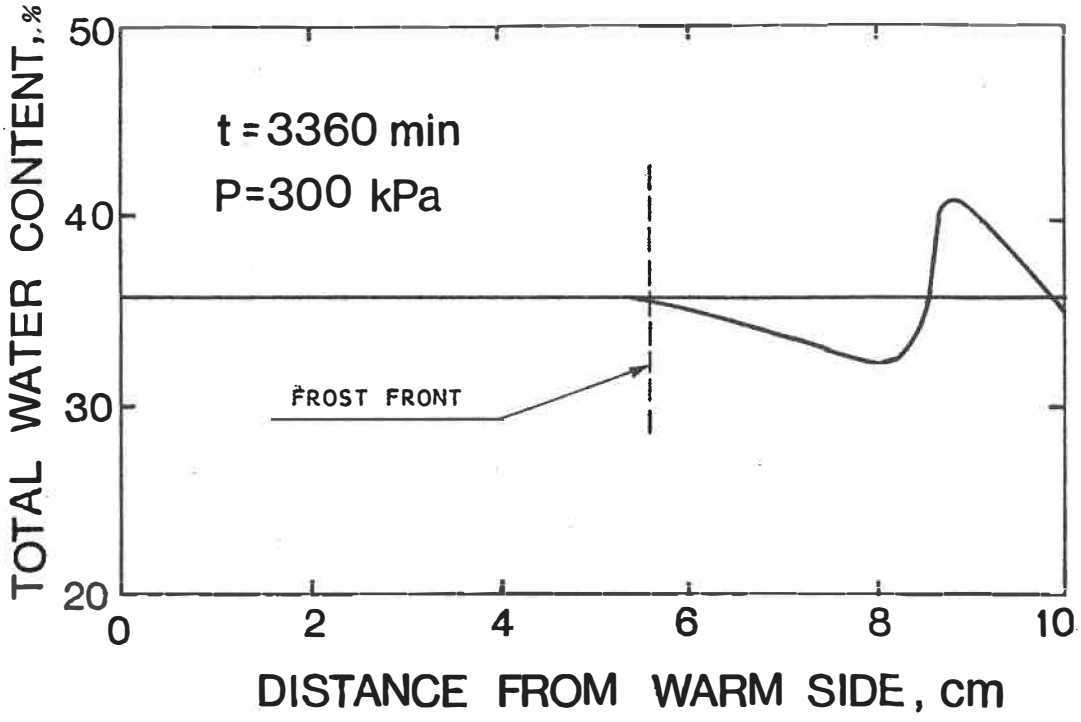

Figure 3.7: Calculated moisture distribution in the sample after 3360 min, under 300 kPa

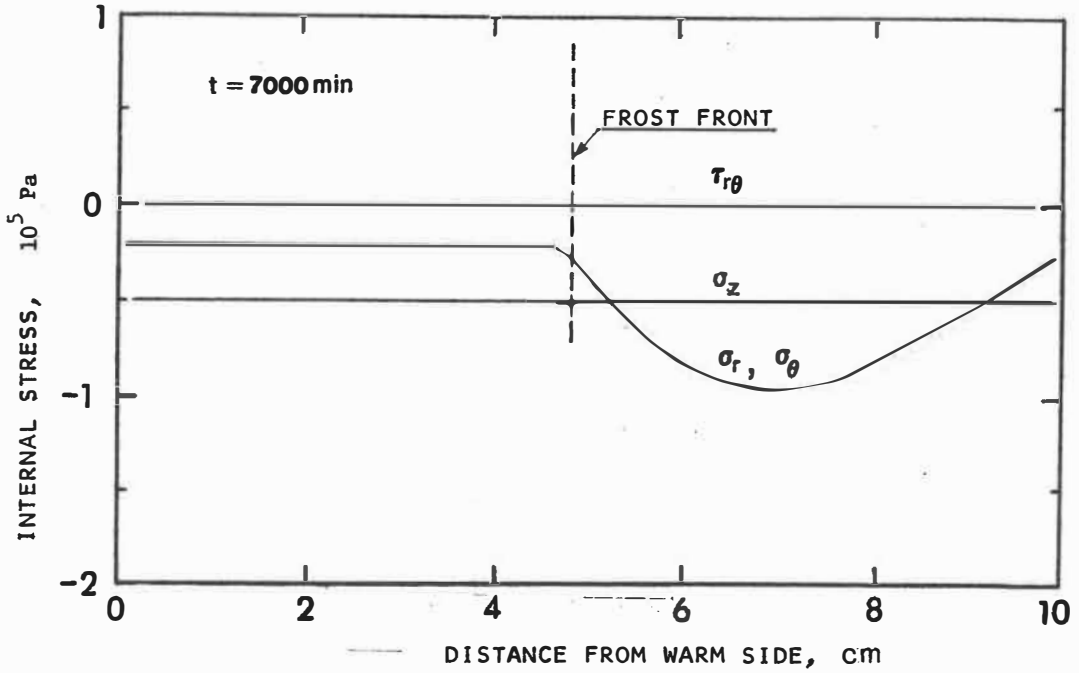

Figure 3.8: Calculated stress field after 7000 min, under 50 kPa

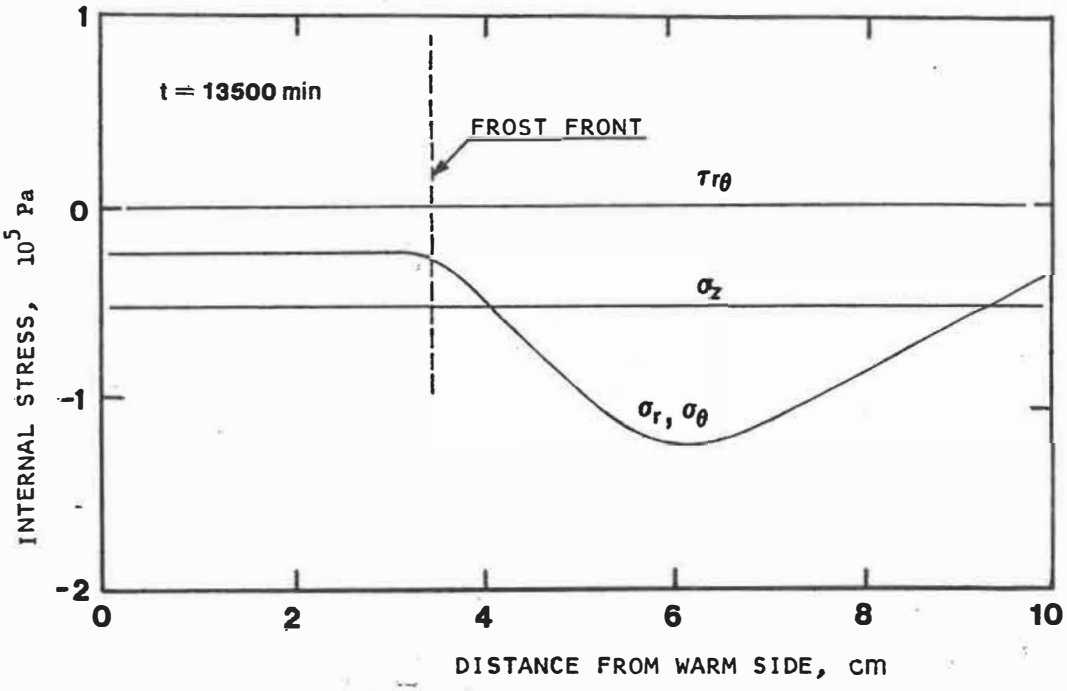

Figure 3.9: Calculated stress field after 13500 min, under 50 kPa

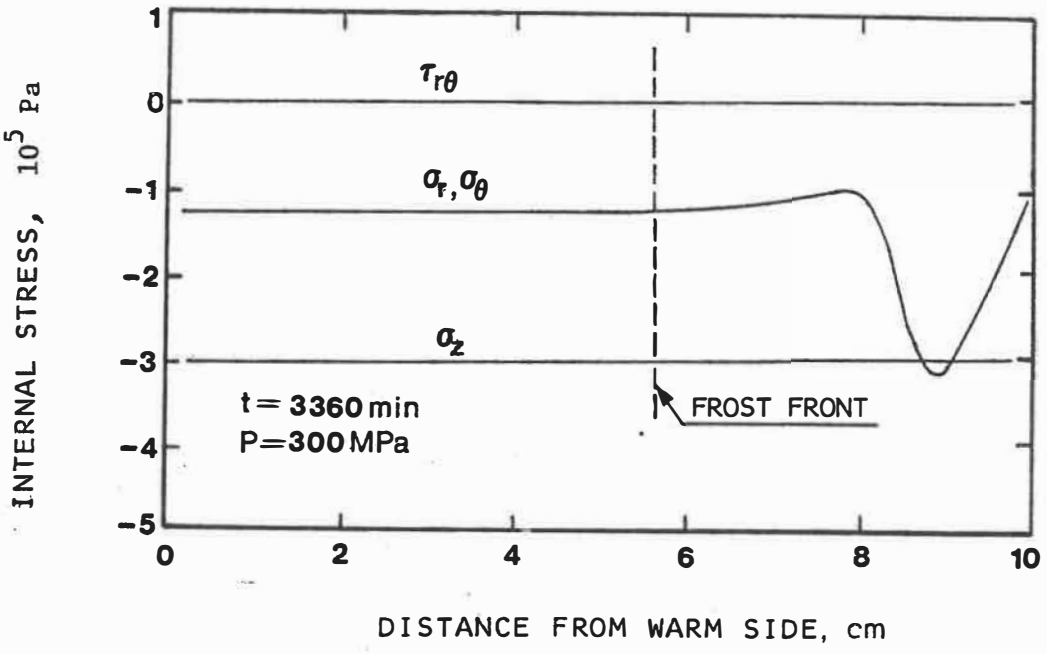

Figure 3.10: Calculated stress field after 3360 min, under 300 kPa

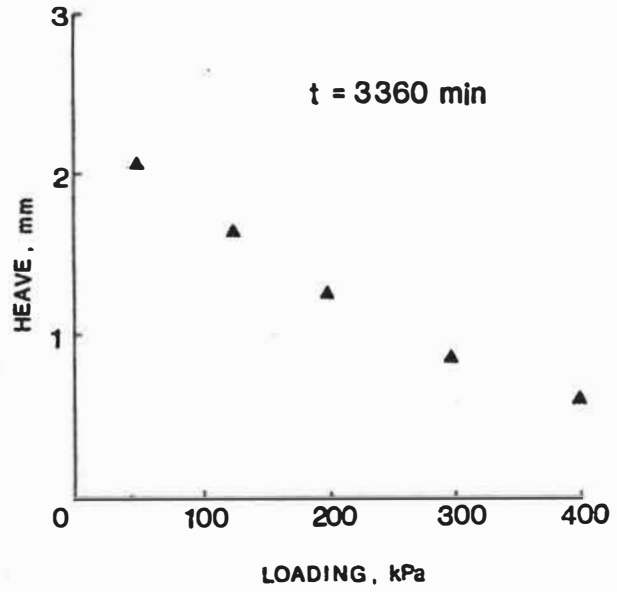

Figure 3.11: Calculated relationship between heave and applied loading after 3360 min

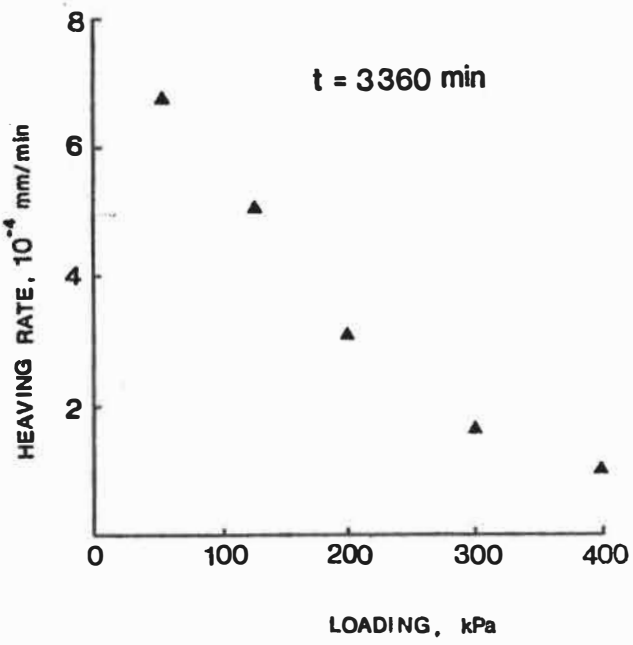

Figure 3.12: Calculated relationship between heave rate and applied loading after 3360 min

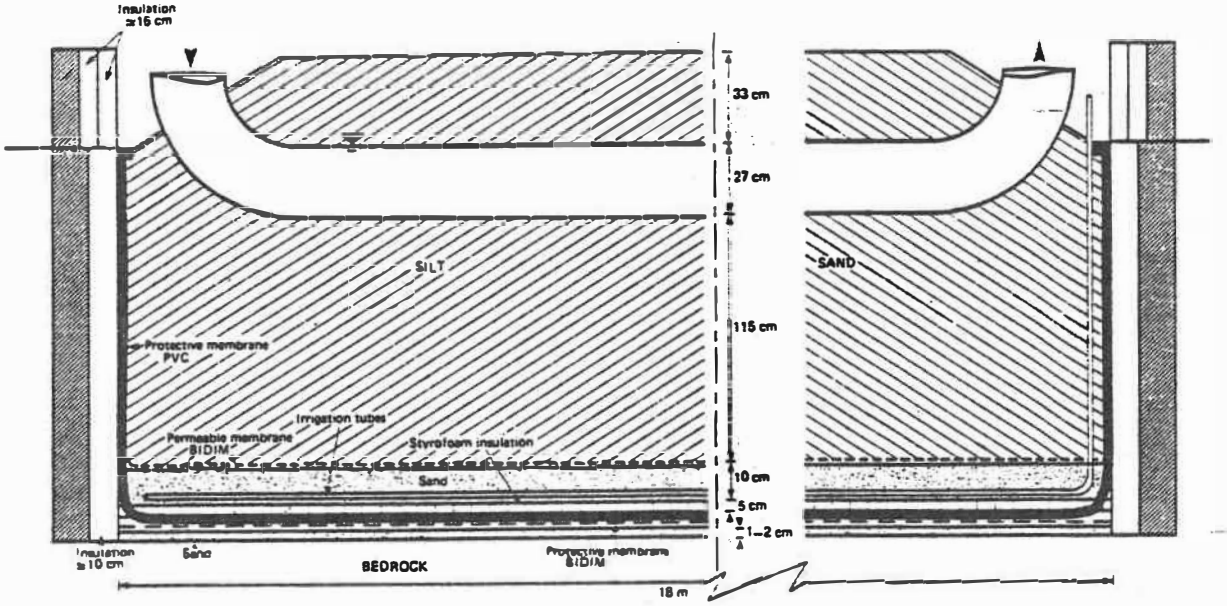

Figure 4.1: Longitudinal section of trough (after Williams, 1983)

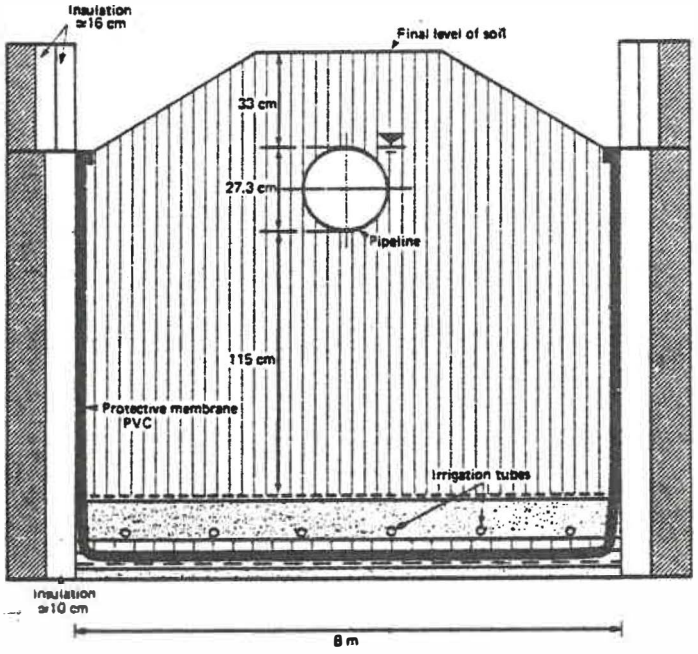

Figure 4.2: Cross-section of trough (after Williams, 1983)

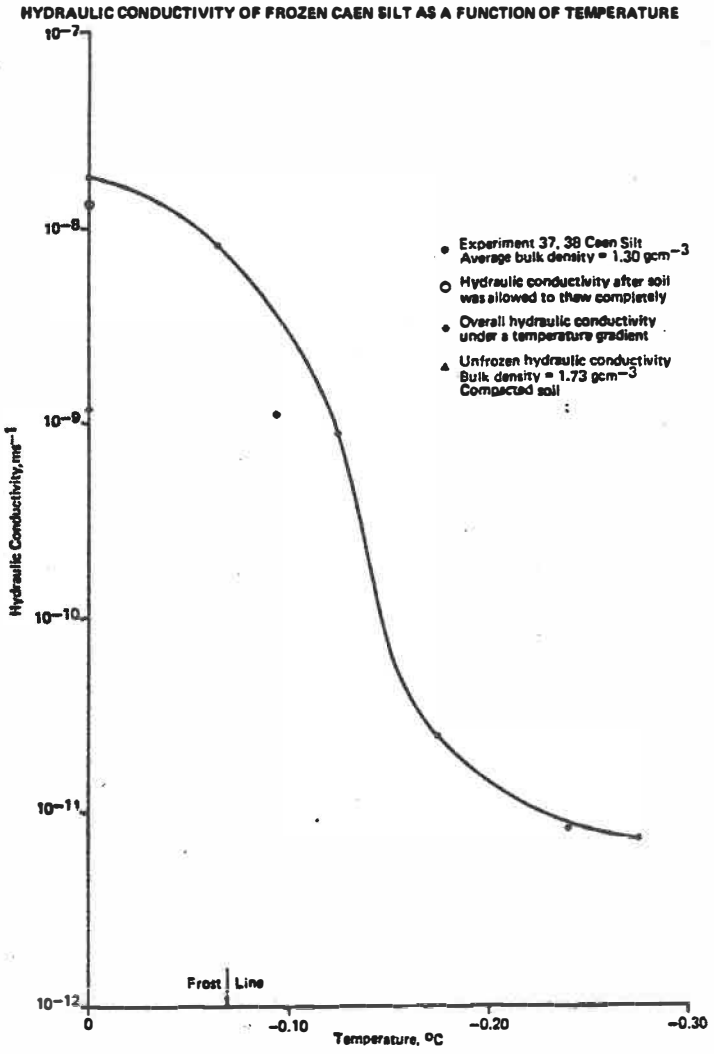

Figure 4.3: Hydraulic conductivity of frozen Caen silt as a function of temperature (after Williams and Wood, 1984)

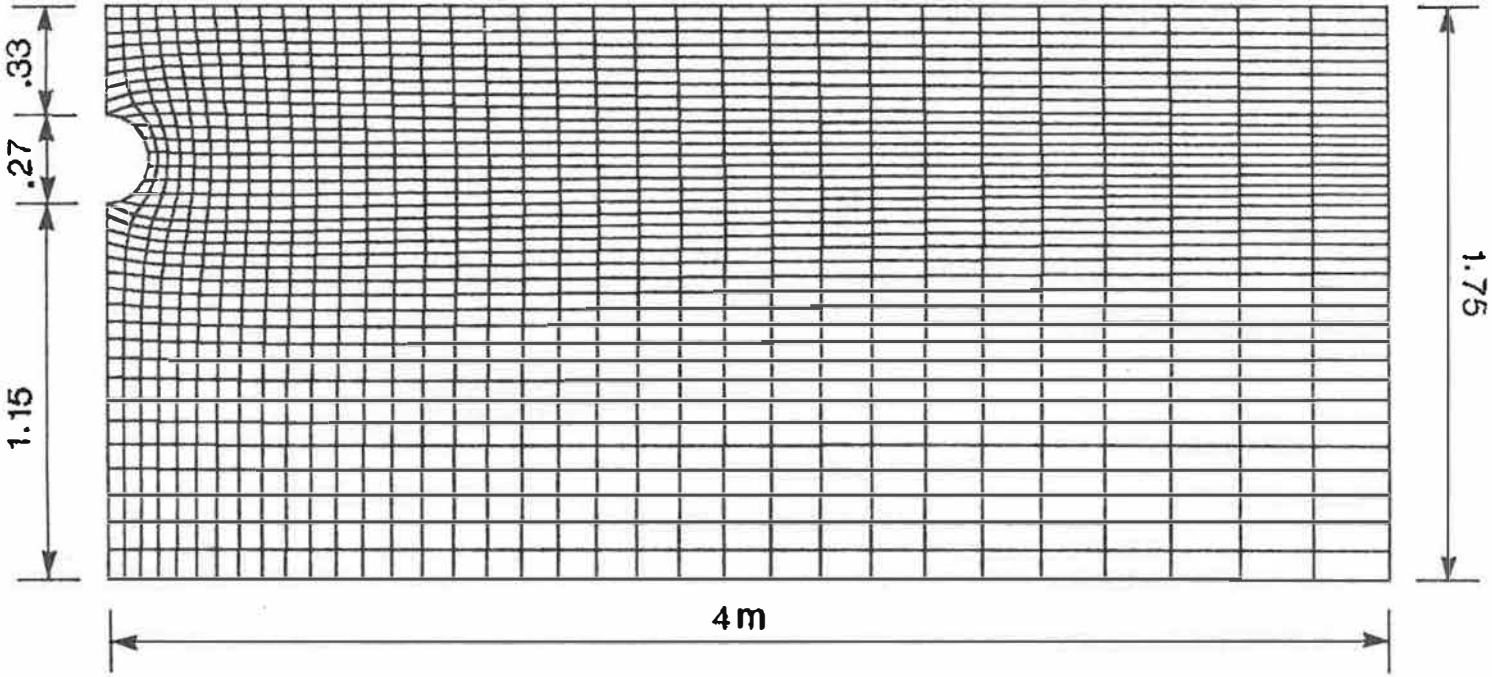

Figure 4.4: The grid mesh system used for the finite difference method

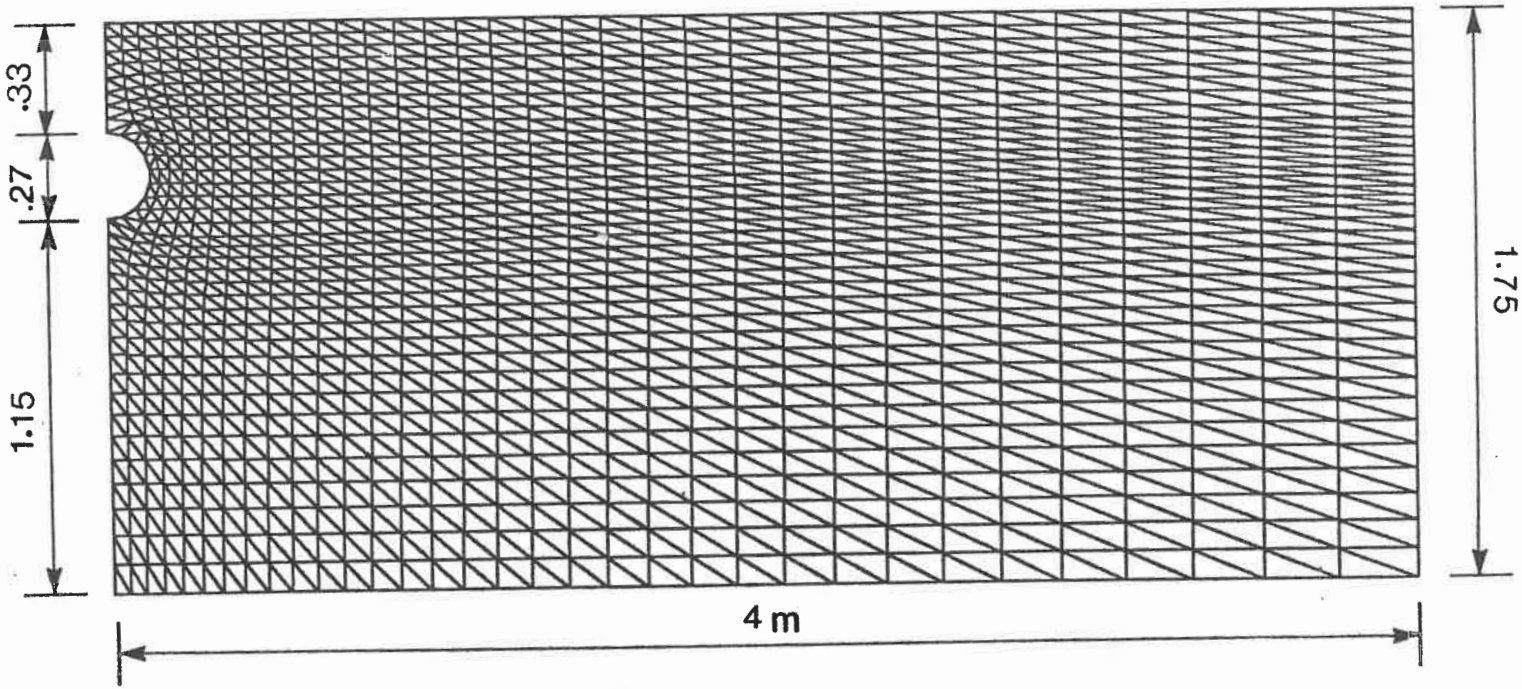

Figure 4.5: The finite element mesh used in the simulation

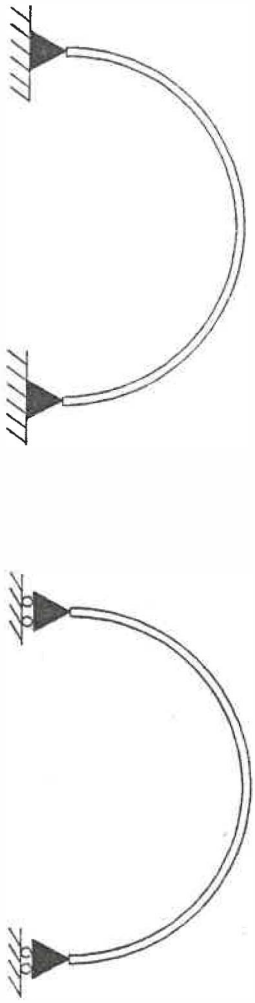

Figure 4.6: Two limiting pipe-confinement case: (a) rigidly fixed; (b) free floating

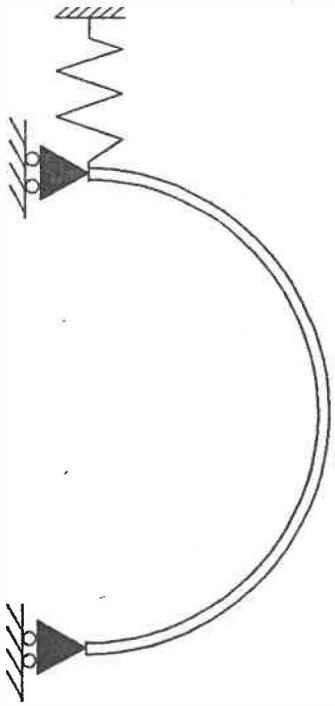

Figure 4.7: Possible pipe-confinement condition: resistance of the pipe to be represented by a virtual spring

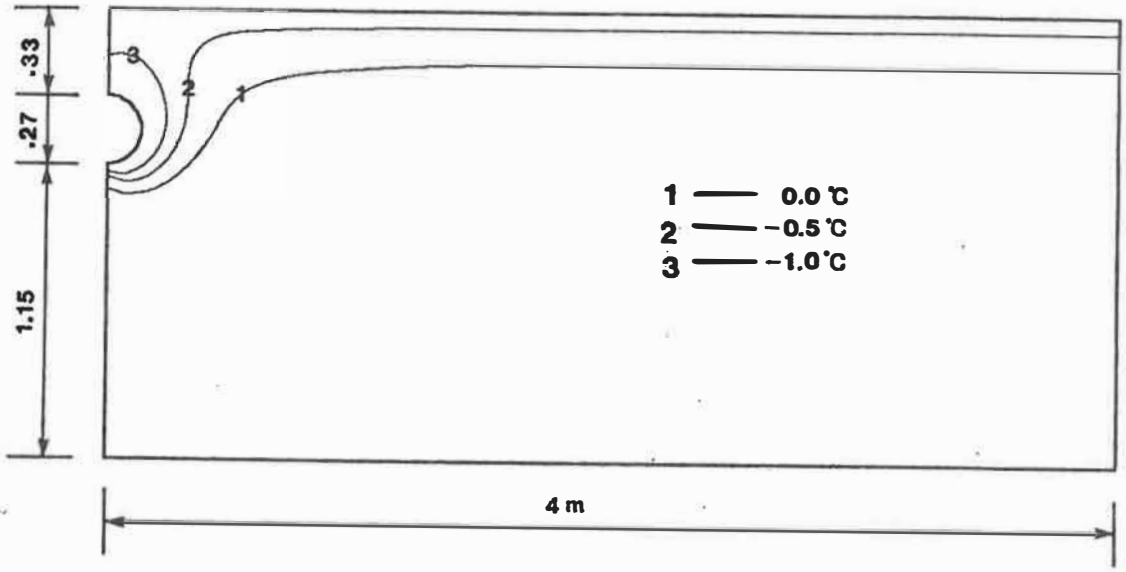

Figure 4.8: Simulated isotherms in the soil after 400 hours

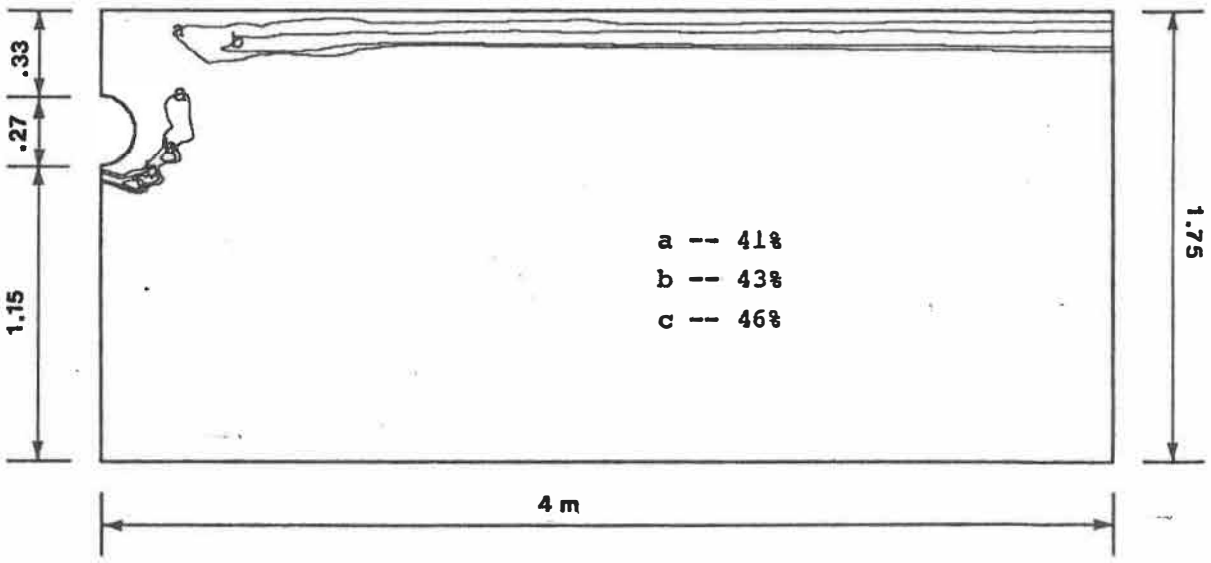

Figure 4.9: Simulated isolines of moisture content in the soil after 400 hours

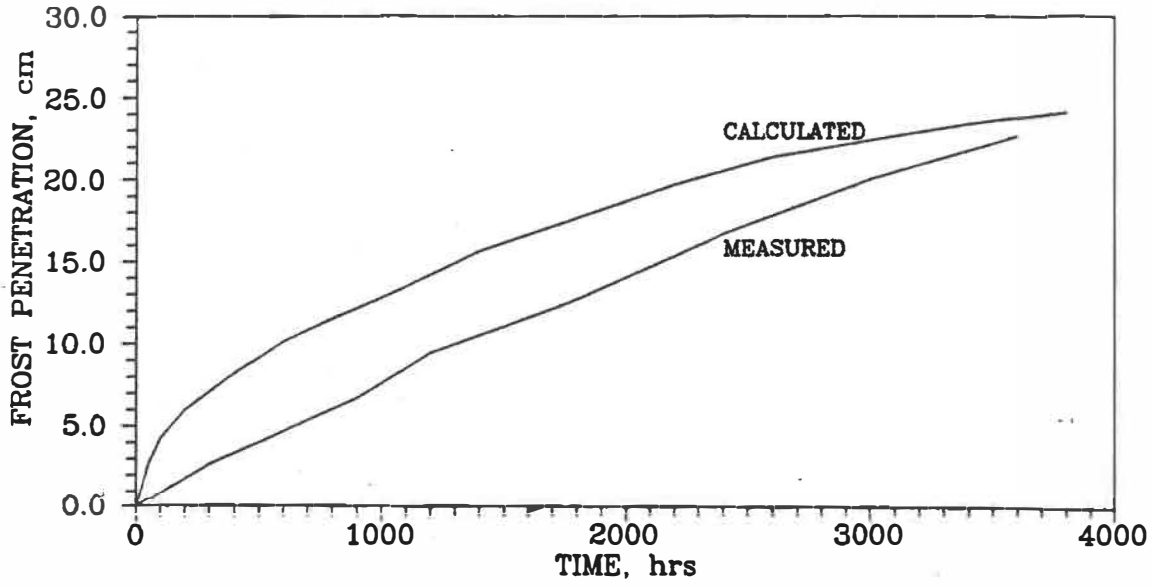

Figure 4.10: Comparison of simulated and measured frost penetration under the centreline of the pipe

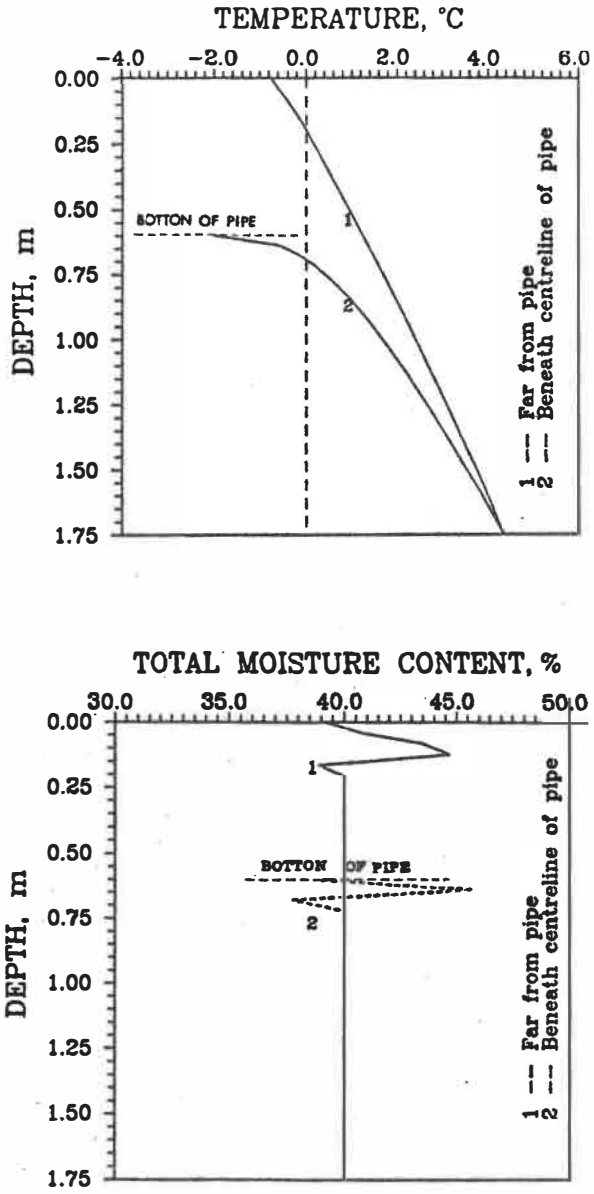

Figure 4.11: Simulated temperature and moisture profiles in the soil after 400 hours

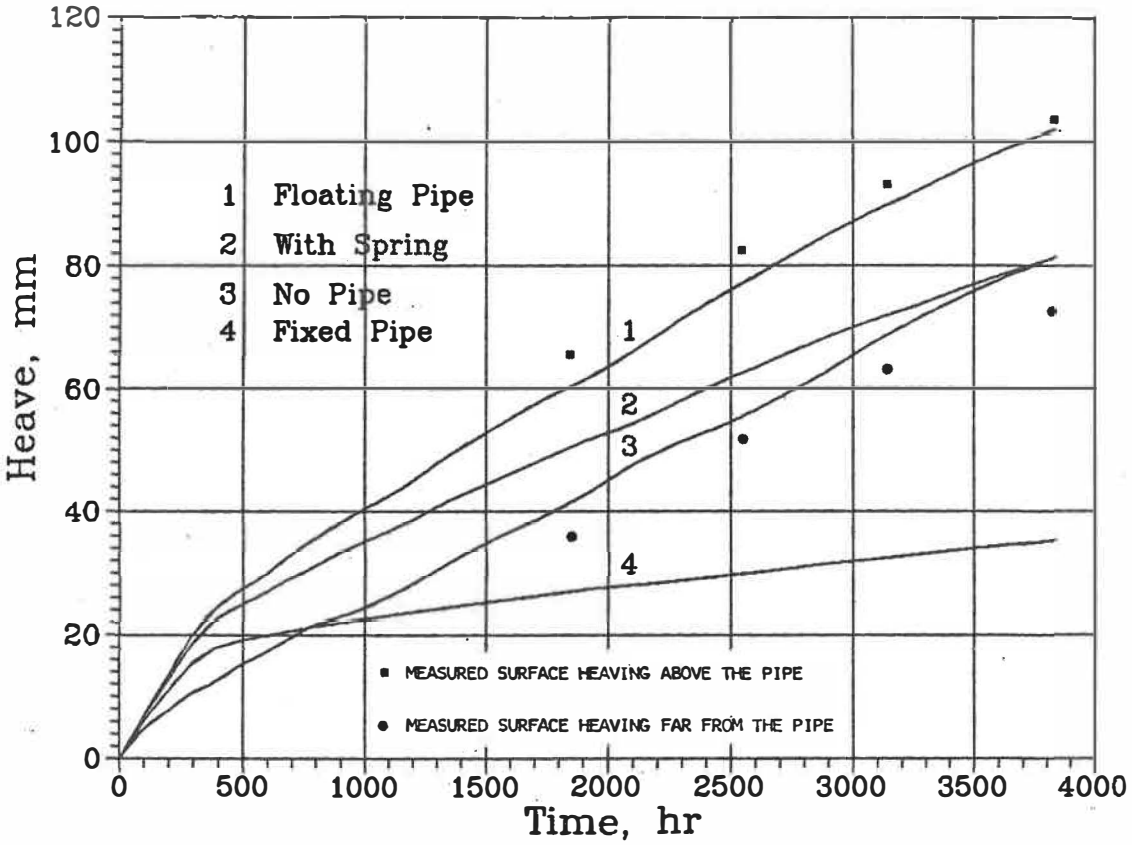

Figure 4.12: Simulated frost heave of the surface, $T_{pipe} = -2°C$

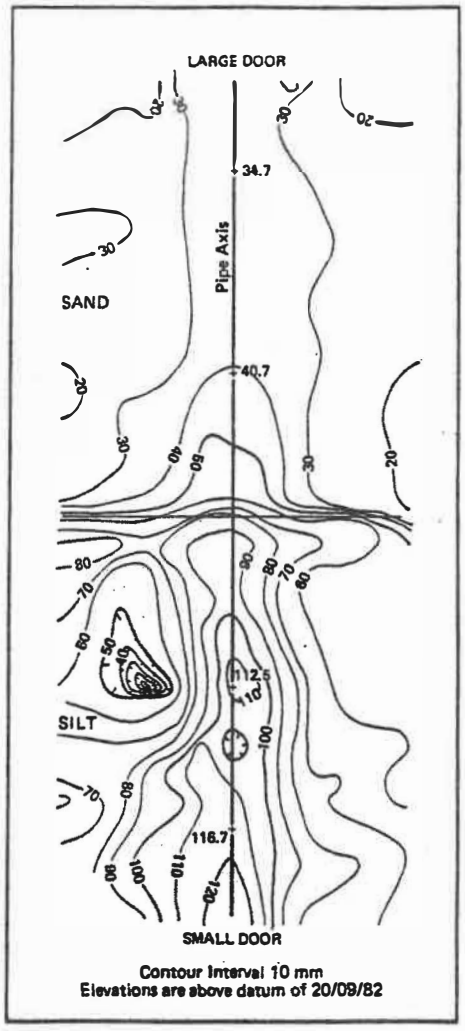

Figure 3.16 Elevation of soil surface, 05/04/83.

Figure 4.13: Measured elevation of soil surface, 04/05/1983 (approximately after 2700 hours; after Williams, 1983)

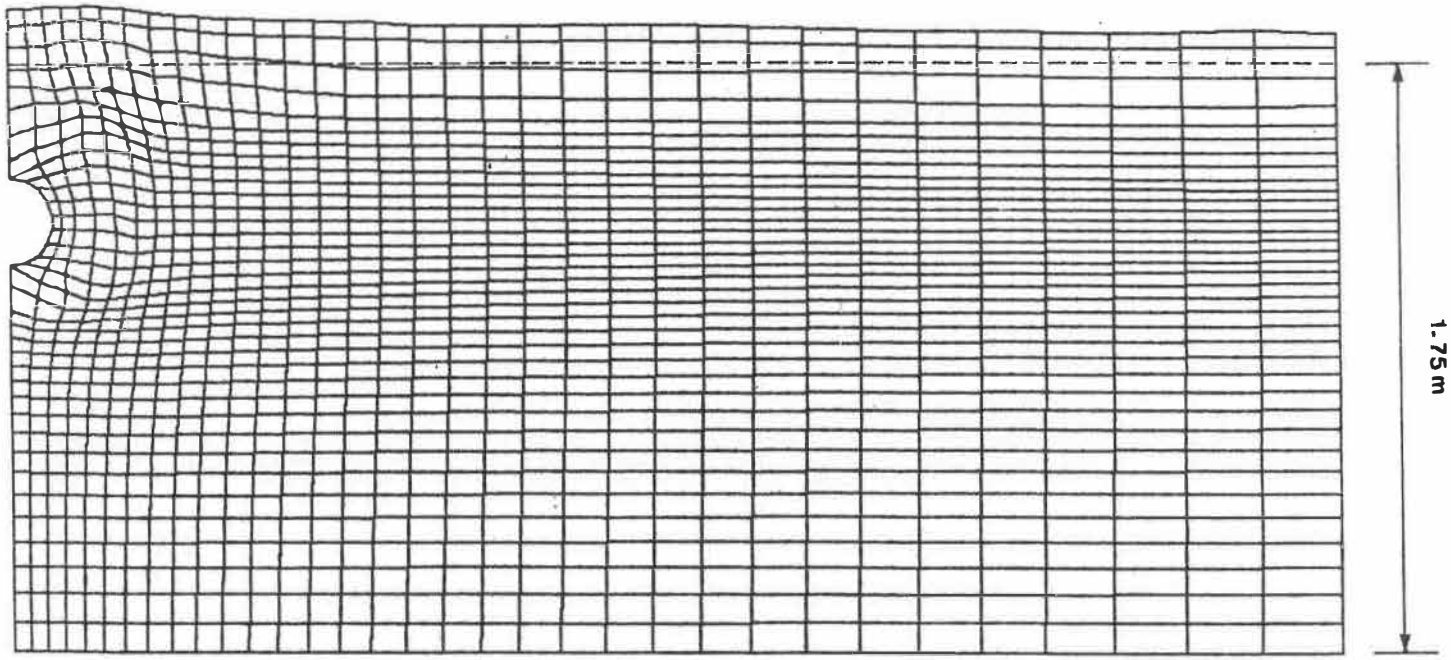

Figure 4.14: Deformed mesh for the fixed pipe case after 400 hours ($amp = 10$)

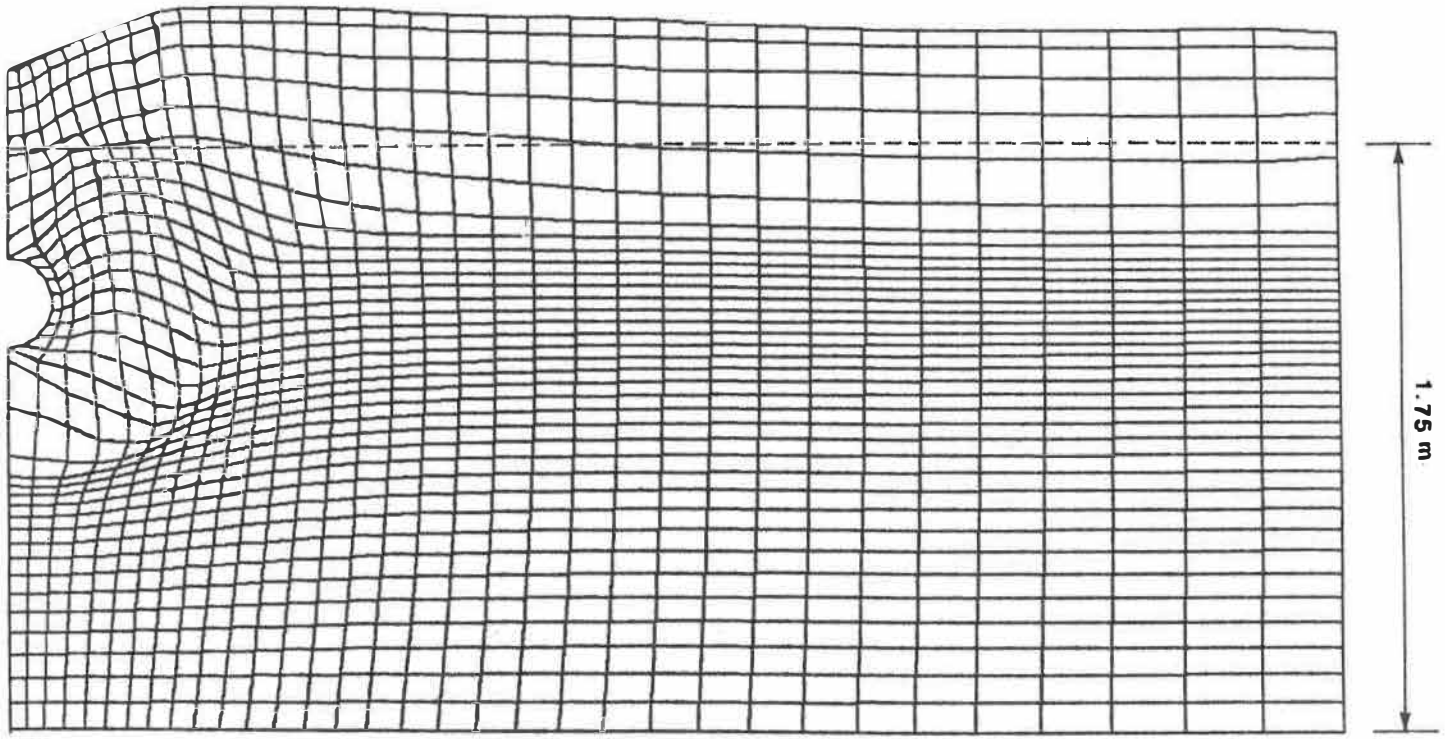

Figure 4.15: Deformed mesh for the fixed pipe case after 1600 hours ($amp = 10$)

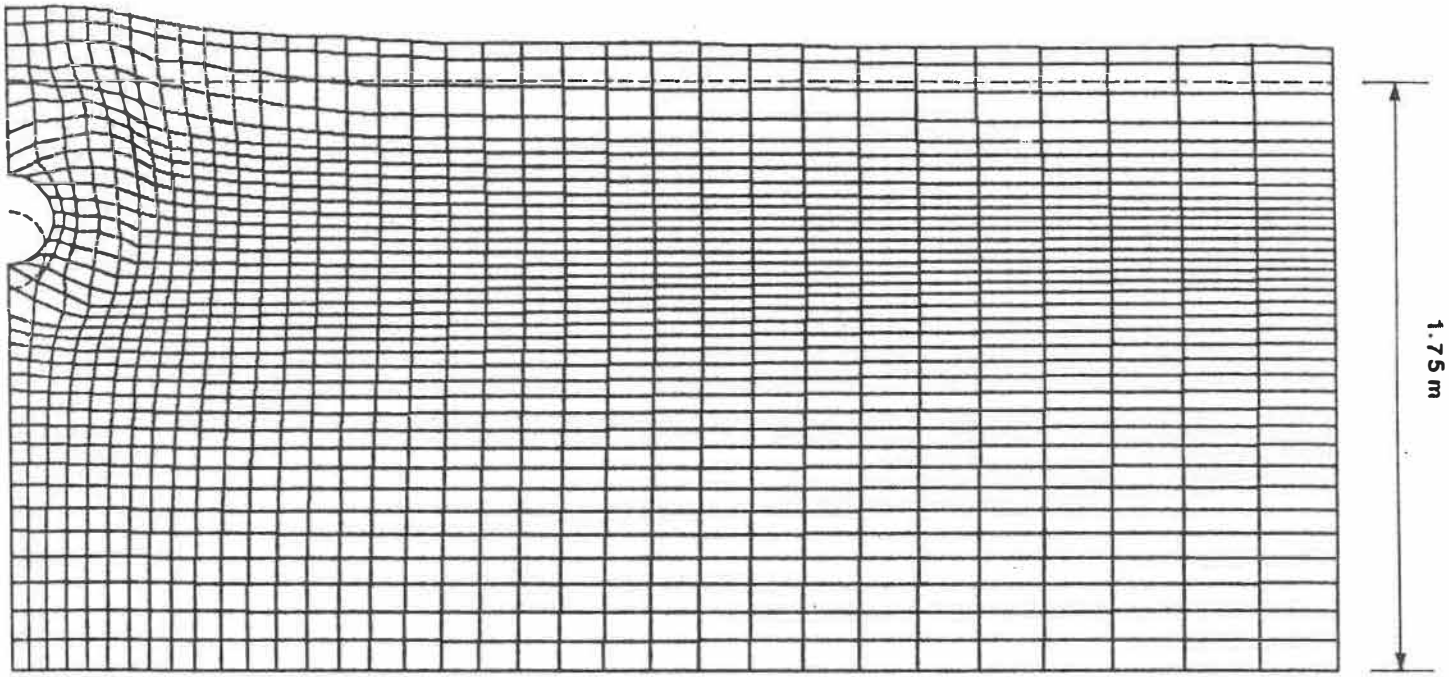

Figure 4.16: Deformed mesh for the floating pipe case after 400 hours ($amp = 10$)

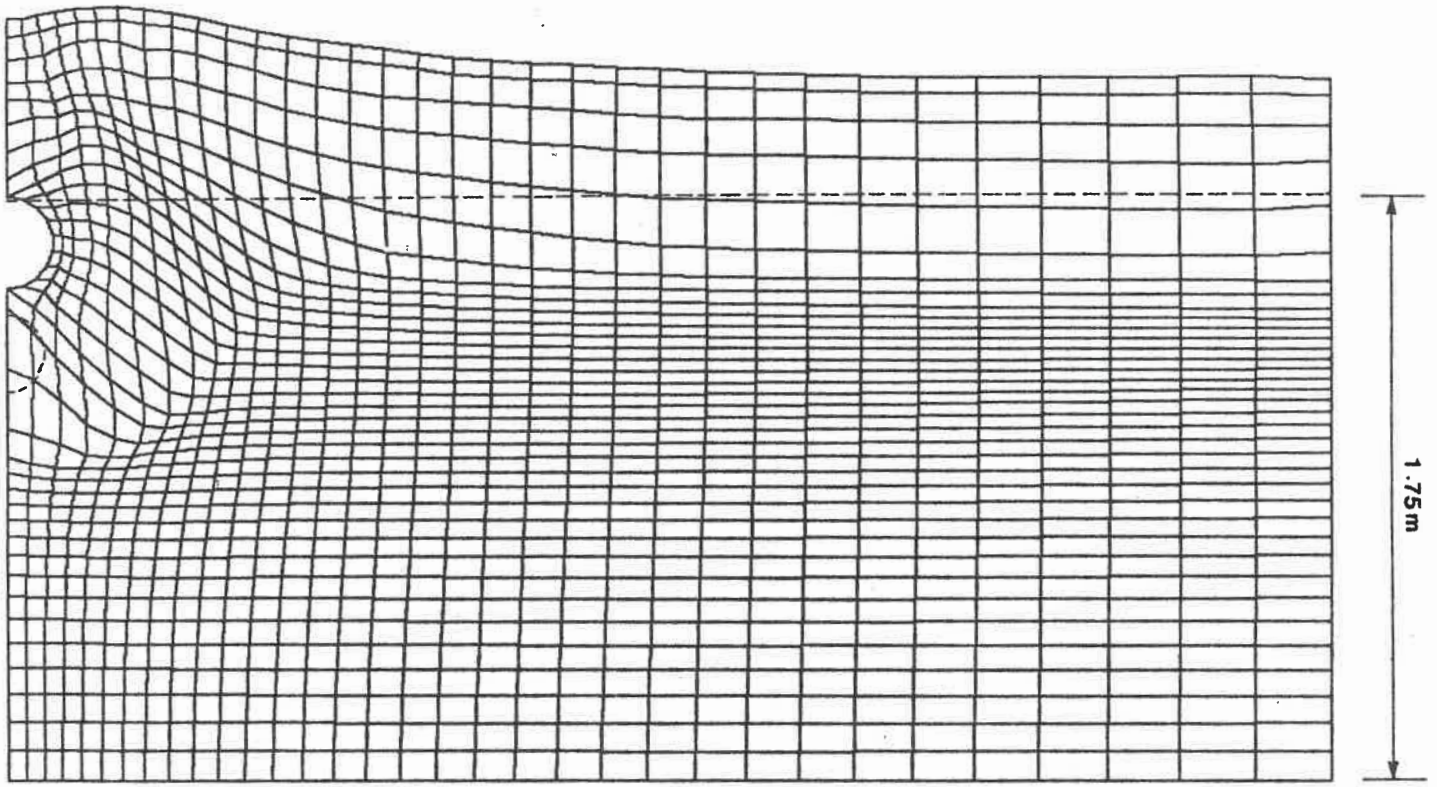

Figure 4.17: Deformed mesh for the floating pipe case after 1600 hours ($amp = 10$)

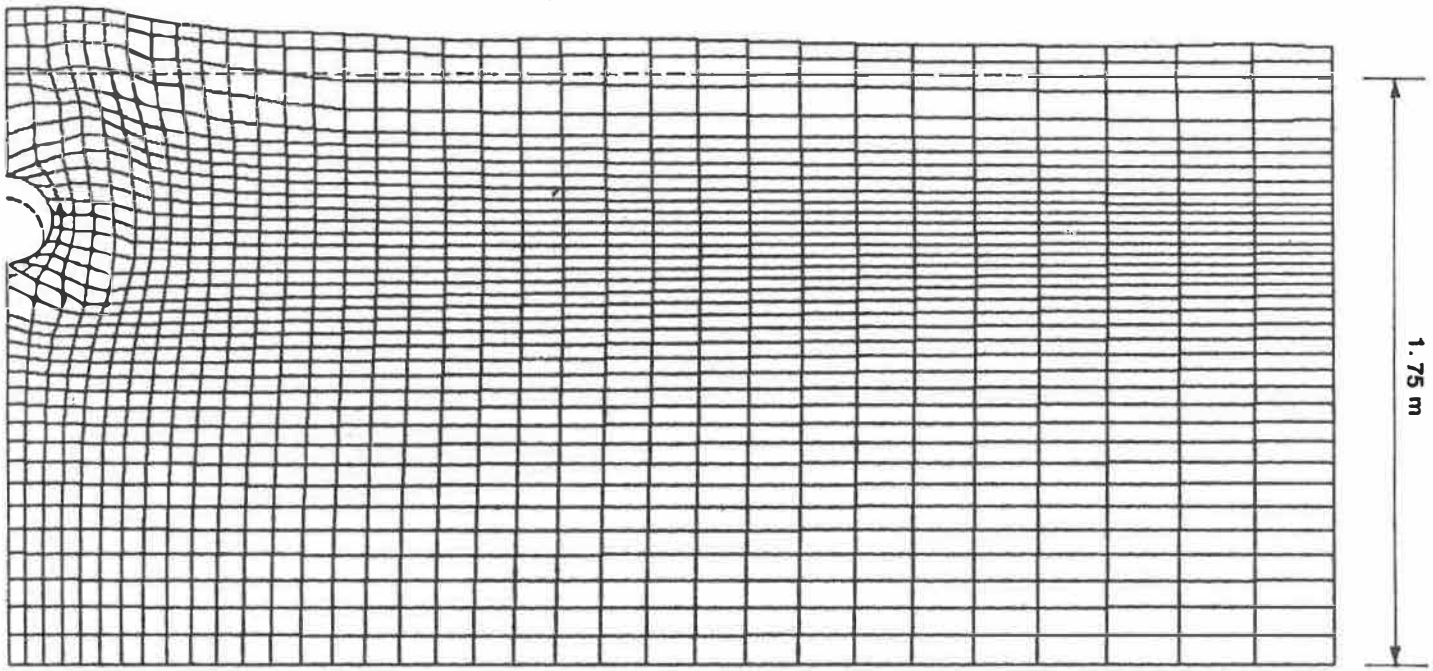

Figure 4.18: Deformed mesh for the virtual spring pipe case after 400 hours ($amp = 10$)

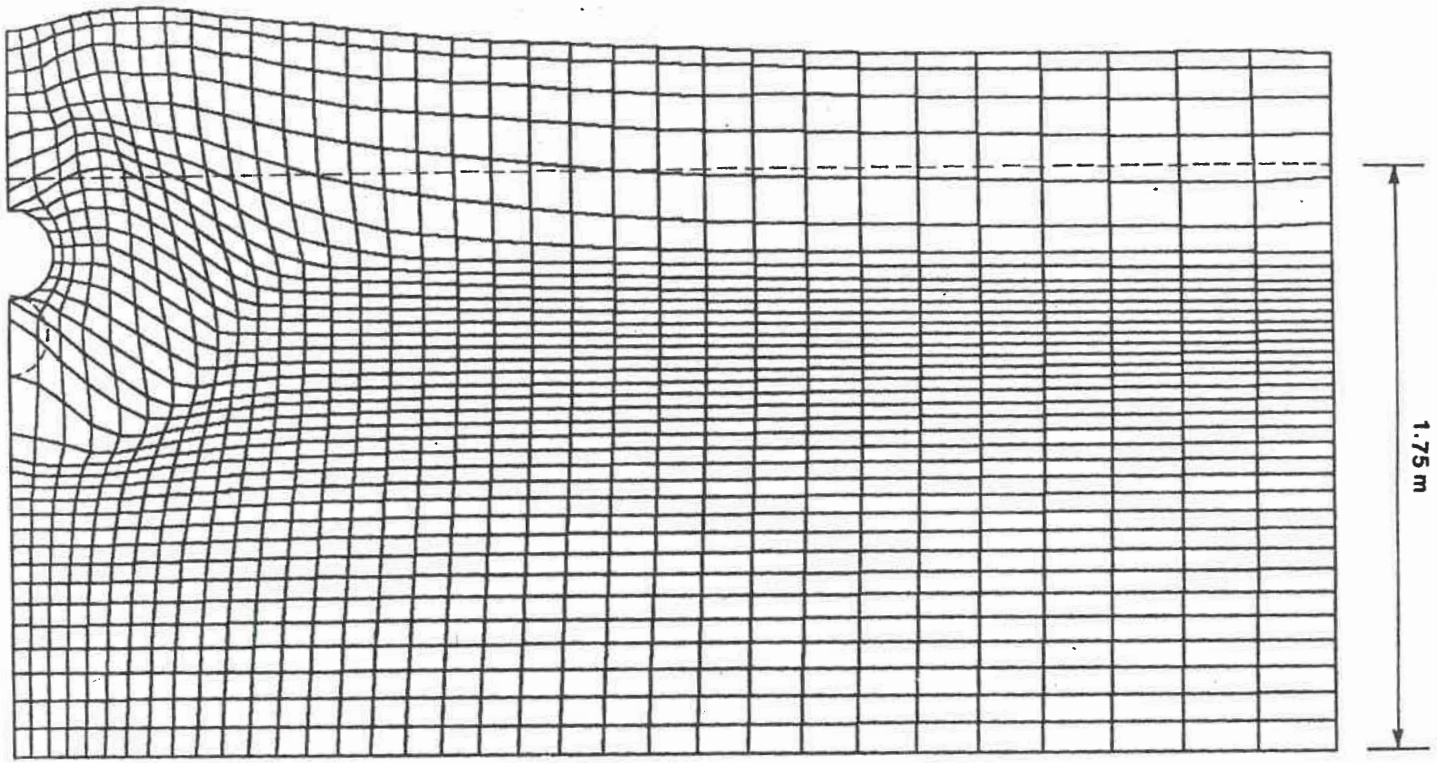

Figure 4.19: Deformed mesh for the virtual spring pipe case after 1600 hours ($amp = 10$)

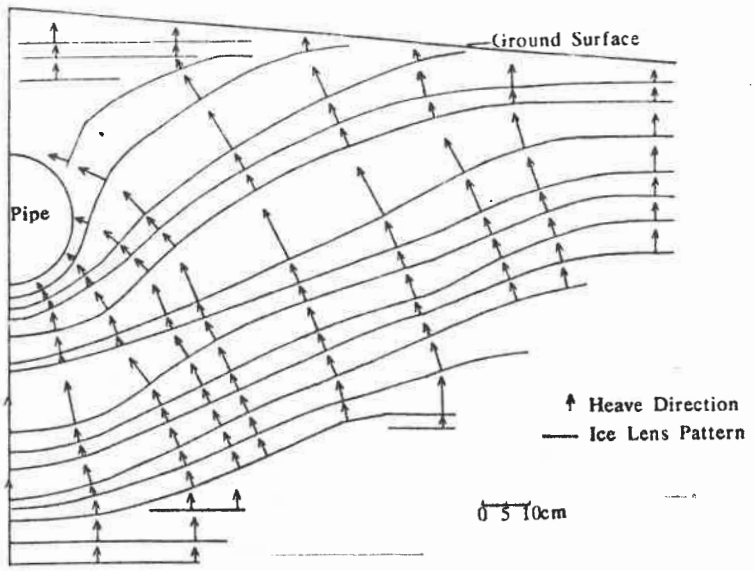

Figure 4.20: Ice lens orientation around a chilled pipe (after Smith and Williams, 1990)

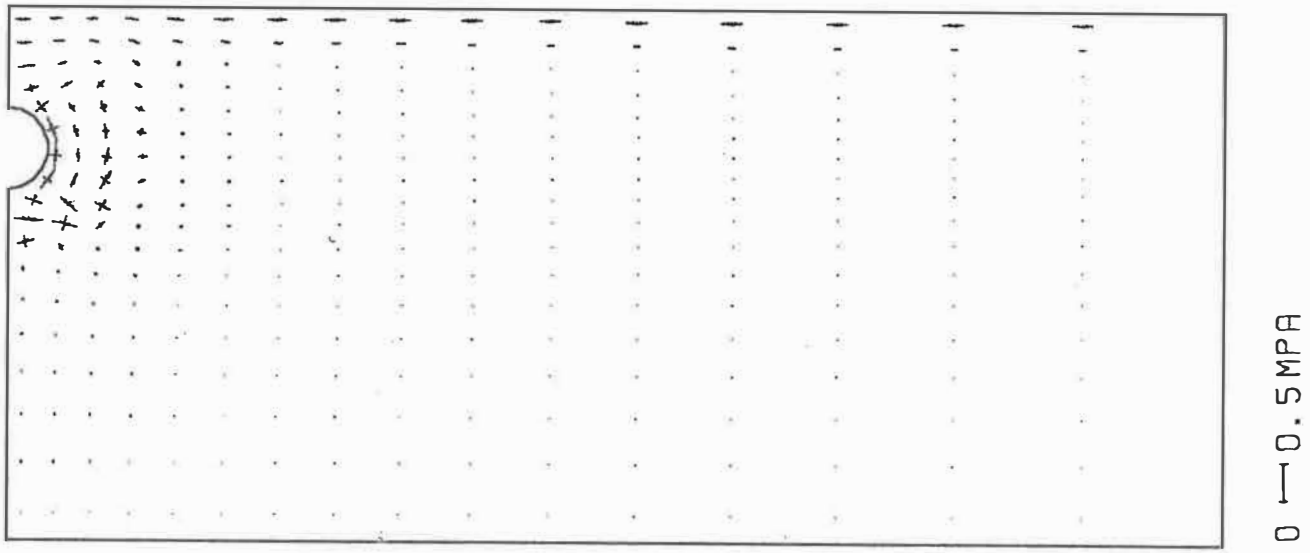

Figure 4.21: The distribution of simulated principal stresses in the soil after 400 hours

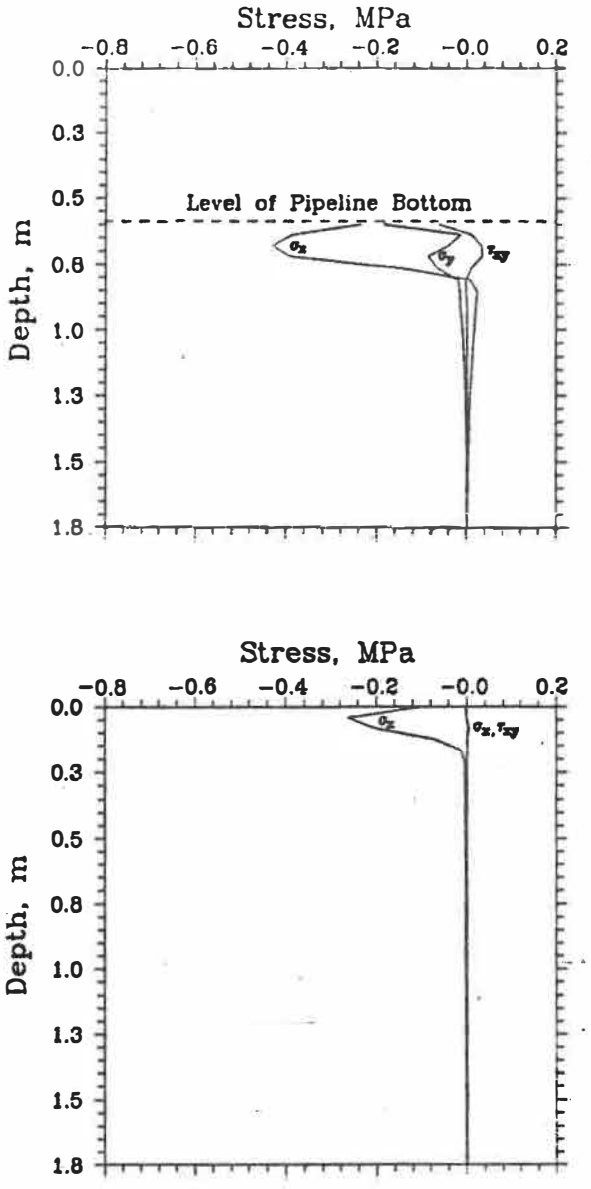

Figure 4.22: Simulated vertical stresses distribution after 400 hours (a) under the pipe; (b) far from the pipe

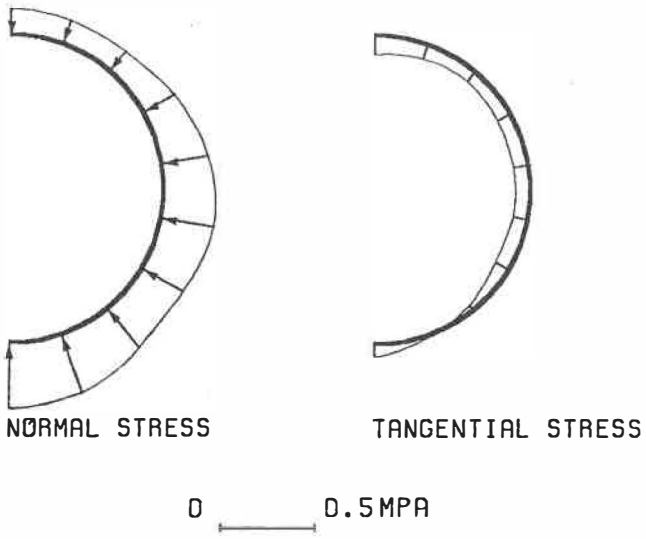

Figure 4.23: Stresses acting on the pipe for the fixed pipe case, after 400 hours

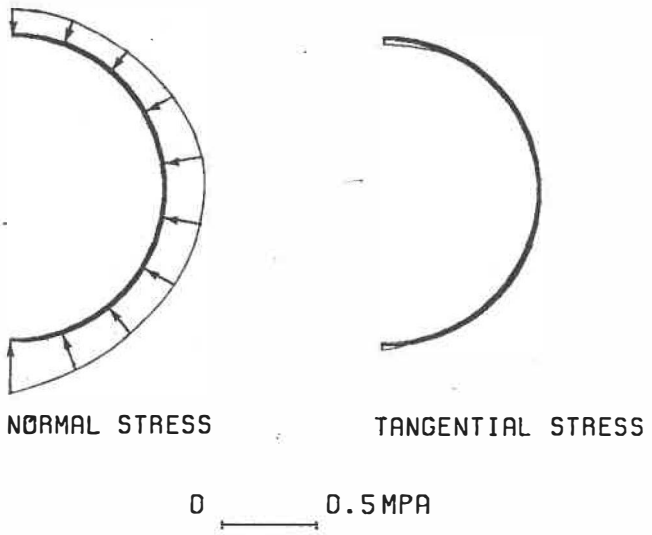

Figure 4.24: Stresses acting on the pipe for the floating pipe case, after 400 hours

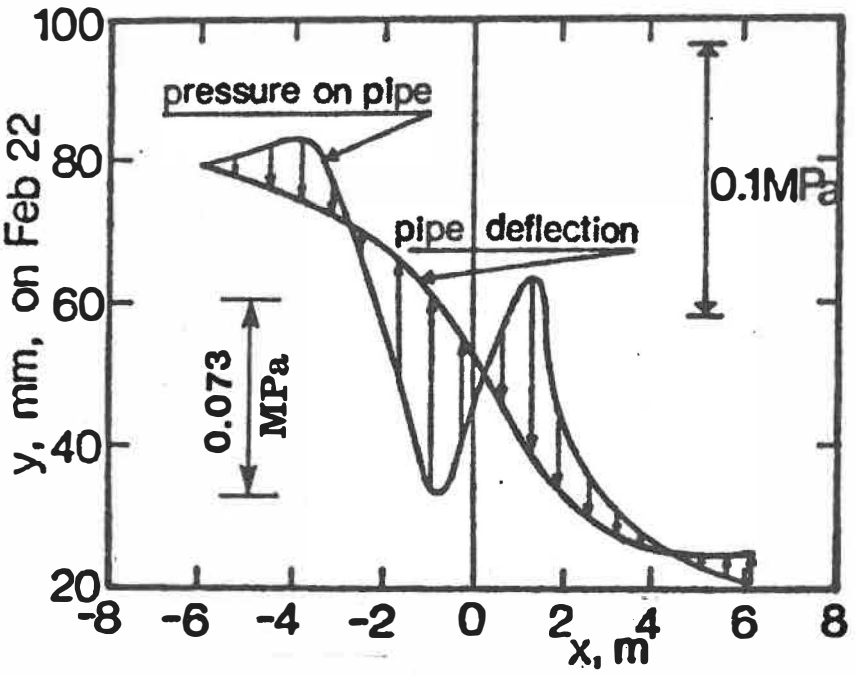

Figure 4.25: Diagram of soil pressure acting on pipeline (after Ladanyi and Lemaire, 1984)

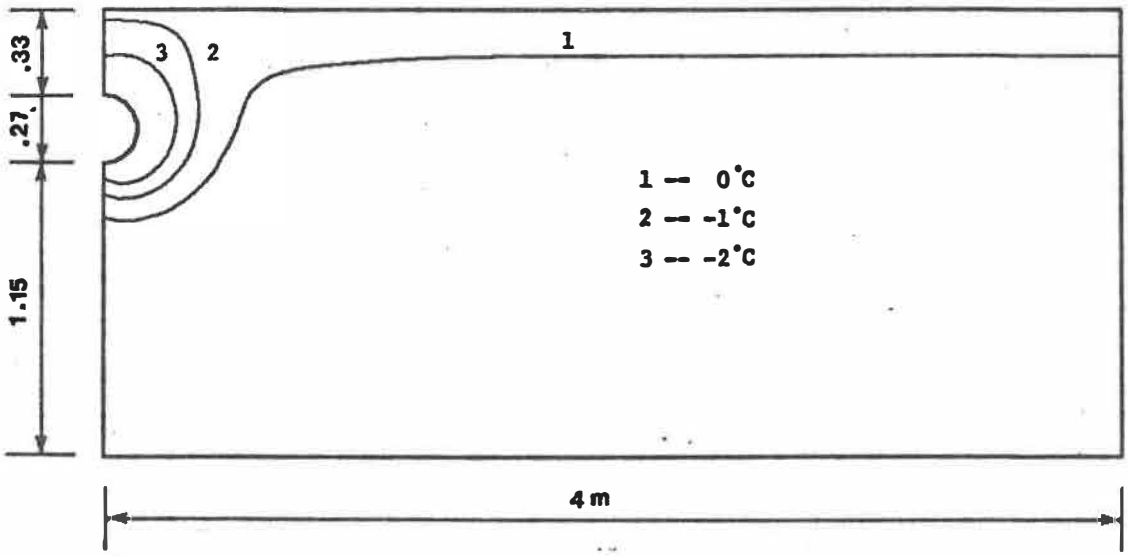

Figure 4.26: Simulated isotherms in the soil after 400 hours ($T_{pipe} = -5°C$)

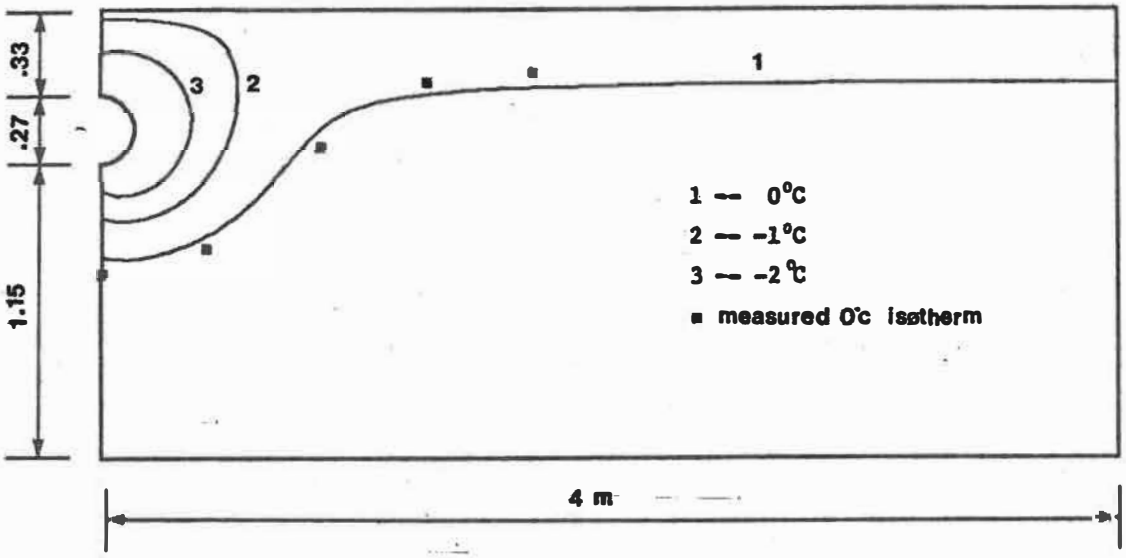

Figure 4.27: Simulated isotherms in the soil after 1600 hours ($T_{pipe} = -5°C$)

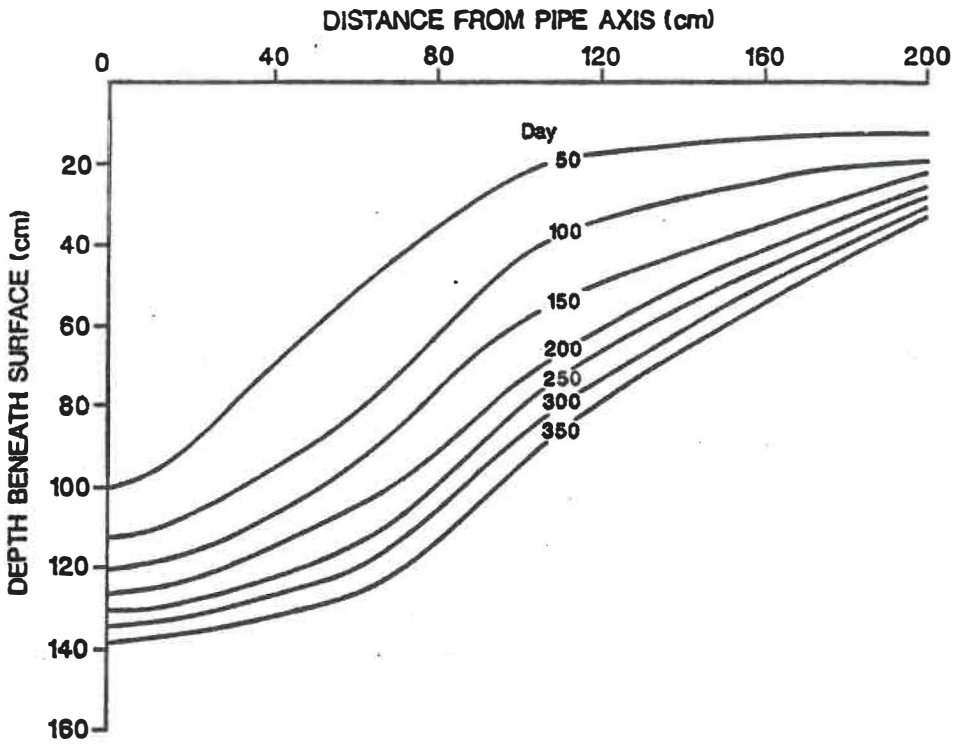

Figure 4.28: Measured $0°C$ isotherm in the silt section after a different time (in the 3rd freeze cycle) (after Williams, 1986c)

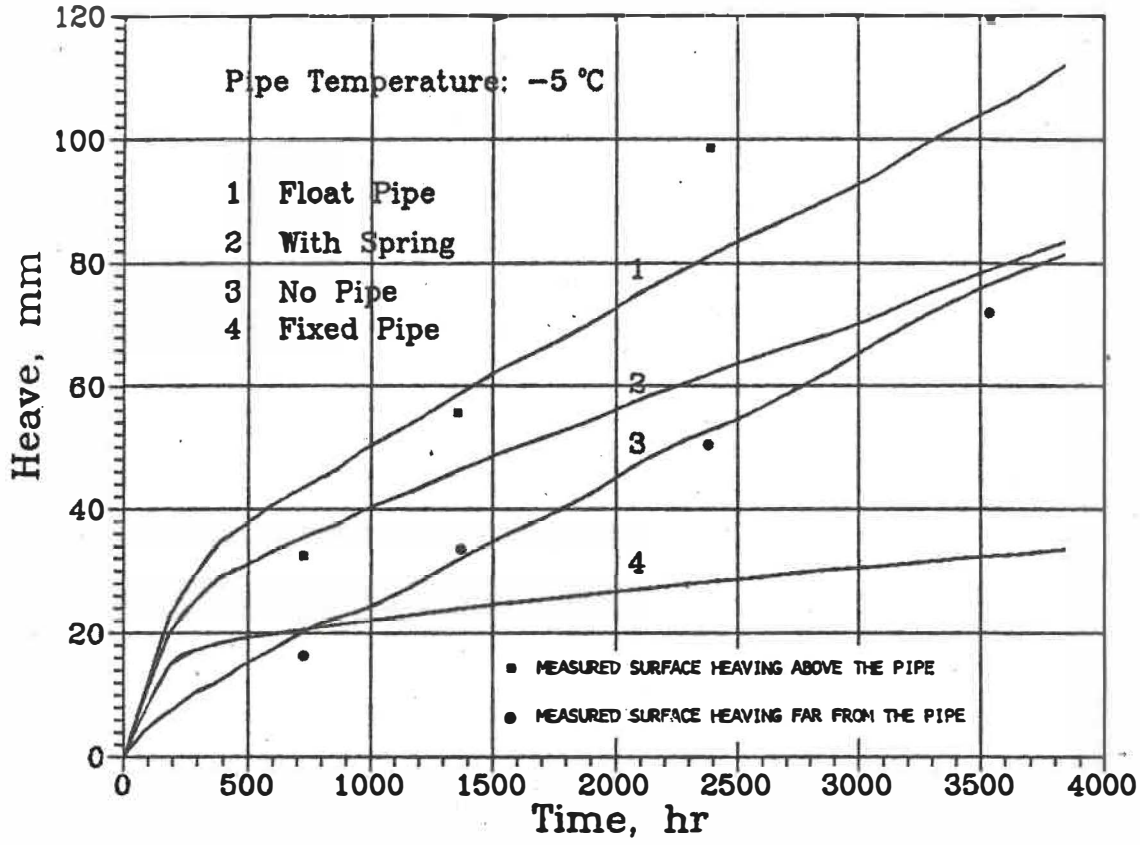

Figure 4.29: Simulated frost heave of surface ($T_{pipe} = -5°C$)

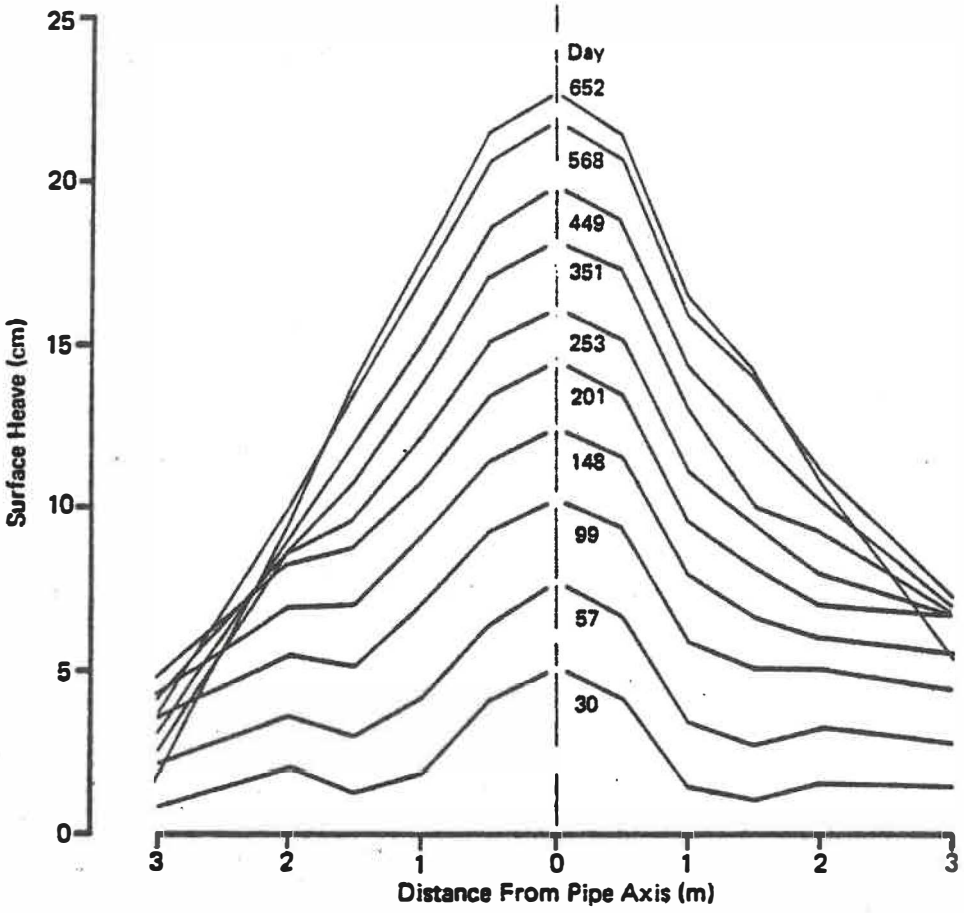

Figure 4.30: Measured surface relief in the silt section after a different time (in the 2nd freeze cycle) (after Williams, 1986b)

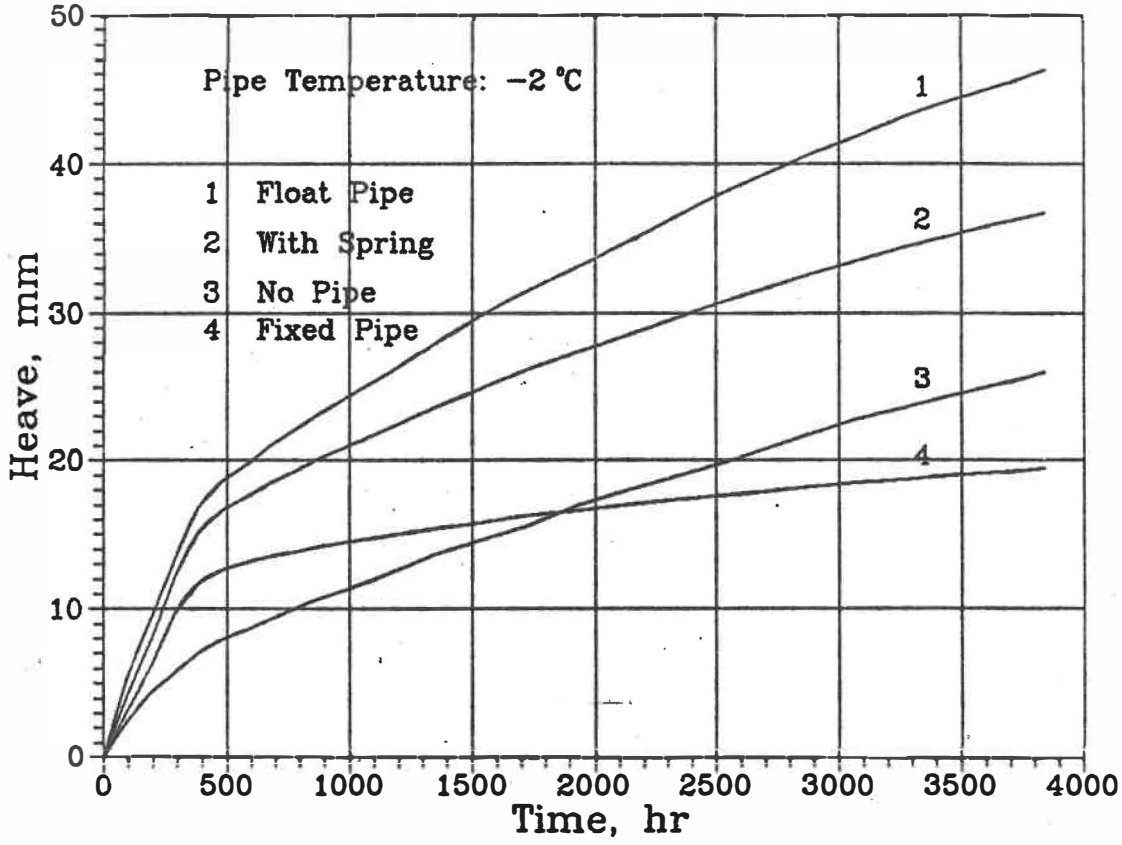

Figure 4.31: Simulated frost heave of surface ($T_{pipe} = -2°C$)

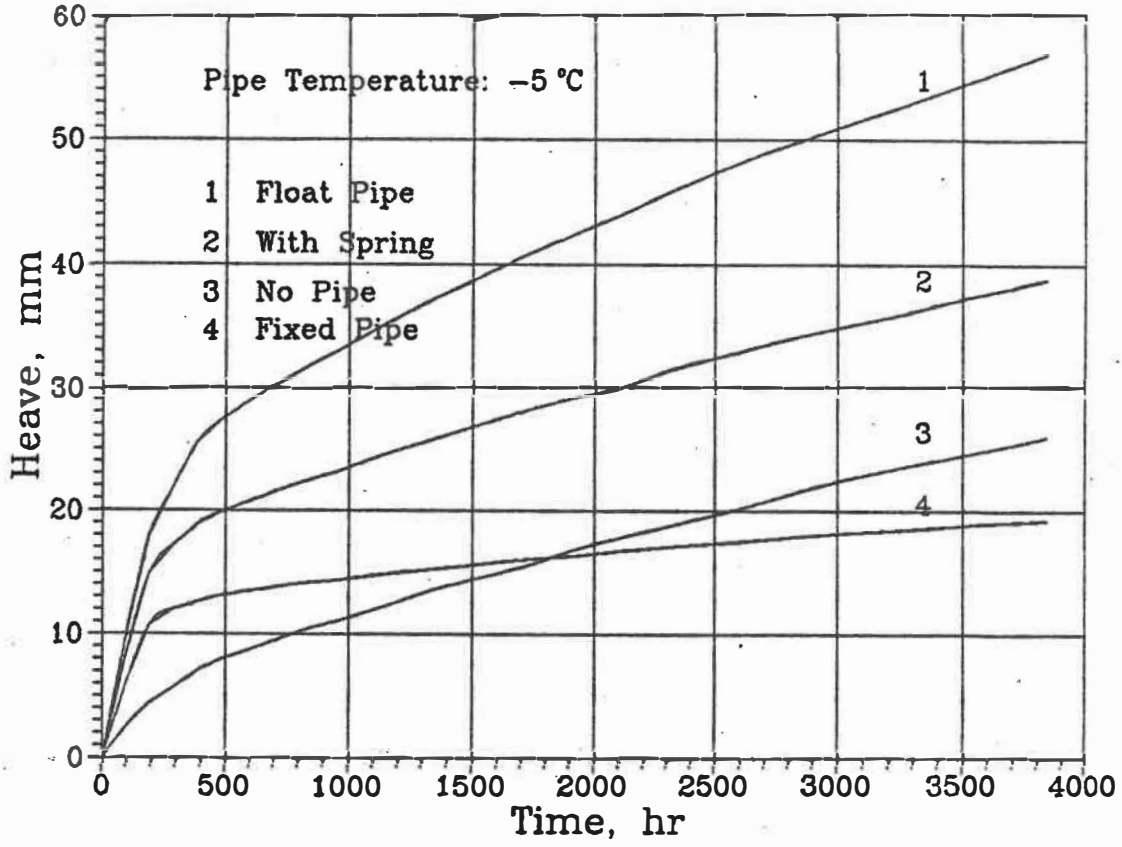

Figure 4.32: Simulated frost heave of surface ($T_{pipe} = -5°C$)

Appendix A

PROGRAM FOR THE SIMULATION OF THE CHILLED PIPELINE GROUND FREEZING TEST

```
C      ****************************************************************
C      *                                                              *
C      *     PROGRAM OF CALCULATING TEMPERATURE,FROST-HEAVING AND     *
C      *               STRESSES AROUND CHILLED PIPELINE               *
C      *        (CO-OPERATIVE FRANCE-CANADA RESEARCH PROJECT)         *
C      *                                                              *
C      *                        BY  SHEN MU                           *
C      *   CINEP, ECOLE POLYTECHNIQUE DE MONTREAL, H3C 3A7, CANADA    *
C      *     CREATED:  28/04/1989    LAST CORRECTION: 24/07/1990      *
C      *   ---------------------------------------------------------  *
C      *   MAIN ARGUMENTS:                                            *
C      *      (1)    MX,MY -- MAX. NUMBER OF GRID POINTS IN X AND Y   *
C      *                      DIRECTIONS. ( MX*MY MESH )              *
C      *      (2) G11(MX,MY),G12(MX,MY),G22(MX,MY)                   *
C      *                   -- COVARIANT METRIC TENSOR COMPONENTS      *
C      *                      DIVIDED BY SQUARE OF JACOBIAN           *
C      *      (3) PP(MX,MY),QQ(MX,MY)                                 *
C      *                   -- LAPLACIANS OF XI & ETA                  *
C      *      (4) TIM,DTIM -- TIME AND TIME STEP (HOUR)               *
C      *      (5)    ICTLF -- CONTROL VARIATION FOR CONFINEMENT       *
C      *                        = 0   FREE FLOATING PIPELINE          *
C      *                        = 1   FIXED PIPELINE                  *
C      *                                                              *
C      *   NOTES:                                                     *
C      *     (1)  ALL REALS IN DUMMY ARGUMENTS ARE SINGLE PRECISION   *
C      *     (2)  THE INCREMENTS OF  XI & ETA  EQUAL 1.0              *
C      *            ( MX*MY  MESH IN  XI-ETA  PLANE )                 *
C      *     (3)  L(F) = G22*FXIXI - 2*G12*FXIETA + G11*FETAETA +     *
C      *                 PP*FXI + QQ*FETA    ( L -- LAPLACIAN )       *
C      *                                                              *
C      ****************************************************************
C
C      PROGRAM    TEMPER
C
       PARAMETER  (MX = 34,   MY = 37,  MSUB=50)
       PARAMETER  (ME=2400,   MJ2=2600)
C
       INTEGER    I,  J,  LPTTW, LPTM, LSTW, LSM, ISTPM, ISM, IS,
     &            NJ, NE, NJ2,   LPTCTL, ISTCTL, ICTLF
       INTEGER*4  UNIT1, UNIT2
C
       REAL*4     TN(MX,MY),  DTN(MX,MY), RKC(MX,MY),
     &            A(MSUB),    B(MSUB),    C(MSUB),      F(MSUB),
     &            WL(MX,MY),  WI(MX,MY),  DV(MX,MY),    ATM(MX,MY),
     &            SEQ(ME),    U(MJ2),     STRAIN(ME,3), STRESS(ME,3)
```

```
      REAL*4     TIM,  DTIM, TMAX, TO,  SS1, SS2, SS3, TAIR, TPIPE,
     &           GAML, GAMI, WO,   TF,  UW1, UWN, UWA, RGLI, RLK
C
      COMMON   /SOIL/ TIM, DTIM, WO, TF, UWN, UWA, RGLI, RLK
      COMMON   /CURV/ G11(MX,MY), G12(MX,MY), G22(MX,MY), PP(MX,MY),
     &                QQ(MX,MY)
      COMMON   /HEAT/ TN,     DTN, WL,  WI,  DV,  ATM
      COMMON  /FORCE/ STRESS, U,   SEQ, STRAIN
C
C     ================================================================
C              INPUT AND DEFINE THE DATA USED IN CALCULATION
C         (1) UNIT1 -- THE NUMBER OF OUTPUT UNIT (CRT OR PRINTER)
C         (2) UNIT2 -- THE NUMBER OF I/O UNIT (DISK)
C     ================================================================
C
      UNIT1 = 6
      UNIT2 = 5
C
      TMAX  = 4000.0
      DTIM  = 4.0
      LPTTW = 2000
      LPTMS = 96
      LPTMD = 2000
      ISTPM = 2
C
      WRITE(*,*) 'PLEASE ENTER ICTLF = ?'
      READ(*,*)  ICTLF
      NJ   = MX*MY
      NE   = (MX - 1)*(MY - 1)*2
      IF  (ICTLF .EQ. 0) THEN
         NJ = NJ + 1
         NE = NE + 9
      END IF
      NJ2  = 2*NJ
C
      READ(UNIT2,*) ((G11(I,J),J=1,MY),I=1,MX)
      READ(UNIT2,*) ((G12(I,J),J=1,MY),I=1,MX)
      READ(UNIT2,*) ((G22(I,J),J=1,MY),I=1,MX)
      READ(UNIT2,*) (( PP(I,J),J=1,MY),I=1,MX)
      READ(UNIT2,*) (( QQ(I,J),J=1,MY),I=1,MX)
C
      TAIR  = -0.75
      TPIPE = -2.0
      TO    =  3.0
      WO    =  0.4
```

```
      UW1    =  0.17
      TF     = -0.1
C
      GAML   = 1000.0
      GAMI   = 916.8
      UWN    = ALOG(UW1/W0)/ALOG(ABS(TF))
      UWA    = W0*ABS(TF)**UWN
      RGLI   = GAML/GAMI
      RLK    = 3600.0/9.8E+03
C
      TIM  = 0.0
      LSTW = 0
      LSMS = 0
      LSMD = 0
      ISM  = 0
      DO 2000  I = 1 , MX
      DO 2000  J = 1 , MY
        TN(I,J)  = T0
        WL(I,J)  = W0
        WI(I,J)  = 0.0
        DV(I,J)  = 0.0
2000  CONTINUE
C
      CALL   SD(ICTLF, TIM, DTIM, TF, W0)
C
C     ================================================================
C             CALCULATING THE TEMPERATURE FIELD BY ADI METHOD
C                  USING CURVILINEAR COORDINATE SYSTEMS
C     ================================================================
C
      LPTCTL = 0
      ISTCTL = 0
C
2100  CONTINUE
      TIM  = TIM + DTIM
C
      IF  ((TIM .GT. 400.0) .AND. (ISTCTL .EQ. 0)) THEN
         ISTCTL = 1
         ISTPM  = 2*ISTPM
      END IF
C
      IF  ((TIM .GT. 1000.0) .AND. (LPTCTL .EQ. 0)) THEN
         LPTCTL = 1
         LPTTW  = 2*LPTTW
         LPTMS  = 2*LPTMS
```

```
         LPTMD  = 2*LPTMD
        END IF
C
C       ------------------------------------------------------------
C        DEFINING BOUNDARY CONDITIONS AND THERMAL PARAMETERS RKC (=K/C)
C           (1)  RKC(MX,MY) -- RATIO BETWEEN  K  AND  C
C       ------------------------------------------------------------
C
        CALL   PARAM1(RKC)
C
        DO 3000  J = 20 , 29
          IF  (ABS(TIM-DTIM) .LT. 1.0E-05) THEN
             DTN(1,J) = TPIPE - T0
          ELSE
             DTN(1,J) = 0.0
          END IF
3000    CONTINUE
C
C       ------------------------------------------------------------
C                              XI-DIRECTION
C       ------------------------------------------------------------
C
        DO 3100  J = 2 , MY-1
          DO 3110  I = 2 , MX-1
            SS1  =  DTIM*RKC(I,J)*0.5
            SS2  =  G22(I,J)*SS1
            SS3  =  PP(I,J) *SS1*0.5
            A(I) = -SS2 + SS3
            B(I) =  SS2 + SS2 + 1.0
            C(I) = -SS2 - SS3
C
            SS1  = TN(I+1,J) - 2.*TN(I,J) + TN(I-1,J)
            SS2  = TN(I,J+1) - 2.*TN(I,J) + TN(I,J-1)
            F(I) = SS1*G22(I,J) + SS2*G11(I,J)
            F(I) = F(I) + PP(I,J)*(TN(I+1,J) - TN(I-1,J))*0.5
            F(I) = F(I) + QQ(I,J)*(TN(I,J+1) - TN(I,J-1))*0.5
C
            SS1  = TN(I+1,J+1) - TN(I+1,J-1) - TN(I-1,J+1) + TN(I-1,J-1)
            F(I) = F(I) - SS1*G12(I,J)*0.5
            F(I) = F(I)*DTIM*RKC(I,J)
3110      CONTINUE
C
          SS1     = G12(MX-1,J)/G22(MX-1,J)
          B(MX-1) = B(MX-1) + C(MX-1)/(1.0 - SS1)
          F(MX-1) = F(MX-1) + C(MX-1)*SS1*DTN(MX,J-1)/(1.0 - SS1)
```

```
C
          IF  ((J .LT. 20) .OR. (J .GT. 29)) THEN
             SS1  = G12(2,J)/G22(2,J)
             B(2) = B(2) + A(2)/(1.0 - SS1)
             F(2) = F(2) + A(2)*SS1*DTN(1,J-1)/(1.0 - SS1)
          ELSE
             F(2) = F(2) - A(2)*DTN(1,J)
          END IF
C
          IS = MX - 1
          CALL   TRID2(MSUB,2,IS,A,B,C,F)
C
          DO 3130  I = 2 , MX-1
            DTN(I,J) = F(I)
3130      CONTINUE
C
3100    CONTINUE
C
C       ------------------------------------------------------------------
C                                ETA-DIRECTION
C       ------------------------------------------------------------------
C
        IF  (TIM .LE. 50.0*24.0) THEN
           SS1 = -2.0*DTIM/(50.*24.)
        ELSEIF (TIM .LE. 100.*24.) THEN
           SS1 = -0.5*DTIM/(50.*24.)
        ELSEIF (TIM .LE. 280.0*24.0) THEN
           SS1 = 0.0
        ELSEIF (TIM .LE. 372.0*24.0) THEN
           SS1 = 2.5*DTIM/(92.*24.)
        END IF
        DO 3010  I = 1 , MX
          IF  (ABS(TIM-DTIM) .LT. 1.0E-05) THEN
             DTN(I,1)  = 2.0
             DTN(I,MY) = TAIR - T0
          ELSE
             DTN(I,1)  = SS1
             DTN(I,MY) = 0.0
          END IF
3010    CONTINUE
C
        DO 3200  I = 2 , MX-1
          DO 3210  J = 2 , MY-1
            SS1  =  DTIM*RKC(I,J)*0.5
            SS2  =  G11(I,J)*SS1
```

```
            SS3  =  QQ(I,J) *SS1*0.5
C
            A(J) = -SS2 + SS3
            B(J) =  SS2 + SS2 + 1.0
            C(J) = -SS2 - SS3
            F(J) =  DTN(I,J)
3210        CONTINUE
C
          F(2)    = F(2)    - A(2)*DTN(I,1)
          F(MY-1) = F(MY-1) - C(MY-1)*DTN(I,MY)
C
          IS = MY - 1
          CALL   TRID2(MSUB,2,IS,A,B,C,F)
C
          DO 3230  J = 2 , MY-1
            DTN(I,J) = F(J)
3230      CONTINUE
C
3200    CONTINUE
C
        DO 3240  J = 2 , MY-1
          IF  ((J .LT. 20) .OR. (J .GT. 29)) THEN
             SS1 = G12(2,J)/G22(2,J)
             DTN(1,J) = (DTN(2,J) - DTN(1,J-1)*SS1)/(1.0 - SS1)
          END IF
          SS1       = G12(MX-1,J)/G22(MX-1,J)
          DTN(MX,J) = (DTN(MX-1,J) - DTN(MX,J-1)*SS1)/(1.0 - SS1)
3240    CONTINUE
C
        DO 3300  I = 1 , MX
        DO 3300  J = 1 , MY
          TN(I,J) = TN(I,J) + DTN(I,J)
3300    CONTINUE
C
        CALL   MOIST
C
        ISM = ISM + 1
        IF  (ISM .GE. ISTPM) THEN
           ISM = 0
           CALL   SD(ICTLF, TIM, DTIM, TF, WO)
C
           DO 3310  I = 1 , MX
             DO 3310  J = 1 , MY
               DV(I,J) = 0.0
3310       CONTINUE
```

```
      END IF
C
C     ---------------------------------------------------------------
C
      LSTW = LSTW + 1
      IF  (LSTW .EQ. LPTTW) THEN
         LSTW = 0
         WRITE(UNIT1,'(1X//1X,''TIME='',F7.1,1X,''HOUR'',1X/)') TIM
         WRITE(UNIT1,'(1X,''TEMPERTURE FIELD'',1X/)')
         WRITE(UNIT1,4000) ((TN(I,J), J=1,MY), I=1,MX)
4000     FORMAT(1X,10(F6.3,1X))
C
         DO 4010  I = 1 , MX
         DO 4010  J = 1 , MY
           SS1 = WL(I,J) + WI(I,J) - W0
           IF  (SS1 .LT. 0.0) THEN
              ATM(I,J) =  WL(I,J) + WI(I,J)/RGLI
           ELSE
              ATM(I,J) = (WL(I,J) + WI(I,J)/RGLI)/(1.0 + SS1)
           END IF
4010     CONTINUE
         WRITE(UNIT1,'(1X/1X,''TOTAL MOISTURE CONTENT FIELD'',1X/)')
         WRITE(UNIT1,4020) ((ATM(I,J), J=1,MY), I=1,MX)
4020     FORMAT(1X,10(F6.3,1X))
      END IF
C
      LSMS = LSMS + 1
      LSMD = LSMD + 1
      IF  (LSMS .EQ. LPTMS) THEN
         LSMS = 0
         IF  (LPTMS .LT. LPTTW) THEN
            WRITE(UNIT1,'(1X//1X,''TIME='',F7.1,1X,''HR'')') TIM
         END IF
         WRITE(UNIT1,'(1X,''STRESS FIELD'',1X/)')
         WRITE(UNIT1,4030) ((STRESS(IE,J), J=1,3), IE=1,NE)
4030     FORMAT(1X,6E12.4)
      END IF
C
      IF  (LSMD .EQ. LPTMD) THEN
         LSMD = 0
         IF  ((LPTMD .LT. LPTTW) .AND. (LPTMD .LT. LPTMS))  THEN
            WRITE(UNIT1,'(1X//1X,''TIME='',F7.1,1X,''HR'')') TIM
         END IF
         WRITE(UNIT1,'(1X,''DISPLACEMENT'',1X/)')
         WRITE(UNIT1,'(8(E10.3,1X))') (U(I), I=1,NJ2)
```

```
      END IF
C
C
      IF  (ABS(TIM-TMAX) .GT. 1.0E-05)  THEN
        GOTO 2100
      END IF
C
      STOP
      END
C
C     ****************************************************************
C                 SUBROUTINE OF CALCULATING MOISTURE FIELD
C
C     (1)     WL, WI -- VOLUMETRIC FRACTIONS OF LIQUID WATER AND ICE
C     (2)  GAML,GAMI -- DENSITIES OF LIQUID WATER AND ICE, kg/m*m*m
C     (3)          L -- LATENT HEAT OF FUSION, 3.336E+05 J/kg
C     (4)       H(T) -- HYDRAULIC CONDUCTIVITY OF FREEZING SOIL
C                       (-0.3 < T < TF),  m/sec
C     (5)         HT -- HYDRAULIC CONDUCTIVITY OF THAW SOIL, m/sec
C     (6)        HDT -- HYDRAULIC CONDUCTIVITY OF FROZEN SOIL (T<-.3)
C     ****************************************************************
C
      SUBROUTINE   MOIST
C
      PARAMETER  (MX = 34,   MY = 37)
C
      REAL*4   TN(MX,MY),  WL(MX,MY), WI(MX,MY), DV(MX,MY),
     &         ATM(MX,MY), DTN(MX,MY)
      REAL*4   L,   GAML,  GAMI,  RGLI,  RLK,  ALF,  SSW,  SS1, SS2,
     &         TXP, TXM,   TYP,   TYM,   HIJ,  HXP,  HXM,  HYP, HYM,
     &         PIJ, PIPJP, PIPJM, PIMJP, PIMJM,PIPJ, PIMJ, PIJP,PIJM
C
      COMMON   /SOIL/ TIM, DTIM, WO, TF, UWN, UWA, RGLI, RLK
      COMMON   /CURV/ G11(MX,MY), G12(MX,MY), G22(MX,MY), PP(MX,MY),
     &                QQ(MX,MY)
      COMMON   /HEAT/ TN, DTN, WL, WI, DV, ATM
C
      DATA     L/0.3336E+06/,   GAML/1000.0/,    GAMI/916.8/,
     &         HT/0.0000E-00/,  HFD/8.0499E-13/
C
      H(T)    = 1.0750E-09*EXP(23.99*T)
      P(T,TF) = 0.3336E+09*ALOG((T+273.16)/(TF+273.16))
C
      DO 3000  I = 2 , MX-1
      DO 3000  J = 2 , MY-1
```

```
C
C       ------------------------------------------------------
C                 DETERMINING THE HYDRAULIC CONDUCTIVITIES
C          (1)      HIJ -- HYDRAULIC CONDUCTIVITY AT (I,J)
C          (2)  HXP,HXM -- HYDRAULIC CONDUCTIVITIES AT (I+.5, J)
C                          AND (I-.5, J)
C          (3)  HYP,HYM -- HYDRAULIC CONDUCTIVITIES AT (I, J+.5)
C                          AND (I, J-.5)
C
C          ( * -- THE UNIT OF HYDRAULIC CONDUC. IS 'm*m/Hour/Pa' )
C       ------------------------------------------------------------
C
        TIJ = TN(I,J)
        TXP = (TN(I+1,J) + TN(I,J)) * 0.5
        TXM = (TN(I-1,J) + TN(I,J)) * 0.5
        TYP = (TN(I,J+1) + TN(I,J)) * 0.5
        TYM = (TN(I,J-1) + TN(I,J)) * 0.5
C
        HIJ = HT
        HXP = HT
        HXM = HT
        HYP = HT
        HYM = HT
C
        IF  (TN(I,J) .LE. TF) THEN
           HIJ = HFD
           IF  (TN(I,J) .GE. -0.3)  HIJ = H(TN(I,J))
        END IF
C
        IF  (TXP .LE. TF) THEN
           HXP = HFD
           IF  (TXP .GE. -0.3)  HXP = H(TXP)
        END IF
C
        IF  (TXM .LE. TF) THEN
           HXM = HFD
           IF  (TXM .GE. -0.3)  HXM = H(TXM)
        END IF
C
        IF  (TYP .LE. TF) THEN
           HYP = HFD
           IF  (TYP .GE. -0.3)  HYP = H(TYP)
        END IF
C
        IF  (TYM .LE. TF) THEN
```

```
            HYM = HFD
            IF  (TYM .GE. -0.3)  HYM = H(TYM)
         END IF
C
         HIJ = HIJ*RLK
         HXP = HXP*RLK
         HXM = HXM*RLK
         HYP = HYP*RLK
         HYM = HYM*RLK
C
C        ------------------------------------------------------------
C                  DETERMINING THE LIUQID WATER PRESSURE
C           (1)          PIJ -- LIQUID WATER PRESSURE AT (I,J), Pa
C           (2)  PIPJP,PIPJM -- LIQUID WATER PRESSURE AT (I+1, J+1)
C                               AND (I+1, J-1)
C           (3)  PIMJP,PIMJM -- LIQUID WATER PRESSURE AT (I-1, J+1)
C                               AND (I-1, J-1)
C           (4)   PIJP, PIJM -- LIQUID WATER PRESSURE AT (I, J+1)
C                               AND (I, J-1)
C           (5)   PIPJ, PIMJ -- LIQUID WATER PRESSURE AT (I+1, J)
C                               AND (I-1, J)
C        ------------------------------------------------------------
C
         SSW = WL(I,J)
         PIJ = 0.0
         IF  (TN(I,J) .LE. TF) THEN
            WL(I,J) = UWA/ABS(TN(I,J))**UWN
            PIJ     = P(TN(I,J), TF)
         END IF
C
         PIPJP = 0.0
         IF  (TN(I+1,J+1) .LE. TF) THEN
            PIPJP = P(TN(I+1,J+1), TF)
         END IF
C
         PIPJM = 0.0
         IF  (TN(I+1,J-1) .LE. TF) THEN
            PIPJM = P(TN(I+1,J-1), TF)
         END IF
C
         PIMJP = 0.0
         IF  (TN(I-1,J+1) .LE. TF) THEN
            PIMJP = P(TN(I-1,J+1), TF)
         END IF
C
```

```
          PIMJM = 0.0
          IF  (TN(I-1,J-1) .LE. TF) THEN
             PIMJM = P(TN(I-1,J-1), TF)
          END IF
C
          PIPJ = 0.0
          IF  (TN(I+1,J) .LE. TF) THEN
             PIPJ = P(TN(I+1,J), TF)
          END IF
C
          PIMJ = 0.0
          IF  (TN(I-1,J) .LE. TF) THEN
             PIMJ = P(TN(I-1,J), TF)
          END IF
C
          PIJP = 0.0
          IF  (TN(I,J+1) .LE. TF) THEN
             PIJP = P(TN(I,J+1), TF)
          END IF
C
          PIJM = 0.0
          IF  (TN(I,J-1) .LE. TF) THEN
             PIJM = P(TN(I,J-1), TF)
          END IF
C
C         ------------------------------------------------------------
C                          DETERMINING THE ICE CONTENT
C         ------------------------------------------------------------
C
          SS1 =       G22(I,J)*(HXP*(PIPJ - PIJ) - HXM*(PIJ - PIMJ))
          SS1 = SS1 + G11(I,J)*(HYP*(PIJP - PIJ) - HYM*(PIJ - PIJM))
          SS1 = SS1 - G12(I,J)*HIJ*(PIPJP - PIMJP - PIPJM + PIMJM)*0.5
          SS1 = SS1 +  PP(I,J)*HIJ*(PIPJ - PIMJ)*0.5
          SS1 = SS1 +  QQ(I,J)*HIJ*(PIJP - PIJM)*0.5
          SS2 = WL(I,J) - SSW
          SSW = WI(I,J)
C
          WI(I,J) = WI(I,J) + RGLI*(DTIM*SS1 - SS2)
          IF  (WI(I,J) .LT. 0.0)  WI(I,J) = 0.0
          DV(I,J) = DV(I,J) + WI(I,J) - SSW + SS2
C
          IF  (DV(I,J) .LT. 0.0)   DV(I,J) = 0.0
C
3000     CONTINUE
C
```

```
C       ---------------------------------------------------------------
C       CALCULATING THE CONTENTS OF LIQUID WATER AND ICE ON BOUNDARIES
C       ---------------------------------------------------------------
C
        DO 3010  I = 1 , MX
          WL(I,1)  = WO
          WI(I,1)  = 0.0
          DV(I,1)  = 0.0
          WL(I,MY) = UWA/ABS(TN(I,MY))**UWN
          WI(I,MY) = RGLI*(WO - WL(I,MY))
          DV(I,MY) = 0.0
3010    CONTINUE
C
        DO 3020  J = 2 , MY-1
          IF  ((J .LT. 20) .OR. (J .GT. 29)) THEN
             SS1     = G12(2,J)/G22(2,J)
             WL(1,J) = (WL(2,J) - WL(1,J-1)*SS1)/(1.0 - SS1)
             WI(1,J) = (WI(2,J) - WI(1,J-1)*SS1)/(1.0 - SS1)
             DV(1,J) = (DV(2,J) - DV(1,J-1)*SS1)/(1.0 - SS1)
          ELSE
             WL(1,J) = UWA/ABS(TN(1,J))**UWN
             WI(1,J) = RGLI*(WO - WL(1,J))
             IF  (TIM .LT. 1.0E-05) THEN
                DV(1,J) = WL(1,J) + WI(1,J) - WO
             ELSE
                DV(1,J) = 0.0
             END IF
          END IF
          IF  (DV(1,J) .LT. 0.0)   DV(1,J) = 0.0
C
          SS1      = G12(MX-1,J)/G22(MX-1,J)
          WL(MX,J) = (WL(MX-1,J) - WL(MX,J-1)*SS1)/(1.0 - SS1)
          WI(MX,J) = (WI(MX-1,J) - WI(MX,J-1)*SS1)/(1.0 - SS1)
          DV(MX,J) = (DV(MX-1,J) - DV(MX,J-1)*SS1)/(1.0 - SS1)
          IF  (DV(MX,J) .LT. 0.0)   DV(MX,J) = 0.0
3020    CONTINUE
C
        DV(1,MY)  = DV(2,MY)
        DV(MX,MY) = DV(MX-1,MY)
C
        RETURN
        END
C
C       ***************************************************************
C       *  SUBROUTINE OF SOLUTION OF TRIDIAGONAL SYSTEMS OF EQUATIONS  *
```

```
C       *                          BY  SHEN MU                            *
C       *     CREATED:   9/11/1988    LAST CORRECTION: 11/11/1988       *
C       ***********************************************************************
C
        SUBROUTINE   TRID2(MSUB,NO,NM,A,B,C,F)
C
        REAL*4    A(MSUB), B(MSUB), C(MSUB), F(MSUB), Q
C
C       =====  DECOMPOSITION AND FORWARD SUBSTITUTION  =====
C
        Q     = B(NO)
        F(NO) = F(NO)/B(NO)
        DO 6000  K = NO , NM-1
          B(K) = C(K)/Q
          Q = B(K+1) - A(K+1)*B(K)
          F(K+1) = (F(K+1) - A(K+1)*F(K))/Q
6000    CONTINUE
C
C       =====  BACKSUBSTITUTION  =====
C
        DO 6010  K = NM-1 , NO , -1
          F(K) = F(K) - B(K)*F(K+1)
6010    CONTINUE
C
C       ======
        RETURN
        END
C
C       ***********************************************************************
C               SUBROUTINE OF CALCULATING THERMAL PARAMETERS RKC
C
C         (1)           K -- APPARENT THERMAL CONDUCTIVITY, J/m/C/hour
C         (2)  KS, KL, KI -- THERMAL CONDUCTIVITY OF SOIL, WATER, ICE
C         (3)           C -- APPARENT HEAT CAPACITY, J/(m*m*m)/C
C         (4)  CS, CL, CI -- HEAT CAPACITY OF SOIL, WATER, ICE
C         (5)           L -- LATENT HEAT OF FUSION, 3.336E+05 J/kg
C       ***********************************************************************
C
        SUBROUTINE   PARAM1(RKC)
C
        PARAMETER  (MX = 34,   MY = 37)
C
        REAL*4     TN(MX,MY),  RKC(MX,MY), WL(MX,MY), WI(MX,MY),
     &             DTN(MX,MY), DV(MX,MY),  ATM(MX,MY)
        REAL*4     GAML, K,   C,   L,  KS, KL, KI, CS, CL, CI,
```

```
     &            XS,   XL,  XI,  SS1
C
        COMMON   /SOIL/ TIM, DTIM, WO, TF, UWN, UWA, RGLI, RLK
        COMMON   /HEAT/ TN,  DTN,  WL, WI, DV,  ATM
C
        DATA  L/0.3336E+06/,  CS/2.2E+06/, CL/4.18E+06/, CI/1.93E+06/,
     &        KS/4.34/,       KL/0.602/,   KI/2.22/,     GAML/1000./
C
        DO 4000  I = 1 , MX
        DO 4000  J = 1 , MY
          SS1 = WL(I,J) + WI(I,J) - WO
          IF  (SS1 .LE. 0.0) THEN
             XS = 1.0 - WO
             XL = WL(I,J)
             XI = WI(I,J)
          ELSE
             XS = (1.0 - WO)/(1.0 + SS1)
             XL =    WL(I,J)/(1.0 + SS1)
             XI =    WI(I,J)/(1.0 + SS1)
          END IF
C
          C   = 0.0
          IF  (TN(I,J) .LE. TF)  THEN
             IF  (TN(I,J) .GT. -2.00)  C = 0.02274
             IF  (TN(I,J) .GT. -1.50)  C = 0.0368
             IF  (TN(I,J) .GT. -1.00)  C = 0.0592
             IF  (TN(I,J) .GT. -0.75)  C = 0.0952
             IF  (TN(I,J) .GT. -0.50)  C = 0.2780
             IF  (TN(I,J) .GT. -0.35)  C = 0.5045
             IF  (TN(I,J) .GT. -0.20)  C = 1.55
             C = C*GAML*L
          END IF
          C = C + CS*XS  + CL*XL  + CI*XI
          K =     KS**XS * KL**XL * KI**XI
          RKC(I,J) = K*3600.0/C
4000    CONTINUE
C
        RETURN
        END
```

```
C      ****************************************************************
C      *                                                              *
C      *    SUBROUTINES OF CALCULATING THE STRESS AND DEFORMATION     *
C      *            FIELDS AROUND CHILLED PIPELINE BY FEM             *
C      *        (CO-OPERATIVE FRANCE-CANADA RESEARCH PROJECT)         *
C      *                                                              *
C      *                        BY  SHEN MU                           *
C      *   CINEP, ECOLE POLYTECHNIQUE DE MONTREAL, H3C 3A7, CANADA    *
C      *     CREATED:  12/09/1989    LAST CORRECTION:  5/09/1989      *
C      *   ---------------------------------------------------------  *
C      *   MAIN ARGUMENTS:                                            *
C      *      (1)    MX,MY -- MAX. NUMBER OF GRID POINTS IN X AND Y   *
C      *                      DIRECTIONS. ( MX*MY MESH )              *
C      *      (2) TIM,DTIM -- TIME AND TIME STEP (HOUR)               *
C      *   NOTES:                                                     *
C      *     (1)  ALL REALS IN DUMMY ARGUMENTS ARE SINGLE PRECISION   *
C      *     (2)  THE SYSTEM OF UNIT IN THIS PART: M, HOUR, MPA       *
C      *                                                              *
C      ****************************************************************
C
       SUBROUTINE   SD(ICTLF,TIM, DTIM, TF,W0)
C
       PARAMETER    (MX=34,    MY=37)
       PARAMETER    (ME=2400,  MJ=1300,  MJ2=2600, MAXSK=173000)
C
       INTEGER*4    UNIT1, UNIT2
       INTEGER*2    JM(ME,3), IZC(160),  IB(MJ),  ND(3)
       INTEGER*4    IA(MJ2),  ICN(6),   IHH, IDD, IP, IQ, IMX, IA4,
     &              NE, NJ,  NGPE, NJ2, NZ,  NPJ, M1, M2, M3,  M4,
     &              IE, ISS, I, J, K, L, ICTLF
C
       REAL*4       TN(MX,MY),  DV(MX,MY),  WL(MX,MY), WI(MX,MY),
     &              DTN(MX,MY), ATM(MX,MY), AJZ(MJ,2), SK(MAXSK),
     &              P(MJ2),     U(MJ2),     SEQ(ME),   STRESS(ME,3),
     &              EIE(ME),    DK(6,6),    S(3,6),  AY(6),  YL(3),
     &              HIE(ME),    PJ(25,2),   TND(3),  DVD(3), DTD(3),
     &              RDT(3,3),   B(3,6),     C(3),    STRAIN(ME,3)
       REAL*4       TIM, DTIM, TF, AMU, SS1, SS2, SS3, SS4, TE, DVE,
     &              DTE, EC,  SM,   AE
C
       COMMON       /HEAT/ TN,     DTN, WL,  WI,  DV,  ATM
       COMMON      /STIFF/ NJ2,    IDD, IA,  SK,  P
       COMMON    /ELEMENT/ AJZ,    JM,  NE,  NJ
       COMMON      /FORCE/ STRESS, U,   SEQ, STRAIN
C
```

```
C     ================================================================
C                        INPUT INITIAL MESH DATA
C         (1)   NE , NJ -- TOTAL NUMBER OF ELEMENTS & NODES
C         (2)      NGPE -- NUMBER OF NODES IN EACH ELEMENT
C         (3)  JM(NE,4) -- NODAL NUMBER OF ELEMENT
C         (4) AJZ(NJ,2) -- NODAL COORDINATES
C     ================================================================
C
      UNIT1 = 6
      UNIT2 = 5
C
      NJ   = MX*MY
      NE   = (MX - 1)*(MY - 1)*2
      NGPE = 3
      NPJ  = 0
      NZ   = 150
      NJ2  = 2*NJ
      AMU  = 0.3
      IF  ((TIM .GT. 1.0E-04) .AND. (ICTLF .EQ. 0)) THEN
         NJ  = NJ + 1
         NE  = NE + 9
         NZ  = NZ - 17
         NJ2 = 2*NJ
      END IF
C
      IF  (TIM .LT. 1.0E-04) THEN
         IF  ((NJ .GT. MJ) .OR. (NE .GT. ME) .OR. (NJ2 .GT. MJ2)) THEN
            WRITE(UNIT1,*) '*** PLEASE CORRECT MJ OR ME ***'
            WRITE(UNIT1,*) '******  STOP IN  SD.FOR  ******'
         END IF
C
         DO 4100  I = 1 , MJ
           AJZ(I,1) = 0.0
           AJZ(I,2) = 0.0
           P(I)     = 0.0
           U(I)     = 0.0
4100     CONTINUE
C
         DO 4110  IE = 1 , ME
           JM(IE,1)     = 0
           JM(IE,2)     = 0
           JM(IE,3)     = 0
           STRAIN(IE,1) = 0.0
           STRAIN(IE,2) = 0.0
           STRAIN(IE,3) = 0.0
```

```
            STRESS(IE,1) = 0.0
            STRESS(IE,2) = 0.0
            STRESS(IE,3) = 0.0
            SEQ(IE)      = 0.0
4110        CONTINUE
C
            READ(UNIT2,*) (( JM(I,J), J=1,NGPE), I=1,NE )
            READ(UNIT2,*) ((AJZ(I,J), J=1,2   ), I=1,NJ )
            READ(UNIT2,*) (   IZC(I), I=1,NZ  )
            READ(UNIT2,*) (( PJ(I,J), J=1,2   ), I=1,NPJ)
C
            IF  (ICTLF .EQ. 0) THEN
               NJ  = NJ + 1
               NE  = NE + 9
               NZ  = NZ - 17
               NJ2 = 2*NJ
C
               AJZ(NJ,1) = 0.0
               AJZ(NJ,2) = 1.285
               IZC(NZ)   = 2*NJ - 1
C
               ISS = (MX - 1)*(MY - 1)*2
               DO 4200  I = 1 , 9
                 K = ISS + I
                 JM(K,1) = NJ
                 JM(K,2) = 647 + (I-1)*MX
                 JM(K,3) = JM(K,2) + MX
4200           CONTINUE
            END IF
         END IF
C        ================================================================
C                 DEFINING THE VOLUME OF GLOBAL STIFFNESS MATRIX
C           (1)  IA(MJ2) -- THE NUMBER OF THE DIAGONAL ELEMENT OF THE
C                           GLOBAL STIFFNESS MATRIX
C           (2)      IHH -- VOLUME OF GLOBAL STIFFNESS MATRIX
C        ================================================================
         IF  (TIM .LT. 1.0E-04) THEN
            IMX = 0
            DO 5100  I = 1 , NJ
              IB(I)     = 0
              IA(2*I-1) = 0
              IA(2*I)   = 0
5100        CONTINUE
C
            DO 5110  IE = 1 , NE
```

```
            DO 5120  IP = 1 , NGPE
            DO 5120  IQ = 1 , NGPE
              ISS = JM(IE,IQ) - JM(IE,IP)
              M1  = JM(IE,IQ)
              IF  (ISS .GT. IMX)        IMX = ISS
              IF  (ISS .GT. IB(M1))  IB(M1) = ISS
5120          CONTINUE
5110        CONTINUE
C
            IDD   = 2*IMX + 2
            IA(1) = 1
            DO 5130  I = 1 , NJ
              IF  (I .GT. 1)   IA(2*I-1) = IA(2*I-2) + 2*IB(I) + 1
              IA(2*I) = IA(2*I-1) + 2*IB(I) + 2
5130        CONTINUE
            IHH = IA(NJ2)
            WRITE(UNIT1,'(1X,''IDD='',I4,9X,''IHH='',I6//)')  IDD, IHH
            IF  (IHH .GT. MAXSK) THEN
               WRITE(UNIT1,*) '* THE DIMENSION OF SK(I) IS TOO SMALL *'
               WRITE(UNIT1,*) '**********  STOP IN  SD.FOR  **********'
               STOP
            END IF
          END IF
C         ======================================================================
C                       DEFINING THE GLOBAL STIFFNESS MATRIX
C                  (1)  SK(MAXSK) -- GLOBAL STIFFNESS MATRIX
C         ======================================================================
          DO 5200  I = 1 , MAXSK
            SK(I) = 0.0
5200      CONTINUE
C
          CALL    ELS(0, TF, EIE, HIE)
          IF  (ICTLF .EQ. 0) THEN
             ISS = (MX - 1)*(MY - 1)*2
             DO 5205  K = 1 , 9
               IE = ISS + K
               EIE(IE) = 1.0E+09
               HIE(IE) = -10.0
5205         CONTINUE
          END IF
C
          DO 5210  IE = 1 , NE
            CALL   DYGD(3, IE, EIE, HIE, DK, S, B, AE)
            DO 5220  IQ = 1 , NGPE
              ICN(2*IQ-1) = 2*JM(IE,IQ) - 1
```

```
          ICN(2*IQ)   = 2*JM(IE,IQ)
5220      CONTINUE
          ISS = 2*NGPE
          DO 5230  IP = 1 , ISS
          DO 5230  IQ = 1 , ISS
            IF  (ICN(IP) .GE. ICN(IQ)) THEN
               M1     = ICN(IP)
               M2     = IA(M1) - ICN(IP) + ICN(IQ)
               SK(M2) = SK(M2) + DK(IP,IQ)
            END IF
5230      CONTINUE
5210    CONTINUE
C       ======================================================================
C                       DEFINING INITIAL FORCES VECTOR
C       ======================================================================
        IF  (TIM .LT. 1.0E-04) THEN
           DO 5300  I = 1 ,NPJ
             J = IFIX(PJ(I,2) + 1.0E-06)
             P(J) = PJ(I,1)
5300       CONTINUE
        END IF
C       ======================================================================
C        CALCULATING THE CREEP & VOLUMETRIC EXPANSION IN THE TIME STEP
C              (1)      TE -- AVERAGE TEMPERATURE IN THE ELEMENT
C              (2)     DTE -- TEMPERATURE INCREMENT IN THE ELEMENT
C              (3)     DVE -- VOLUMETRIC EXPANSION OF ELEMENT
C              (4) SEQ(IE) -- EQUIVALENT STRESS
C              (5)      SM -- MEAN STRESS
C              (6)      EC -- CREEP STRAIN INCREMENT
C              (7)   YL(3) -- STRESS DEVIATION
C              (8)    C(3) -- EQUIVALENT INITIAL STRAIN
C       ======================================================================
        IF  (TIM .GT. 1.0E-04) THEN
           DO 5750  I = 1 , NJ2
             P(I) = 0.0
5750       CONTINUE
        END IF
C
        DO 5760  IE = 1 , NE
          C(1) = 0.0
          C(2) = 0.0
          C(3) = 0.0
C
          ISS = (MX - 1)*(MY - 1)*2
          IF  (IE .LE. ISS) THEN
```

```
            DO 5770  K = 1 , NGPE
              ND(K)  = JM(IE,K)
              SS1    = FLOAT(ND(K) -1)/FLOAT(MX)
              J      = IFIX(SS1 + 1.0E-06) + 1
              I      = ND(K) - (J-1)*MX
C
              TND(K) = TN(I,J)
              DVD(K) = DV(I,J)
              DTD(K) = DTN(I,J)
5770          CONTINUE
              TE  = (TND(1) + TND(2) + TND(3))/3.0
              DTE = (DTD(1) + DTD(2) + DTD(3))/3.0
              DVE = (DVD(1) + DVD(2) + DVD(3))/3.0
            ELSE
              TE  = 1.0
              DTE = 0.0
              DVE = 0.0
            END IF
C
C           ----- THE UNIT OF STRESS IN CREEP EQUATION IS MPA -----
C
            SS1   = SEQ(IE)*1.0E-06
            IF  ((TE .LE. TF) .AND. (SEQ(IE) .GT. 0.0)) THEN
              SM  = (1.0 + AMU)*(STRESS(IE,1) + STRESS(IE,2))/3.0
              IF  (SM .GT. 0.0) THEN
                SS2 = (TIM + 0.1)**0.56*(1.0 - TE)**2.326
                EC  = 2.12E-08*SS1**2.326/SS2
              ELSE
                SS2 = (TIM + 0.1)**0.80*(1. - TE)**1.429
                EC  = 2.80E-06*SS1**1.429/SS2
              END IF
C
              YL(1) = STRESS(IE,1) - SM
              YL(2) = STRESS(IE,2) - SM
              YL(3) = STRESS(IE,3)
C
              SS2  = 1.5*EC*DTIM/SEQ(IE)
              C(1) = YL(1)*SS2
              C(2) = YL(2)*SS2
              C(3) = YL(3)*SS2*2.0
            END IF
C
            SS1  = DVE/3.0
            C(1) = C(1) + SS1
            C(2) = C(2) + SS1
```

```
C       ================================================================
C         CALCULATING THE CORRECTION OF TEMPERATURE EFFECT ON ELASTIC
C                              CONSTANT MATRIX
C            (1) RDT(3,3) -- DERIVATIVE OF ELASTIC CONSTANT MATRIX
C                            WITH RESPECT TO TEMPERATURE
C       ================================================================
          IF  (TE .LT. TF) THEN
             RDT(1,1) =  1.0 - AMU
             RDT(1,2) = -AMU
             RDT(1,3) =  0.0
             RDT(2,1) = -AMU
             RDT(2,2) =  1.0 - AMU
             RDT(2,3) =  0.0
             RDT(3,1) =  0.0
             RDT(3,2) =  0.0
             RDT(3,3) =  2.0
C
             IF  (TE .GT. TF) THEN
                SS2 = 0.0
             ELSE
                IF  (SM .LE. 0.0) THEN
                   SS1 = 0.636/(EIE(IE)*(ABS(TE)**1.364))
                ELSE
                   SS1 = 0.381/(EIE(IE)*(ABS(TE)**1.619))
                END IF
                SS2 = -DTE*(1.0 + AMU)*SS1
             END IF
             DO 5800  I = 1 , 3
               DO 5800  J = 1 , 3
                 RDT(I,J) = RDT(I,J)*SS2
5800         CONTINUE
C
             DO 5810  I = 1 , 3
               YL(I) = 0.0
               DO 5820  K = 1 , 3
                 YL(I) = YL(I) + RDT(I,K)*STRESS(IE,K)
5820           CONTINUE
5810         CONTINUE
C
             C(1) = C(1) + YL(1)
             C(2) = C(2) + YL(2)
             C(3) = C(3) + YL(3)
          END IF
C       ================================================================
C        CALCULATING THE EQUIVLENT NODAL FORCES FROM CREEP & EXPANSION
```

```
C             (1)  AY(3) -- EQUIVALENT NODAL FORCES INCREMENT
C       ================================================================
          CALL   DYGD(2, IE, EIE, HIE, DK, S, B, AE)
          DO 5900  I = 1 , 6
            AY(I) = 0.0
            DO 5910  K = 1 , 3
              AY(I) = AY(I) + S(K,I)*C(K)*AE
5910        CONTINUE
5900      CONTINUE
C
          DO 5920  I = 1 , NGPE
            DO 5930  J = 1 , 2
              IP = 2*(I-1) + J
              IQ = 2*(JM(IE,I) - 1) + J
              P(IQ) = P(IQ) + AY(IP)
5930        CONTINUE
5920      CONTINUE
C
5760    CONTINUE
C       ================================================================
C         MODIFIED GLOBAL STIFFNESS MATRIX AND FORCES VECTOR ACCORDING
C                     TO DISPLACEMENT BOUNDARY CONDITIONS
C       ================================================================
        DO 5400  I = 1 , NZ
          ISS = IZC(I)
          M1  = IA(ISS-1) + 1
          M2  = IA(ISS)   - 1
          DO 5410  J = M1 , M2
            SK(J) = 0.0
5410      CONTINUE
          M3 = ISS + 1
          DO 5420  IP = M3 , NJ2
            IA4 = IP - ISS
            IF  (IA4 .LE. (IA(IP) - IA(IP-1) -1)) THEN
               M4     = IA(IP) - IA4
               SK(M4) = 0.0
            END IF
5420      CONTINUE
          SK(M2+1) = 1.0
          P(ISS)   = 0.0
5400    CONTINUE
C       ================================================================
C                       CALCULATING THE NODEL DISPLACEMENT
C       ================================================================
C
```

```
      CALL   CHOL
C
      DO 5500  I = 1 , NJ2
        U(I) = U(I) + P(I)
5500  CONTINUE
C     ================================================================
C                 CALCULATING THE STRESSES IN EACH ELEMENT
C       (1)  YL(3) -- ELEMENT STRESS INCREMENT IN THE TIME STEP
C       (2)  AL(6) -- NODAL DISPLACEMENT INCREMENT IN THE TIME STEP
C     ================================================================
      DO 5550  IE = 1 , NE
        CALL   DYGD(2, IE, EIE, HIE, DK, S, B, AE)
        DO 5560  I = 1 , NGPE
          DO 5560  J = 1 , 2
            IP     = 2*(I-1) + J
            IQ     = 2*(JM(IE,I) - 1) + J
            AY(IP) = P(IQ)
5560      CONTINUE
C
          DO 5570  I = 1 , NGPE
            YL(I) = 0.0
            C(I)  = 0.0
            ISS   = 2*NGPE
            DO 5580  J = 1 , ISS
              YL(I) = YL(I) + S(I,J)*AY(J)
              C(I)  = C(I)  + B(I,J)*AY(J)
5580        CONTINUE
            STRESS(IE,I) = STRESS(IE,I) + YL(I)
            STRAIN(IE,I) = STRAIN(IE,I) + C(I)
5570      CONTINUE
C
          SM      = (1.0 + AMU)*(STRESS(IE,1) + STRESS(IE,2))/3.0
          SS1     = STRESS(IE,1) - SM
          SS2     = STRESS(IE,2) - SM
          SS3     = AMU*(STRESS(IE,1) + STRESS(IE,2)) - SM
          SS4     = STRESS(IE,3)
          SEQ(IE) = SQRT(1.5*(SS1*SS1 + SS2*SS2 + SS3*SS3 + 2.*SS4*SS4))
5550  CONTINUE
C     ================================================================
C                     CALCULATING THE STRESSES AT NODE
C     ================================================================
      IF  (ICTLF .EQ. 1) THEN
         DO 5700  K = 1 , NJ
           SS1      = FLOAT(K - 1)/FLOAT(MX)
           J        = IFIX(SS1 + 1.0E-06) + 1
```

```
            I        = K - (J-1)*MX
            ATM(I,J) = 0.0
C
            ISS = 0
            M1  = (J - 3)*(MX + MX - 2)
            M2  = (J + 1)*(MX + MX - 2)
            IF  (M1 .LT. 1 )  M1 = 1
            IF  (M2 .GT. NE)  M2 = NE
            DO 5710  IE = M1 , M2
              DO  5720  L = 1 , NGPE
                IF  (JM(IE,L) .EQ. K) THEN
                   ISS = ISS + 1
                   SS1 = (1.0 + AMU)*(STRESS(IE,1) + STRESS(IE,2))
                   ATM(I,J) = ATM(I,J) + SS1/3.0
                END IF
5720            CONTINUE
5710          CONTINUE
C
              IF  (ISS .GT. 0)  ATM(I,J) = ATM(I,J)/FLOAT(ISS)
5700        CONTINUE
          END IF
C
C         ======
          RETURN
          END
C
C         ****************************************************************
C         *      SUBROUTINE OF SOLVING THE SYSTEM OF BAND EQUATIONS      *
C         *            BY THE CHOLESKY-CROUT METHOD (FOR FEM)            *
C         *      ------------------------------------------------        *
C         *      CREATED: 1985            LAST CORRECTION: 14/08/89      *
C         ****************************************************************
C
          SUBROUTINE    CHOL
C
          PARAMETER     (MJ2=2600, MAXSK=173000)
C
          REAL*4        SK(MAXSK), P(MJ2)
          INTEGER*4     IA(MJ2), IDD, NJ2,  I,  J,  L,  M1, M2, M3, M4,
     &                  IH,  IP, IQ
C
          COMMON        /STIFF/ NJ2, IDD, IA, SK, P
C
C         =====   DECOMPOSITION AND FORWARD SUBSTITUTION   =====
C
```

```
      DO 6100  J = 2 , NJ2
        L = IA(J-1) + J + 1 - IA(J)
        DO 6110  I = L , J
          IQ =   IA(J) - J + I
          IH = IA(I-1) - IA(I) + I
          M1 = I - 1
          DO 6110  IP = L , M1
            IF (IP .GT. IH)  THEN
               M2     =  IA(I) - I + IP
               M3     =  IA(IP)
               M4     =  IA(J) - J + IP
               SK(IQ) = SK(IQ) - SK(M2)*SK(M4)/SK(M3)
            END IF
6110      CONTINUE
6100    CONTINUE
C
        DO 6120  I = 2 , NJ2
          M1 = IA(I-1) + I + 1 - IA(I)
          M2 = I - 1
          DO 6120  IP = M1 , M2
            M3   = IA(I) - I + IP
            M4   = IA(IP)
            P(I) = P(I) - SK(M3)*P(IP)/SK(M4)
6120    CONTINUE
C
C       =====   BACKSUBSTITUTION   =====
C
        DO 6130  I = NJ2 , 1 , -1
          IF  ((I+IDD) .LT. NJ2) THEN
             L = I + IDD
          ELSE
             L = NJ2
          END IF
          M1 = I + 1
          DO 6140  IP = M1 , L
            M2 = IA(IP) - IP + I
            IF  ((IA(IP)-IP+I) .GT. IA(IP-1)) THEN
               P(I) = P(I) - SK(M2)*P(IP)
            END IF
6140      CONTINUE
          M3   = IA(I)
          P(I) = P(I)/SK(M3)
6130    CONTINUE
C
C       ======
```

```
RETURN
END
```

```
C       ****************************************************************
C       *   SUBROUTINE OF DETERMINING THE YOUNG'S MODULES OF ELEMENT   *
C       *                    (TRIANGULAR ELEMENT)                      *
C       *     (1)  EIE(ME) -- YOUNG'S MODULES OF THE ELEMENT           *
C       *     (2)  HIE(ME) -- HARDENING SLOP DURING YIELDING           *
C       *                    ( IF THE ELEMENT IS IN ELASTIC STATUS,    *
C       *                      THE HIE(IE)  IS LESS THAN ZERO )        *
C       *     (3)    ICTL0 -- CONTROL PARAMETER (= 0 OR 1)             *
C       *                      = 0     CALAULATING EIE & HIE           *
C       *                      = 1     CALAULATING HIE ONLY            *
C       *     (4)   TND(3) -- TEMPERATURE AT NODE                      *
C       *   ---------------------------------------------------------  *
C       *   THE UNIT OF THE YOUNG'S MODULES IS 'PA'                    *
C       ****************************************************************
C
        SUBROUTINE   ELS(ICTL0, TF, EIE, HIE)
C
        PARAMETER    (ME=2400,  MJ=1300, MJ2= 2600)
        PARAMETER    (MX=34,    MY=37)
C
        INTEGER*4    UNIT1
        INTEGER*2    JM(ME,3)
        INTEGER*4    NE, NJ, IE, I, J, K, ISS, ICTL0, ICTL1, IK
C
        REAL*4       TN(MX,MY),  WL(MX,MY),    WI(MX,MY),  DV(MX,MY),
     &               DTN(MX,MY), ATM(MX,MY),   EIE(ME),    TND(3),
     &               WND(3),     AJZ(MJ,2),    U(MJ2),     HIE(ME),
     &               SEQ(ME),    STRAIN(ME,3), STRESS(ME,3)
        REAL*4       TF,  TL1, TL2, SS1, SS2, SS3, SS4, SCALE1, SCALE2,
     &               TE,  EUF, EF,  TAE, SY
C
        COMMON       /HEAT/ TN,     DTN, WL,  WI,  DV,  ATM
        COMMON     /ELEMENT/ AJZ,    JM,  NE,  NJ
        COMMON      /FORCE/ STRESS, U,   SEQ, STRAIN
C
        UNIT1 = 6
C
        EUF = 1.12E+07
C
        IK = (MX - 1)*(MY - 1)*2
        DO 7000  IE = 1 , IK
          DO 7010  K = 1, 3
            ISS    = JM(IE,K)
            SS1    = FLOAT(ISS - 1)/FLOAT(MX) + 1.0E-06
            J      = IFIX(SS1) + 1
```

```
            I      = ISS - (J-1)*MX
            TND(K) = TN(I,J)
7010      CONTINUE
C
          TL1 = (TND(1) -TF)*(TND(2) - TF)
          TL2 = (TND(1) -TF)*(TND(3) - TF)
          IF  ((TL1 .GE. 0.0) .AND. (TL2 .GE. 0.0)) THEN
             ICTL1  = 0
             SCALE1 = 0.0
             SCALE2 = 0.0
             IF  ((TND(2) .GT. TF) .OR. (TND(3) .GT. TF)) THEN
                TE = 1.0
             ELSE
                TE = (TND(1) + TND(2) + TND(3))/3.0
             END IF
          ELSE
             ICTL1 = 1
             IF  ((TL1 .LT. 0.0) .AND. (TL2 .GE. 0.0)) THEN
                SS1    = TND(1)
                SS2    = TND(2)
                SS3    = TND(3)
                TND(1) = SS2
                TND(2) = SS3
                TND(3) = SS1
             ELSEIF ((TL1 .GE. 0.0) .AND. (TL2 .LT. 0.0)) THEN
                SS1    = TND(1)
                SS2    = TND(2)
                SS3    = TND(3)
                TND(1) = SS3
                TND(2) = SS1
                TND(3) = SS2
             END IF
             SCALE1 = (TND(1) -TF)/(TND(1) - TND(2))
             SCALE2 = (TND(1) -TF)/(TND(1) - TND(3))
C
             IF  (TND(1) .LE. TF) THEN
                TE = (TND(1) + TF + TF)/3.0
             ELSE
                TE = (TND(2) + TND(3) + TF + TF)*0.25
             END IF
          END IF
C       ================================================================
C                          DEFINING THE YOUNG'S MODULES
C               (1)  EUF -- YOUNG'S MODULES OF UNFROZEN SOIL
C               (2)   EF -- YOUNG'S MODULES OF FROZEN SOIL
```

```
C       ================================================================
          IF  (ICTLO .LT. 1) THEN
             IF  (TE .GT. TF) THEN
                EIE(IE) = EUF
             ELSE
                SS1 = STRESS(IE,1) + STRESS(IE,2)
                SS2 = ABS(TE - TF) + 0.005
                IF  (SS1 .GT. 0.0) THEN
                   EF = 5.31E+07*(SS2**0.381)
                ELSE
                   EF = 4.00E+07*(SS2**0.636)
                END IF
C
                IF  (ICTL1. EQ. 0) THEN
                   EIE(IE) = EF
                ELSE
                   SS1 = SCALE1*SCALE2
                   IF  (TND(1) .GT. TF) THEN
                      EIE(IE) = SS1*EUF + (1.0 - SS1)*EF
                   ELSE
                      EIE(IE) = (1.0 - SS1)*EUF + SS1*EF
                   END IF
                END IF
             END IF
C
             SS1 =     STRESS(IE,1) + STRESS(IE,2)
             SS2 = ABS(STRAIN(IE,1) + STRAIN(IE,2))
             IF  (SS1 .GT. 0.0) THEN
                IF  (SS2 .GE. 0.01)   EIE(IE) = 2.0E+06
             ELSE
                IF  (SS2 .GE. 0.04)   EIE(IE) = 2.0E+06
             END IF
C
             IF  (EIE(IE) .LE. 0.0) THEN
                WRITE(UNIT1,7020) IE
7020            FORMAT(1X,34HTHE YOUNG'S MODULES < 0 IN ELEMENT,I4)
                STOP
             END IF
          END IF
C       ================================================================
C                DEFINING THE HARDEN SLOP DURING YIELDING
C                    (1)   SY -- YIELD STRESS
C                    (2)  SEQ -- EQUIVALENT STRESS
C       ================================================================
          IF  (ICTLO .LT. 2) THEN
```

```
            TAE     = (TND(1) + TND(2) + TND(3))/3.0
            HIE(IE) = -10.0
            IF  (TAE .LE. TF) THEN
               IF  (SM .LE. 0.0) THEN
                  SY = 0.255E+06*(ABS(TAE) + 0.005)**0.710
               ELSE
                  SY = 0.531E+06*(ABS(TAE) + 0.005)**0.404
               END IF
            ELSE
               SY = 0.25E+05
            END IF
C
            IF  (SEQ(IE) .GE. SY) THEN
               HIE(IE) = EIE(IE)*0.2
            END IF
         END IF
7000    CONTINUE
C
C       ======
        RETURN
        END
C
C       ***************************************************************
C       *    SUBROUTINE OF DETERMINING THE ELEMENT STIFFNESS MATRIX    *
C       *                    (TRIANGULAR ELEMENT)                      *
C       *    CREATED: 1985               LAST CORRECTION: 23/11/89     *
C       *    ---------------------------------------------------       *
C       *         (1)  ICTL0 -- CONTROL PARAMETER                      *
C       *                         = 1  DEFINING ELEMENT AREA ONLY      *
C       *                         = 2  DEFINING MATRIZES  B,D & S      *
C       *                         = 3  DEFINING STIFFNESS MATRIX  DK   *
C       ***************************************************************
C
        SUBROUTINE   DYGD(ICTL0, IE, EIE, HIE, DK, S, B, AE)
C
        PARAMETER    (ME=2400,  MJ=1300, MJ2= 2600)
C
        INTEGER*4    UNIT1
        INTEGER*2    JM(ME,3)
        INTEGER*4    NE,  NJ,  IE,  I,   J,   ND1, ND2, ND3, ICTL0
C
        REAL*4       AJZ(MJ,2),    B(3,6),   D(3,3),   S(3,6),  DK(6,6),
     &               DP(6,6),      EIE(ME),  HIE(ME),  DST(3),  U(MJ2),
     &               SSM1(3,3),    SSM2(3),  SSM3(3),  SEQ(ME),
     &               STRAIN(ME,3), STRESS(ME,3)
```

```
      REAL*4       AE,  XE,  YE,  BI,  BJ,  BM,  CI,  CJ,  CM,  AMU,
     &             SS1, SM
C
      COMMON     /ELEMENT/ AJZ,    JM,  NE,  NJ
      COMMON       /FORCE/ STRESS, U,   SEQ, STRAIN
C
      UNIT1 = 6
C     ================================================================
C                  CALCULATING THE AREA OF THE ELEMENT
C          (1)   XE --  X COORDINATE OF THE POINT OF GRAVITY
C          (2)   YE --  Y COORDINATE OF THE POINT OF GRAVITY
C          (3)   AE --  AREA OF THE ELEMENT
C     ================================================================
      ND1 = JM(IE,1)
      ND2 = JM(IE,2)
      ND3 = JM(IE,3)
C
      BI = AJZ(ND2,2) - AJZ(ND3,2)
      CI = AJZ(ND3,1) - AJZ(ND2,1)
      BJ = AJZ(ND3,2) - AJZ(ND1,2)
      CJ = AJZ(ND1,1) - AJZ(ND3,1)
      BM = AJZ(ND1,2) - AJZ(ND2,2)
      CM = AJZ(ND2,1) - AJZ(ND1,1)
C
      AE = (BJ*CM - BM*CJ)*0.5
      XE = (AJZ(ND1,1) + AJZ(ND2,1) + AJZ(ND3,1))/3.0
      YE = (AJZ(ND1,2) + AJZ(ND2,2) + AJZ(ND3,2))/3.0
      IF  (AE .LE. 0.0) THEN
         WRITE(UNIT1,7500)   IE
7500     FORMAT(5X, 'INCORRECT NODAL NUMBER IN ELEMENT  #', I4)
         WRITE(UNIT1,*)  'AE=',AE
         STOP
      END IF
C     ================================================================
C            CALCULATING THE STRAIN-DISPLACEMENT MATRIX  B
C                    (1)   AMU --  POISSON'S RATIO
C     ================================================================
      IF  (ICTL0 .GT. 1) THEN
         AMU = 0.3
C
         DO 7510  I = 1 , 3
           DO 7510  J = 1 , 6
             B(I,J) = 0.0
7510     CONTINUE
C
```

```
            B(1,1) = BI
            B(1,3) = BJ
            B(1,5) = BM
            B(2,2) = CI
            B(2,4) = CJ
            B(2,6) = CM
            B(3,1) = CI
            B(3,2) = BI
            B(3,3) = CJ
            B(3,4) = BJ
            B(3,5) = CM
            B(3,6) = BM
C
            SS1 = 0.5/AE
            DO 7520  I = 1 , 3
              DO 7520  J = 1 , 6
                B(I,J) = B(I,J)*SS1
7520        CONTINUE
C       ================================================================
C                     CALCULATING THE MATRIZES  D AND DP
C                (1)   D(3,3) --  ELASTICITY MATRIX
C                (2)  DP(3,3) --  ELASTICITY-PLASTICITY MATRIX
C       ================================================================
C
            D(1,1) = 1.0 - AMU
            D(1,2) = AMU
            D(1,3) = 0.0
            D(2,1) = AMU
            D(2,2) = 1.0 - AMU
            D(2,3) = 0.0
            D(3,1) = 0.0
            D(3,2) = 0.0
            D(3,3) = 0.5 - AMU
C
            SS1 = EIE(IE)/((1.0 + AMU)*(1.0 - 2.0*AMU))
            DO 7550  I = 1 , 3
              DO 7550  J = 1 , 3
                D(I,J) = D(I,J)*SS1
7550        CONTINUE
C
            DO 7560  I = 1 , 3
              DO 7560  J = 1 , 3
                SSM1(I,J) = 0.0
7560        CONTINUE
            IF  (HIE(IE) .GE. 0.0) THEN
```

```
            SM     = (1.0 + AMU)*(STRESS(IE,1) + STRESS(IE,2))/3.0
            SS1    = 1.5/SEQ(IE)
            DST(1) = (STRESS(IE,1) - SM)*SS1
            DST(2) = (STRESS(IE,2) - SM)*SS1
            DST(3) = 2.0*STRESS(IE,3)*SS1
C
            DO 7570  I = 1 , 3
              SSM2(I) = 0.0
              DO 7570  K = 1 , 3
                SSM2(I) = SSM2(I) + D(I,K)*DST(K)
7570        CONTINUE
            DO 7580  J = 1 , 3
              SSM3(J) = 0.0
              DO 7580  K = 1 , 3
                SSM3(J) = SSM3(J) + DST(K)*D(K,J)
7580        CONTINUE
C
            DO 7590  I = 1 , 3
              DO 7590  J = 1 , 3
                SSM1(I,J) = SSM2(I)*SSM3(J)
7590        CONTINUE
C
            SS1 = 0.0
            DO 7600  K = 1 , 3
              SS1 = SS1 + DST(K)*SSM2(K)
7600        CONTINUE
            SS1 = SS1 + HIE(IE)
C
            DO 7610  I = 1 , 3
              DO 7610  J = 1 , 3
                SSM1(I,J) = SSM1(I,J)/SS1
7610        CONTINUE
          END IF
C
          DO 7620  I = 1 , 3
            DO 7620  J = 1 , 3
              DP(I,J) = D(I,J) - SSM1(I,J)
7620      CONTINUE
C       ================================================================
C                  CALCULATING THE STRESS-DISPLACEMENT  S
C       ================================================================
          DO 7650  I = 1 , 3
            DO 7650  J = 1 , 6
              S(I,J) = 0.0
              DO 7660  K = 1 , 3
```

```
                S(I,J) = S(I,J) + DP(I,K)*B(K,J)
7660          CONTINUE
7650       CONTINUE
        END IF
C       ================================================================
C                 CALCULATING THE ELEMENT STIFFNESS MATRIX
C               (1)    DK(6,6)  --  ELEMENT STIFFNESS MATRIX
C       ================================================================
        IF  (ICTL0 .GT. 2) THEN
           DO 7700  I = 1 , 6
             DO 7700  J = 1 , 6
               DK(I,J) = 0.0
               DO 7710  K = 1 , 3
                 DK(I,J) = DK(I,J) + S(K,I)*B(K,J)*AE
7710           CONTINUE
7700       CONTINUE
        END IF
C
C       ======
        RETURN
        END
```